DESIGN OF LOW LOSS HELIX CIRCUITS FOR INTERFERENCE FITTED AND BRAZED CIRCUITS

FINAL REPORT

A. JACQUEZ

CONTRACT NOs. NAS3-21509 and NAS3-22441

CR168313

JANUARY 1983

Prepared for:
NASA LEWIS RESEARCH CENTER
CLEVELAND, OHIO 44135

Prepared by:
Varian Associates, Inc.
Microwave Tube Division
611 Hansen Way
Palo Alto, CA 94303

SUMMARY

This final report reviews study programs on fabricating brazed helix circuits and interference fitted circuits to evaluate the rf loss properties and thermal capability. The objective was to produce design circuits with minimum rf loss and maximum heat transfer. These circuits were to be designed to operate at 10 kV and at 20 GHz using a γa approximately equal to 1.0. This represents a circuit diameter of only 0.75 millimeters. The fabrication of this size circuit and the 0.48 millimeter high support rods required considerable refinements in the assembly techniques and fixtures used on lower frequency circuits. The transition from the helices to the waveguide was designed and the circuits were matched from 20 to 40 GHz since the helix design is a broad band circuit and at a γa of 1.0 will operate over this band. The loss measurement was a transmission measurement and therefore had two such transitions. This resulting double-ended match required tuning elements to achieve the broad band match and external E-H tuners at each end to optimize the match for each frequency where the loss measurement was made. The test method used was a substitution method where the test fixture was replaced by a calibrated attenuator. In each case the power in and out was recorded for the test circuit and the attenuator replaced the test circuit and was varied to achieve the same power out for the same power in. This method is different from the one used for lower frequency circuits, where a perturbation method is used with an Automatic Network Analyzer (ANA). The latter could not be used as the ANA did not cover the higher frequency band.

Several circuits fabricated and studied were of a design similar to the lower frequency designs. That is, the helices were made of tungsten and supported with BeO and APBN rods but had the dimensions and TPI to operate at 10 kV and 20 GHz to 40 GHz. This met the requirements of the study program and provided loss data at millimeter frequencies for circuits where considerable rf loss data exists below 18 GHz. This provided the data necessary to determine the change in loss characteristics with frequency. It also provided a known standard to compare with other circuit designs unique to millimeter frequencies. One circuit not used at lower frequencies is the brazed circuit. One variation of this brazed circuit studied was

diamond rods brazed to a Amzirc helix and a copper barrel. This circuit represents an order of magnitude improvement over the thermal capability of an APBN rod supported tungsten helix, interference fitted in a copper barrel.

The results of the tests indicate that:

- the loss of the standard circuit is just a linear extension of the data below 18 GHz. That is, there is no sudden change in the rf loss as the frequency goes from below 18 GHz to 40 GHz;

- the loss in dB per wavelength is either constant or decreasing with frequency for the circuits measured;

- the value of loss in dB/in yields a loss parameter i which is low enough that millimeter tubes will have an acceptable conversion efficiency;

- the interference circuits studied and the brazed circuit studied all had approximately the same rf losses in dB/in over the measured frequency band;

- the study showed that the factors which do effect rf losses are material fabrication, material finishes, and processing; these were not evaluated in sufficient detail to determine the lowest rf loss circuit with the best heat transfer;

- the assembly procedure and control of the rod-helix design are a major factor in the thermal capability of a circuit design.

The study program results in extending the rf loss knowledge of a standard and other design circuits up to 40 GHz. The study resolved that the loss was not excessive and helix tubes could be designed at millimeter frequencies with reasonable efficiencies. Finally the techniques needed to assemble this type of circuit were refined and the factors that required further study were determined.

TABLE OF CONTENTS

LIST OF ILLUSTRATIONS

LIST OF ILLUSTRATIONS

1. INTRODUCTION

This final report covers work done on two NASA contracts on "Low-Loss Helix Study at 20 GHz". The work covering a loss study on an interference (pressure) fitted helix circuit was done under Contract NAS3-22441 and the work covering a loss study on a brazed helix circuit was done under Contract NAS3-21509. The following paragraphs are in reference to Specifications outlined in the work statements.

2.0 OBJECTIVES

The objectives of each contract was to produce design circuits with minimum rf loss and maximum heat transfer. To accomplish this the various losses due to the circuit, dielectric and the body were to be defined.

3.0 DESIGN REQUIREMENTS

The design requirements of the contract are as follows:

3.1 The basic helix design for each study was for a tube operating at 10 kV and with a Ya = 1.

3.2 The helix itself was to be made of copper, copper plated molybdenum or copper plated tungsten and surrounded by a copper plated barrel. The assembly was to be in vacuum.

3.3 The three types of dielectric to be used for support rods were to be:

a. Diamond rods or posts
b. Single crystal BeO
c. A low loss dielectric material other than a and b.

4.0 CONSTRUCTION

The statement of work also defined the following construction requirements.

4.1 Design and construct a helix to waveguide transformer which will accept samples of the helices and have a VSWR of 1.5 or less over the frequency range of 17.7 to 21.2 GHz.

4.1.1 The transformer system shall be able to accept helix samples of 2 and 4 inches for measurement of circuit loss.

4.2 The transformer system should be tunable to allow lower VSWR over a more restricted frequency.

4.2 Construct complete helical circuits with the three types of dielectric supports, barrels and transformers. The helical circuits shall be in high vacuum.

5.0 TEST PROCEDURES

The last technical item in the statement of work covered the test procedures and was as follows.

5.1 Devise techniques to measure the thermal heat transfer and rf loss of the circuit. The rf loss measurements shall be accomplished by the substitute techniques utilizing the difference between a 2 inch and 4 inch long helical circuit.

5.2 Perform the following measurements:

1. Determine transformer coupling losses;
2. Determine the circuit losses
3. Determine the breakdown of skin effect and dielectric losses to overall rf losses.

5.3 Generate design and assembling criteria for circuits with minimum rf circuit losses and maximum heat transfer.

The basic helix design used was a circuit that would operate at 10 kV and with a γa near 1.0 at 20 GHz. The choice of the circuit dimensions and the rod and barrel loading would, of course, determine the exact operating voltage and γa for the chosen design.

For example, a heavy dielectric loaded circuit will have a lower TPI helix or a smaller helix diameter (lower ka cotχ) to raise the operating voltage to 10 kV compared to a low dielectric loaded circuit.

Having chosen the basic helix dimension, the helix materials evalulated were tungsten tape and Amzirc tape. The Amzirc tape being 99.8% pure OFHC copper. Also evaluated as a possible material was copper evaporated on tungsten tape. All of the tapes were prepared according to the documented processing procedures used to process manufacturing's tapes and helices. Some SEM photographs were taken of the surfaces at various stages of processing and the results are presented in Section 2. The two tape materials used on actual helices measured were tungsten and Amzirc.

Two of the three dielectric materials studied were diamond rods and BeO rods. Single crystal BeO was not available and data from a paper on the thermal properties of single crystal BeO show that the properties above $0^{\circ}C$ were identical to regular pressed BeO. The last material studied was APBN which is the conventional support rod below 18 GHz for interference fitted circuits.

Since BeO and APBN are used below 18 GHz, the interference fitted circuits using these dielectrics were studied above 18 GHz, since considerable loss data existed below 18 GHz to compare the measured loss data to the new measured loss data above 18 GHz.

The diamond rods' advantage is mainly the thermal improvement and because of the cost of diamonds and rod manufacturing it would be only considered at millimeter frequencies. Thus the diamond rod and copper (Amzirc) helix would mainly be used for an optimum thermal design. This design would be the brazed design and was the one brazed circuit where the loss was measured up to 40 GHz.

It was noted that existing loss data on various circuits existed from 4 to 18 GHz for conventional circuits. It was further noted that the loss data up to 22 GHz was truly an extension of the known data but that the helix design chosen was capable of operating up to 40 GHz ($\gamma a = 2.2$) and loss data up to this frequency would determine the capability of the helix circuit to extend its usefullness into these millimeter wave bands. This additional frequency bandwidth loss was actually measured.

The construction of loss test fixture was modeled after lower frequency conventional fixtures. These fixtures are normally a coaxial transition design to the helix. The advantage is broad bandwidth and flexibility to transition from a coaxial connector to coaxial cable or waveguide transition. Considerable effort was expended on this approach without full success. The conductor contacts and parts tolerances of the small parts of the millimeter circuit and transitions made the results unreproducible. The results were a redesign to make the transition a direct helix-to-waveguide transformer. This design was acceptable after several modifications. The transitions and circuit fixtures were designed to accept any of the design under study. The measurement was a transmission one and therefore included two such transformers and transitions. This resulted in some long line effects which were eliminated in the measurements by E-H tuners on each end of the loss fixture. The single ended match at each frequency measured was no greater than 1.5 over the frequency range of the waveguide. The circuit fixtures were designed so that they could be used with two different waveguide transitions. One set of waveguide transitions was in WR42 to the circuit fixture and the other set of the waveguide transitions was in WR28 to the circuit fixture. Thus the fixtures had the following capability:

1. The circuit fixtures could support any of the circuit designs such as the BeO or the APBN interference fitted circuits with a copper liner body or the brazed diamond supported Amzirc helix brazed to a copper liner body.

2. The circuit fixtures could be matched to either the WR42 or the WR28 waveguide transitions. The matching elements used to match the various

waveguide transition to the circuit fixtures were the moveable waveguide back short and the helix antenna short.

Circuit fixtures were made for various lengths of helix circuits. Actual measurements on the longer fixtures were not made because existing loss literature on waveguide losses in the millimeter frequencies indicated these losses would be only 0.08 dB or beyond the accuracy of the measuring setup. These are discussed in Section 2.

Finally the test procedure devised for rf loss measurement was a substitute method. The data for the various circuits measured and the test procedure are given in Section 2. A thermal heat transfer study was made on the various circuits and refinements that effect the study are presented.

One of the final consequences of this loss study was the revealing of the areas which need further study. These areas are listed below

Helix Material - fabrication procedures and finishes for low loss
- materials used and their processes

Rod Material - material used and their processing for low loss and thermal properties
- method and measurement of adding distributed loss and tip loss to the dielectric rod material

Some of the processing effects on these materials are presented and indicate the need for closer study.

The results of these study programs extend the knowledge of the various properties of the helix circuit through 40 GHz. These results show that the loss of the designs studied for use in millimeter circuits are acceptable and below 0.05 dB/in above 20 GHz. In fact the loss of these circuits does not increase in loss per wavelength as feared, but essentially stays constant.

The study also results in circuit design and assembly criteria for helix circuits using either interference or brazed assembly design, for millimeter frequencies.

These helices and rods were inspected and processed by existing factory procedures which were not varied and they are not optimized to produce the lowest rf loss or the best thermal capability. These need further study.

All of these results are presented in further detail in Section 2.

2. ACCOMPLISHMENTS

Varian has actively worked on low loss helix assembly, both brazed and interference fitted, for a 20 GHz TWT under NASA Contracts NAS-3-21509 and NAS-3-22441. The results of this work are summarized in this section.

The helix design was for a TWT operating at approximately 10 kV with a Ya of 1 at 20 GHz. The circuit dimensions for such a helix assembly are shown in Figure 1. The helix inner diameter is only 0.024" which is 0.6 millimeter. The helix tape is 0.004" thick x 0.008" wide (0.1 millimeter thick x 0.2 millimeter wide). This makes the diameter of the helix 0.032" (or 0.81 millimeter). The helix is supported on rods which are approximately 0.010" x 0.010" in cross section (0.25 millimeter x 0.25 millimeter). The rods are mounted on support strips as shown and fit within a copper barrel liner whose ID is 0.059" (1.5 millimeters).

A helix assembly with the dimensions shown in Figure 2 is extremely small and is difficult to fabricate to the required tolerances with standard available machine tools. To obtain a phase velocity tolerance of 1%, required a 0.2 mil (0.0051 millimeters)tolerance on the helix pitch. Expressed another way, this tolerance is only 5 microns, and this type of tolerance is difficult to obtain except with specially designed helix winding equipment.

Figure 2 shows an actual circuit made of Amzirc with diamond support rods brazed to it with the dimensions indicated in Figure 1. A standard size paperclip made of wire of approximately 1 millimeter diameter illustrates the small size required of the helices.

On the NASA programs listed above, the following three circuits were studied in detail:

Helix Material	Support Rod Material	Assembly Technique
Tungsten	APBN	Interference Fit
Tungsten	Beryllia	Interference Fit
Amzirc	Diamond	Braze

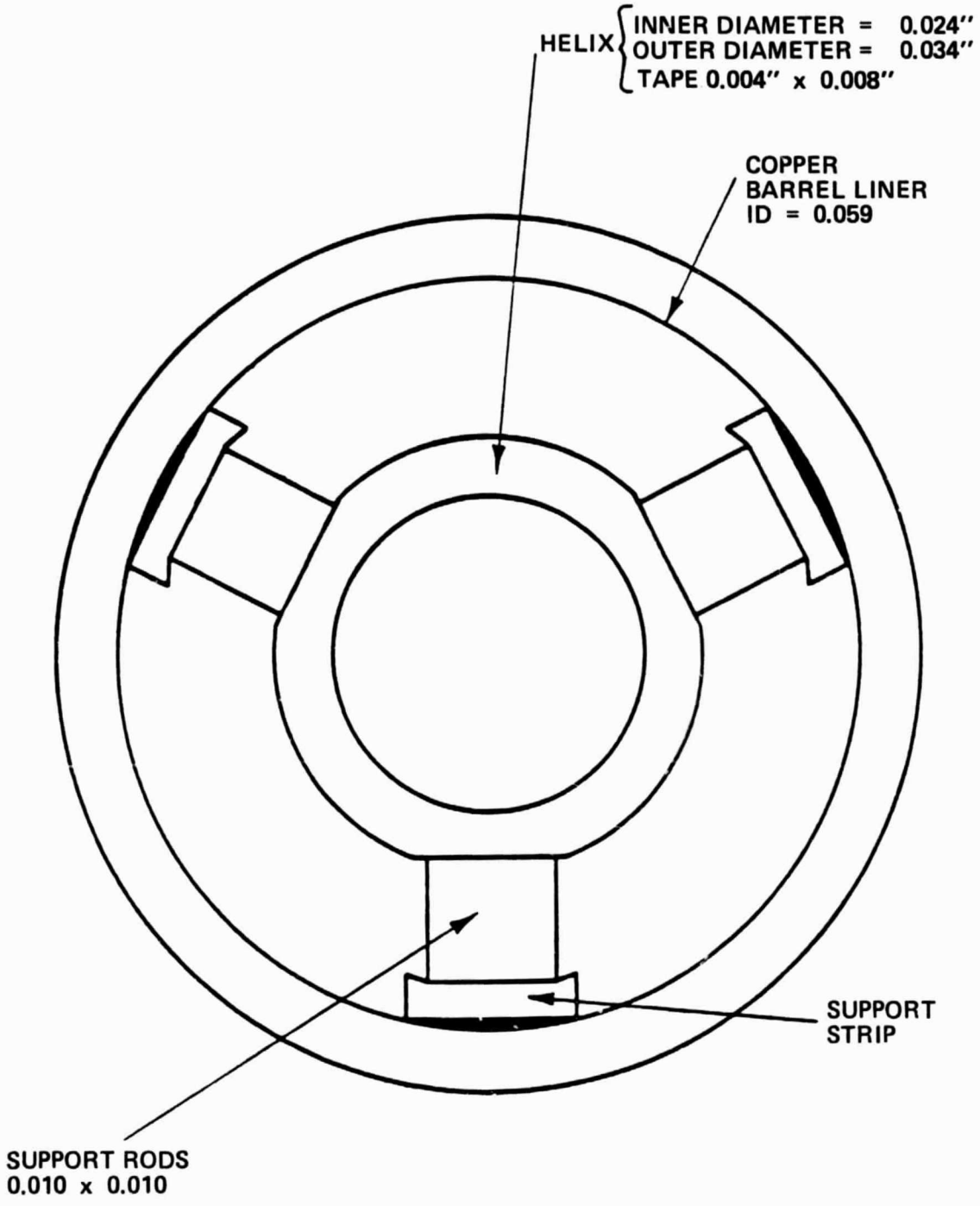

Figure 1. Circuit Dimensions for 20 GHz TWT

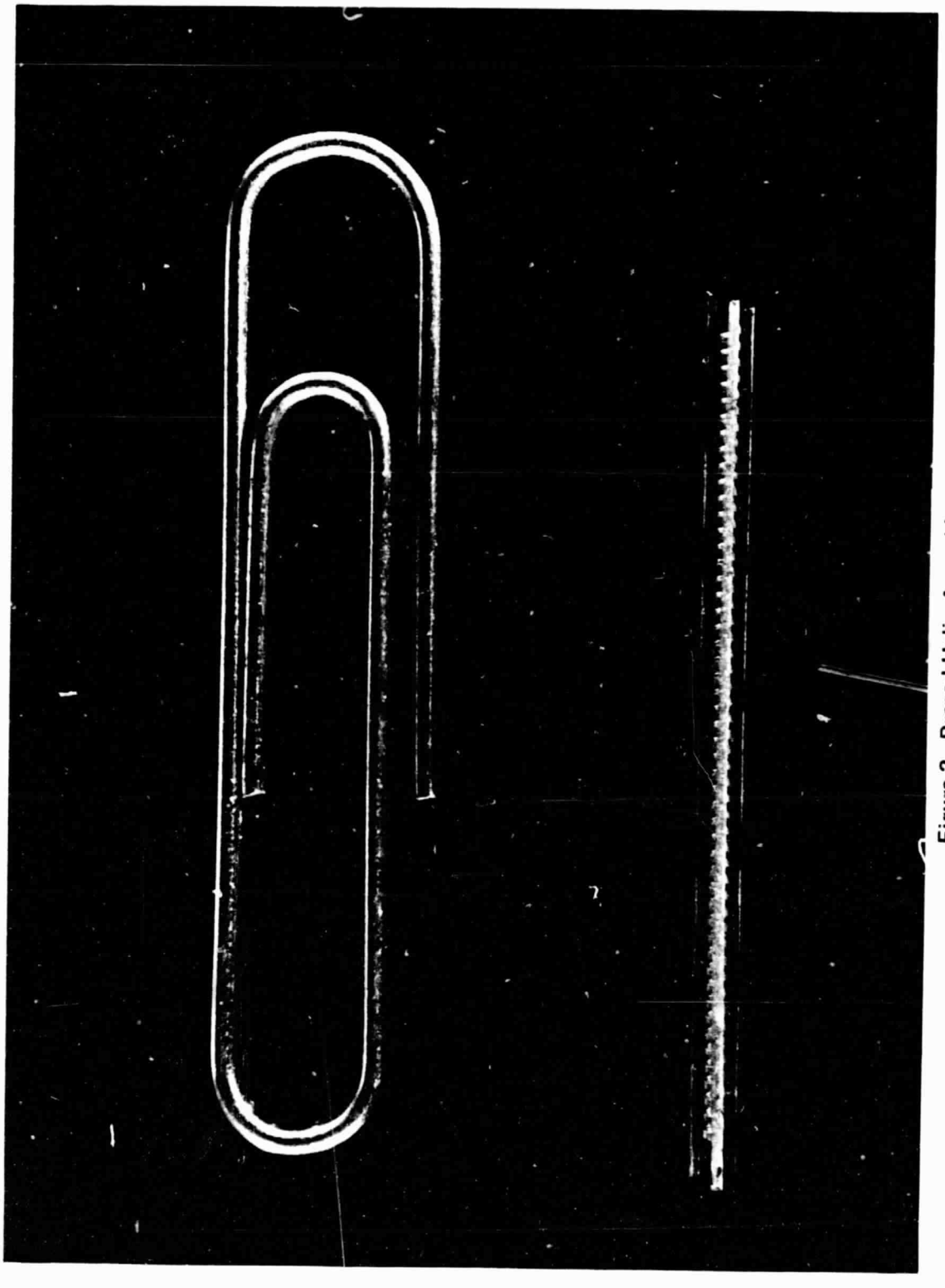

Figure 2. Brazed Helix Assembly

In all cases, fabrication techniques were worked out to assemble these helices with the dimensions shown in Figure 1 and rf loss measurements were made. The individual losses of a dielectric supported helix circuit are discussed in Section 2.1. The development and design of the test vehicle and the test method are discussed in Section 2.2 Fabrication of these helices is discussed in Section 2.3. The measured microwave properties of the circuits, particularly microwave loss, are discussed in Section 2.3. Finally, calculated thermal properties are discussed in Section 2.4.

Important conclusions to be drawn from the NASA loss measurements programs that have been conducted by Varian are that the loss of either an interference fitted tungsten helix on APBN or beryllia or an Amzirc helix brazed to diamond support rods is not excessive. The loss is approximately what would have been expected by extrapolating low frequency measurements; and for any tube design over reasonable ranges of perveance, even for the low perveance values that may be required for PPM focusing of a millimeter wave tube, results in a loss parameter of less than 0.05. Therefore, the loss creates only a small decrease in interaction efficiency, typical of what would be obtained on lower frequency tubes.

One caution must be noted in using the results of Figures 22 and 25 and that is that the loss characteristics are extremely sensitive to the technique by which the circuit is assembled, particularly in the case of the brazed diamond. Although the measured loss characteristics of the circuit are extremely reasonable, much higher values may be obtained if other fabrication techniques other than those described in Section 2.3 are used.

2.1 LOSSES OF A HELIX STRUCTURE

Helix structure losses are due to the following:

barrel losses
dielectric losses
helix circuit losses

The theoretical analysis and measured loss of the helix structure have been made by the Department of Electrical Engineering at the State University of New York in Buffalo. The report from this study is included as Appendix A. The effect on loss of the dielectric support rods for the helix are taken into account. In addition, the helix losses are separated from the barrel losses. The loss variations are given with respect to frequency, helix pitch, helix radius, barrel to helix diameter ratio, helix and barrel resistivity and the effective relative dielectric constant of the helix support rods.

The effect of the circuit loss on the overall efficiency may be shown by considering the expression for η_{ov}. Following the work of Kosmahl, et al, may be written as;

$$\eta_{ov} = \frac{\eta_e \eta_{ct}}{1-\eta_c+\eta_c \eta_e+\eta_c \left(\frac{P_{int} + P_{sig}}{P_o}\right)}$$

where η_c = electronic efficiency
η_{ct} = circuit efficiency
η_c = collector efficiency
Pint = beam power intercepted by helix
Psig = harmonic and unuseable signal loss
Po = beam power

Figure 3 plots the overall efficiency as a function of the circuit efficiency for various values of collector efficiency. This figure shows that by increasing the circuit efficiency from 70% to 90% will increase the overall efficiency nearly 10% for the case of 85% collector efficiency.

The circuit efficiency determines the upper power limit of every circuit. In many cases, this is not evident due to other limitations, such as insufficient gain in the output or thermal degradation due to circuit rf loss or heating due to beam interception in the output. The result is that a reduction in circuit losses would reflect a corresponding increase in the power limit.

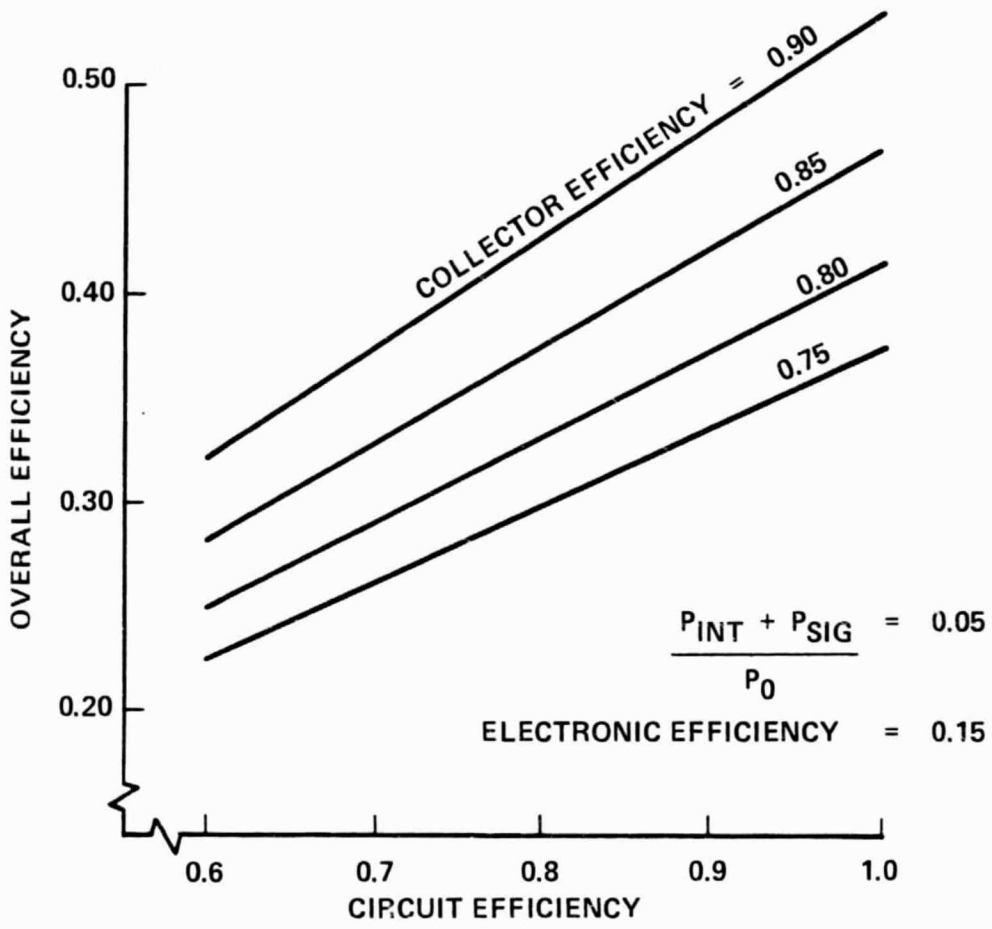

Figure 3. Overall Tube Efficiency as a Function of Circuit Efficiency for Various Values of Collector Efficiency

It is shown that a large fraction of the total loss of a helix structure results from the losses in the helix. These losses are due to the effect of helix surface roughness on skin effective resistance and on the resistivity of the helix material. The loss of the helix structure varies approximately as the square root of the helix resistivity. Figure 4 shows that the helix loss represents a large percentage of the total loss of the entire structure. Barrel losses are small and variations in total loss due to different values of barrel resistivity are small compared to the effect of barrel to helix diameter ratio. The effect of this ratio on an impedance reduction factor are discussed below with other reduction factors.

Besides the direct effect of circuit efficiency on maximum power level there is the effect of all the losses on interaction impedance. The theoretical impedance of the sheath helix is reduced by each loss. Or as normally defined, the effective impedance is:

$$K_{eff} = F_1 F_2 F_3 K_{sh}$$

where

$$F_1 = \frac{\text{tape impedance in free space}}{\text{sheath impedance in free space}}$$

$$F_2 = \frac{\text{tape impedance with dielectric}}{\text{tape impedance in free space}}$$

$$F_3 = \frac{\text{tape impedance with dielectrics and shield}}{\text{tape impedance with dielectric}}$$

The reduction factor due to an actual tape helix compared to a sheath helix is given by F_1. The effect of various tape to gap ratios for values of γa on F_1 is shown in Figure 5.

The reduction factor due to the dielectric is a function of the dielectric loading factor and is shown in Figure 6. This loading factor is

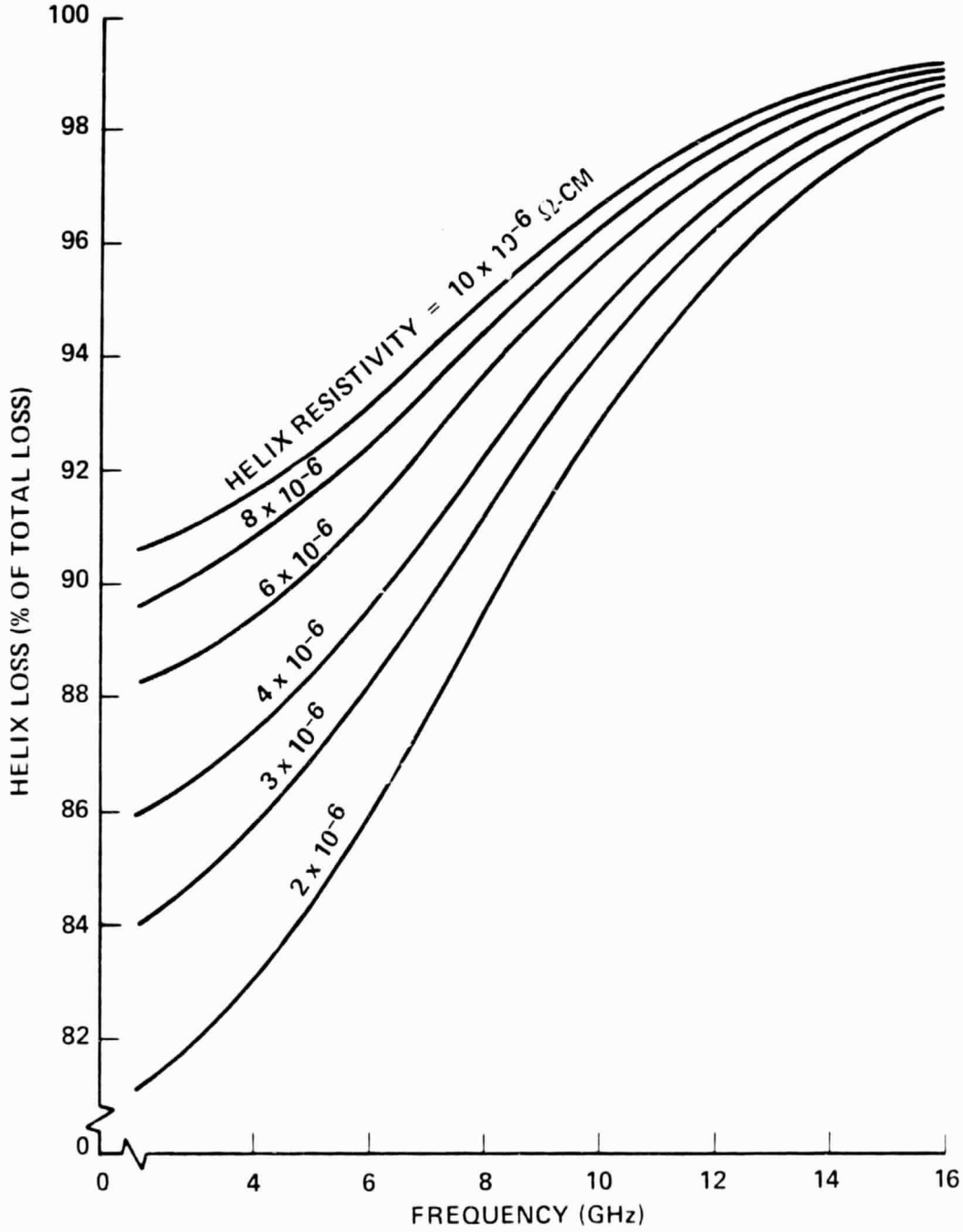

Figure 4. Helix Loss as Functions of Frequency and Helix Resistivity

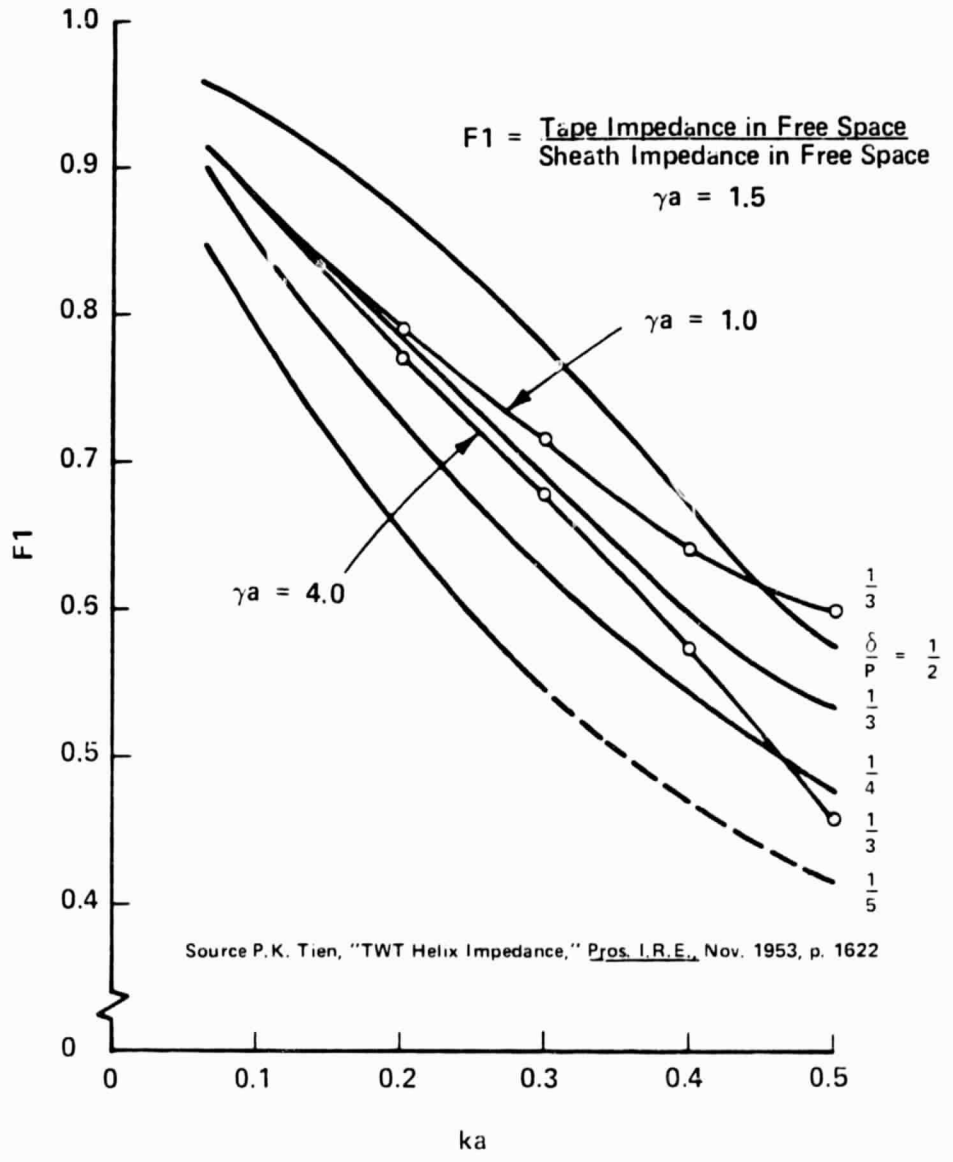

Figure 5. Impedance Reduction Factor F1 for a Tape Helix

a function resulting strictly of the change in impedance in free space to that in the dielectric. It is given by

$$DLF = \frac{(ka \cot\chi)_{actual}}{(ka \cot\chi)_{sheath}} \quad \text{at the same value of ka and } \gamma a$$

The relationship between the DLF and the reduction factor F_2 is given in reference listed in Figure 6.

The last reduction Factor F3 is due to the barrel loading and is shown in Figure 7.

All of the reduction factors lower the interaction impedance which in turn reduces the Pierce gain parameter C by the one-third power of this reduced impedance. Since the efficiency is directly proportional to the gain parameter C, it is also reduced by only one-third power of any increase in the reduction factor.

The circuit loss results in a direct increase in the loss parameter d which directly affects the circuit efficiency. In Section 2.1.3 the importance of the loss parameter on efficiency is discussed in detail including the effect the various losses have on the microwave characteristics. The loss parameter and the reduced impedance effects on the gain per inch are also detailed in this section. Finally, the dielectric loading and barrel loading effects on the backward wave frequency and starting conditions are discussed in Section 2.1.2. Methods to control the helix surface and processing of material to reduce circuit loss are discussed in Section 2.1.1.

2.1.1 Circuit Losses

The fabrication of the helix to minimize rf loss poses different problems depending on whether an Amzirc helix is used or whether a tungsten, moly, or copper plated tungsten, or copper-plated moly helix is used.

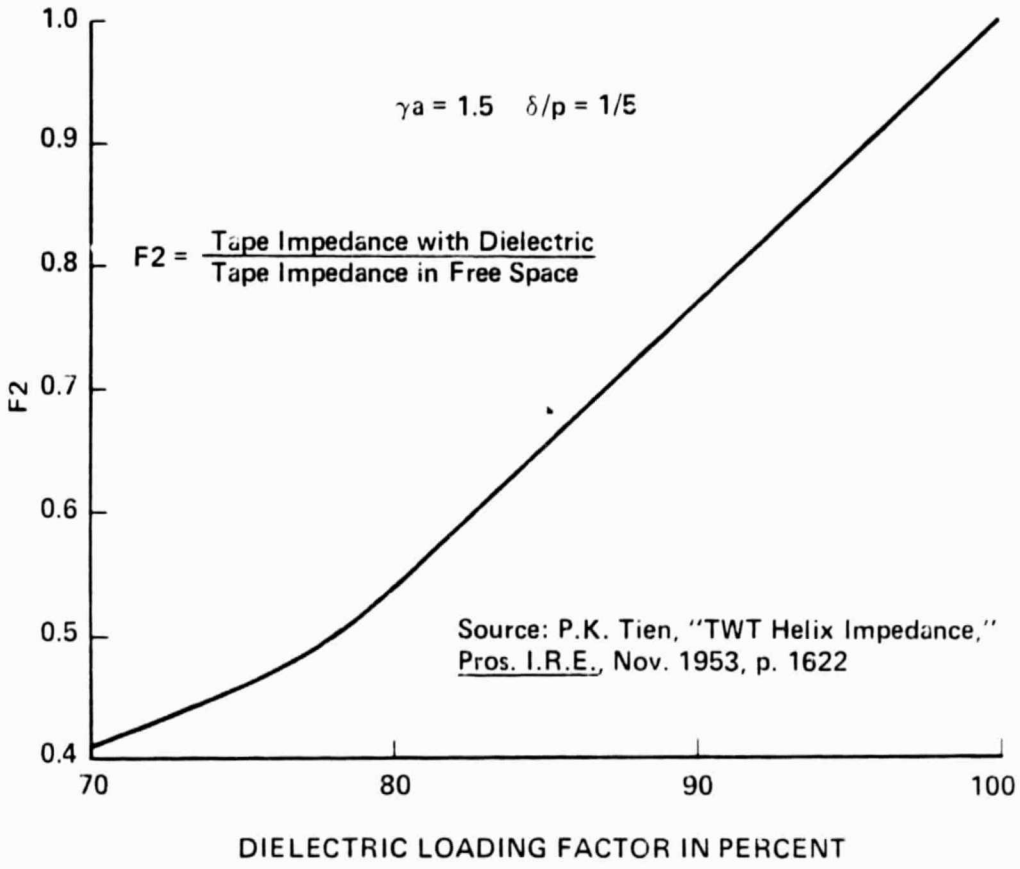

Figure 6. Impedance Reduction Factor F2 for a Tape Helix

Source: B.J. McMurtry, "Fundamental Interaction Impedance of a helix surrounded by a Dielectric and a metal shield." IRE Transaction Electron Devices, pp. 210-216, March 1962.

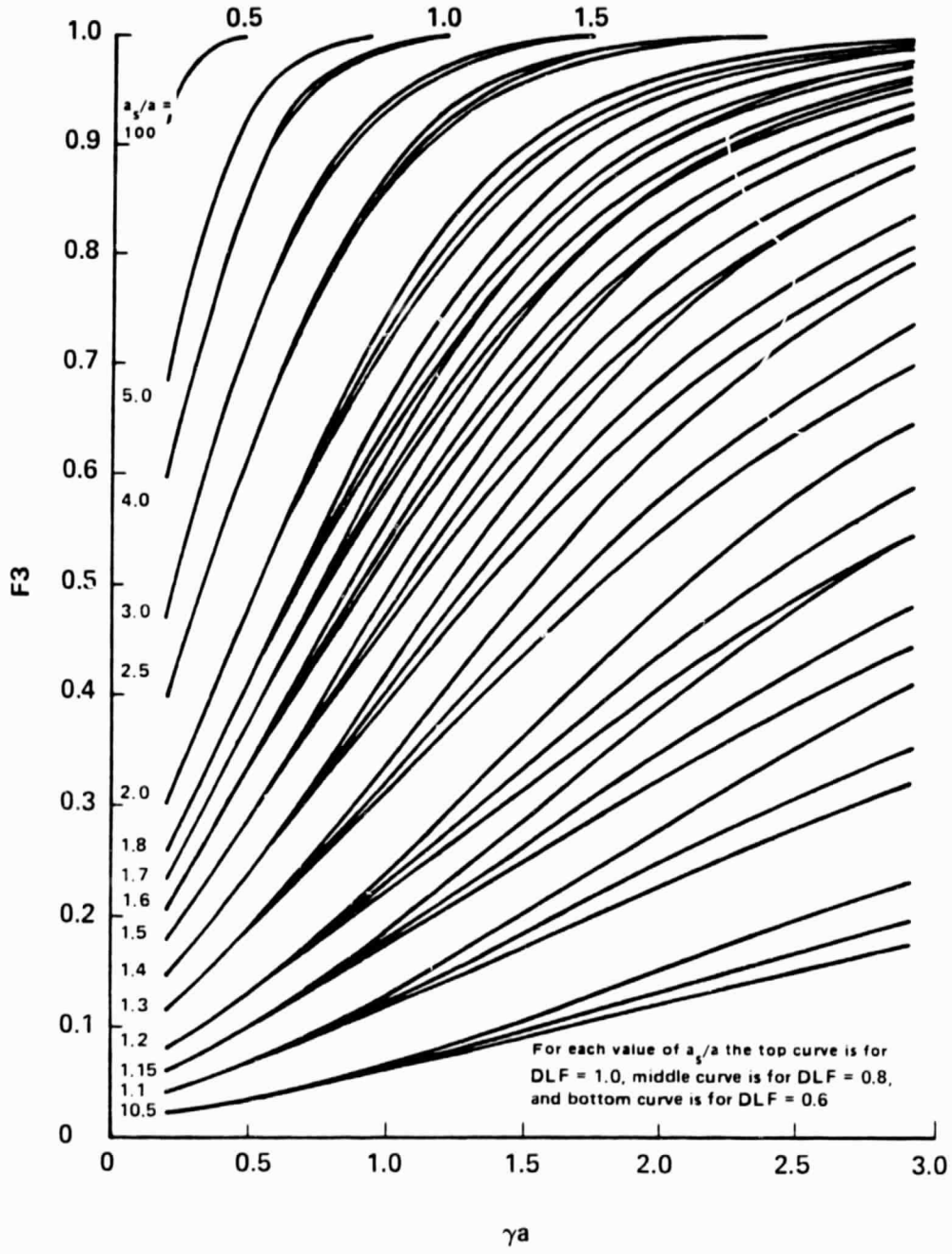

Figure 7. Impedance Reduction Factor for F-3 Tape Helix

The fabrication of tungsten helices will be discussed first with the same comments appling to moly- or copper-coated tungsten or moly helices. The major supplier of factory metal helices is H. Cross Company. Cross will produce tape with a $\pm$ 0.2 mil (5 microns) tolerance on the width and $\pm$ 0.5 mil (12.7 microns) tolerance on the height and control the tungsten tape fabrication to eliminate tape fractures. In the tape itself, the winding process which is accomplished at Varian is carefully controlled to insure that the tape does not fracture and is annealed properly as the helix is wound onto the mandrel. Once it has been established that the helix is free of fractures, the surface finish of the helix tape itself is the major factor controlling loss. The surface finish is controlled by the helix fabrication process which is as follows:

1. The helix is first wound on a molybdenum mandrel.
2. The wound helix is then brazed to the molybdenum mandrel so that it can be centerless ground.
3. The helix mandrel assembly is centerless ground and this grinding determines the finish of the outer diameter of the helix.
4. The molybdenum mandrel is then etched out of the tungsten helix.
5. The resulting tungsten helix is then electropolished.

Varian has established standard processes for each one of these steps. The first step in the program was to use these standard processes on the helix with the dimensions shown in Figure 1 and take photographs at magnification levels of 1000, 2000 and 3000 of the surfaces of the helix after each step has been accomplished. These photographs are shown in Figures 8 through 10 and indicate the significance of processing on the final surface finish.

A copper coating on the tungsten helix should significantly reduce loss if the coating is properly applied so that the bulk resistivity of copper is obtained. Electroplating has never been successful in accomplishing this; the standard technique used within the microwave tube industry is to evaporate copper in a vacuum onto the helix. Varian has

Magnification 1000 X

Magnification 2000 X

Magnification 3000 X

TUNGSTEN WOUND HELIX BRAZED TO THE MANDREL
BEFORE GRINDING AND POLISHING

Figure 8

Magnification 1000 X

Magnification 2000 X

Magnification 3000 X

HELIX SURFACE AFTER CENTERLESS GRINDING

Figure 3

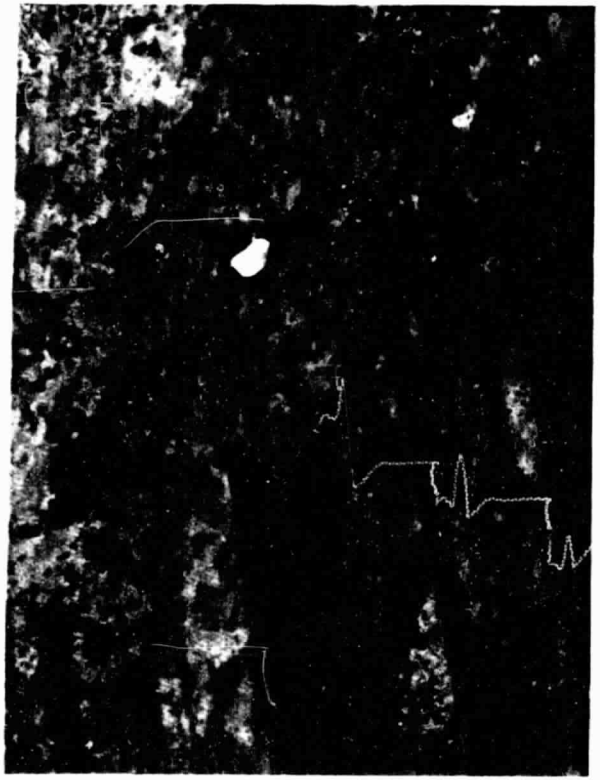

Magnification 1000 X

Magnification 2000 X

Magnification 3000 X

HELIX SURFACE AFTER ELECTROPOLISHING

Figure 10

standard procedures for this. The helix fabrication technique that provides the best surface finish was chosen. The standard helix coating process has been applied and SEM photographs have been taken to determine the surface finish of the copper coated helix. This is shown in Figure 11 and 12.

The fabrication of an Amzirc helix is somewhat different because the Amzirc is a much more pliable material and is not subject to fracturing during fabrication or winding. However, great care must be taken not to oxidize or hydrize the zirconium in the material so that a good active braze can be made. Amzirc material is manufactured by AMAX and H. Cross rolls it into helix tape. At Varian, the Amzirc tape is wound onto a helix mandrel and then mechanically cleaned, electropolished, and vacuum fired. SEM photographs have been taken at various steps during this procedure and the results are shown in Figure 13, 14 and 15.

2.1.2 Dielectric Loss and Barrel Losses

The support rod materials used on these programs included diamonds, APBN, and beryllia.

Successful brazed helix circuits have been made using unmetallized Type IIa diamonds supplied by Dubbledee Company. These diamonds have been found to be free of carbon contamination on their surfaces. The actual helix circuit shown in Figure 2 and the loss measurement shown in Figure 25 were made with these diamonds. A material procurement specification will be written so that future orders of diamonds can be maintained at the same quality.

The APBN material is fabricated by Union Carbide on a graphite mandrel. Discussions were held with Union Carbide to find a way to control and reduce the carbon content in the APBN. The beryllia rods are made by several ceramic companies including Accuratus Ceramaic Corporation and Ceradyne, Incorporated. Both vendors use beryllia powders supplied by Brush Beryllia Corporation. Discussions were held with each of these vendors to control raw material purity and sintering conditions and, based on these discussions, a procurement specification controlling the dielectric constant

a. Electropolish Tungsten Tape of Processed Helix – 1000X

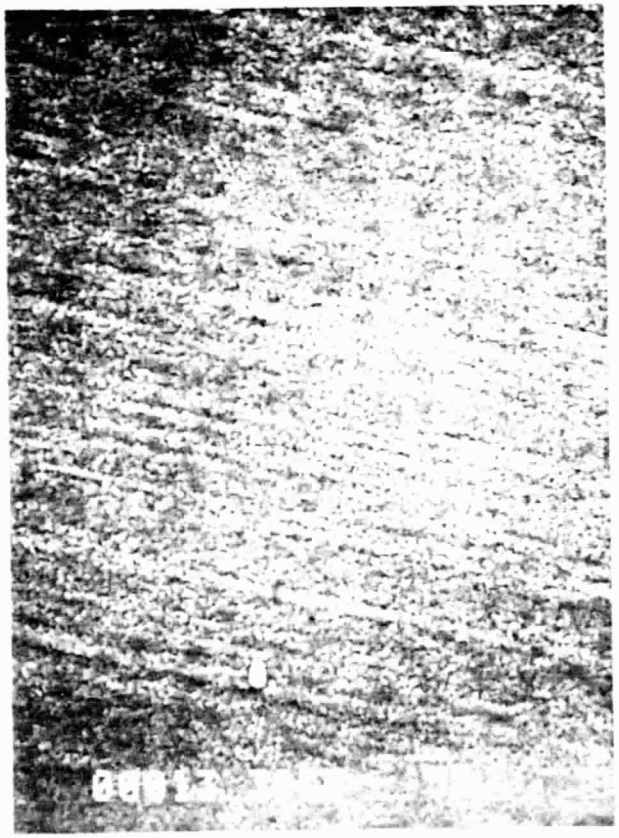

b. Copper Evaporated on Tungsten Processed (Electropolished) Helix – 1000X

Figure 11.

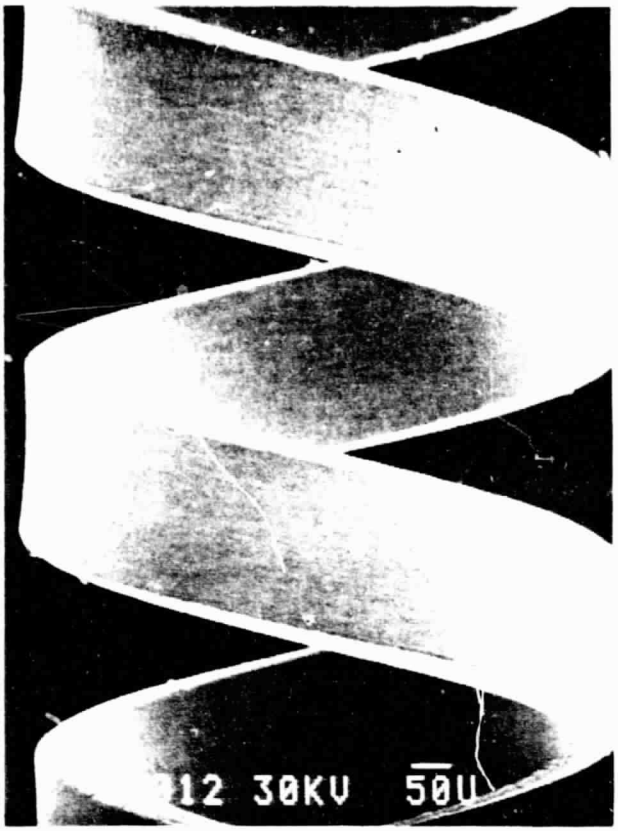

a. Copper Evaporated on Tungsten Processed (Electropolished) Helix 100X

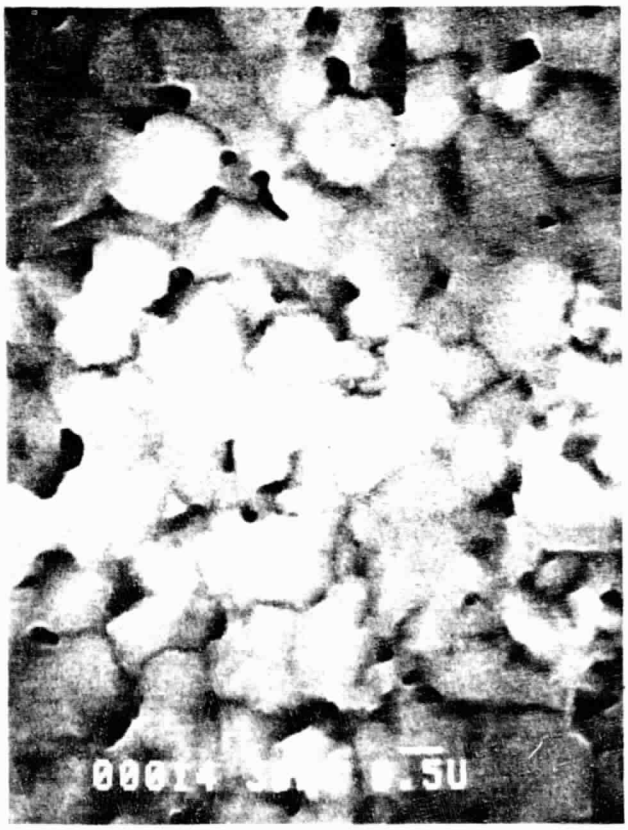

b. Copper Evaporated on Tungsten Processed (Electropolished) 10,000X

Figure 12.

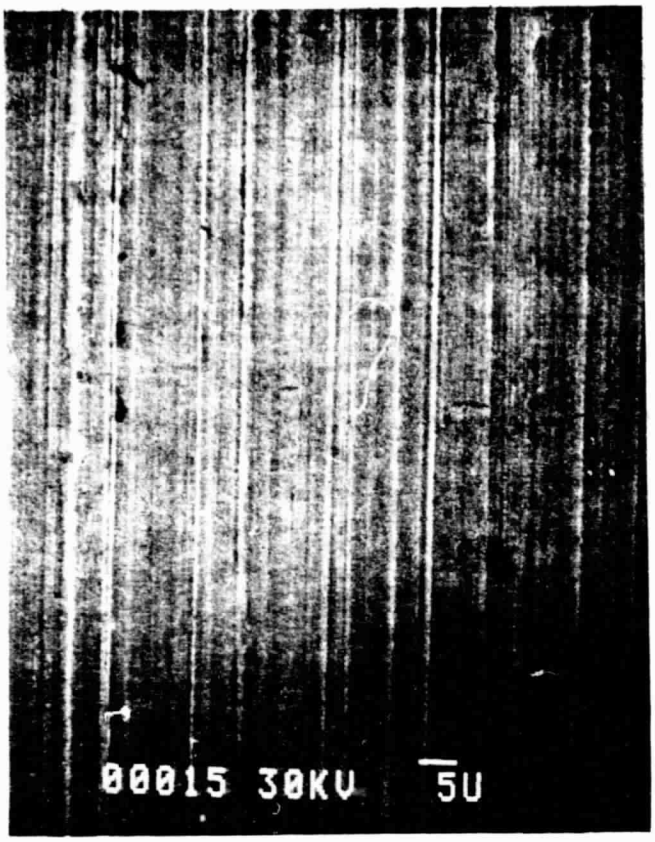

a. 0.005 x 0.010 Amzirc Tape as Received

b. Amzirc Helix as Wound — 100X

c. Amzirc Helix as Wound — 1000X

Figure 13.

a. Amzirc Helix – Chemical Polish (M1-5) and H_2 Fired at 800 °C – 1000X

b. Amzirc Helix – Same Processing as Figure 11. with Final Vacuum Firing at 800 °C – 1000X

Figure 14.

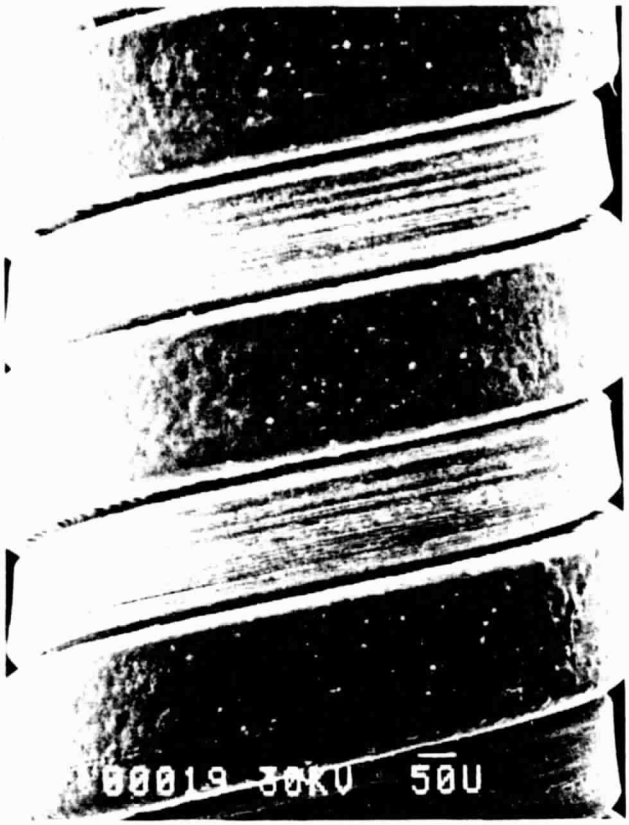

a. Amzirc Helix – Same Process as Figure 11. with Final Vacuum Firing at 800 °C – 1000X

b. Amzirc Helix – Same Processing as Figure 11. with Final Vacuum Firing at 800 °C –10,000X

Figure 15.

and density is required. The density measurement is straight forward while the dielectric will require a rf measure. A resonant frequency shift method is presented in Appendix B.

One effect of the dielectric and barrel loading is that it lowers the π-mode frequency where the tube tends to oscillate. The π-mode frequency is where the forward and backward mode cross over and where the backward wave is synchronous with the beam, that is, the phase velocity of the backward mode is almost equal to the beam velocity. The lower the π-frequency, due to the loading, the closer it comes to the operating band and the closer the synchronism. To show how the loading lowers the π-frequency, we need to consider the following. The π-mode frequency is given by the relation $\beta p=\pi$ which gives:

$$f_{\pi} = \frac{1.879}{(2a)} (v_p/c \cot\chi)$$

For a given helix diameter (2a), as the loading (either or both dielectric or barrel) increases the normalized phase velocity (v_p/c) decreases and to raise the operating voltage back to desired value, the helix TPI must be lowered so that $\cot\chi$ decreases ($\cot\chi = (2a)\ \pi/p$ where p is the helix pitch). Thus the π-frequency is lowered.

The closer the π-frequency is to the operating band the closer the synchronism becomes and for a given circuit length it lowers the starting current for oscillation. To raise the π-frequency once again above the band for a heavily loaded circuit, requires a decrease in the circuit diameter which at millimeter frequency may cause a serious focusing problem.

2.1.3 Microwave Characteristics

The important microwave characteristics in the helix circuit are:

- dispersion
- interaction impedance
- π-mode frequency
- microwave loss

The first three characteristics can easily be determined from scale models of the circuit. The dispersion is important in determining the operating bandwidth of the tube, and for a communication application a nearly constant dispersion is easily obtained over the few GHz bandwidth of the tube. The interaction impedance, when divided by the beam impedance, determines the interaction efficiency of the tube and the gain per wavelength. The π-mode frequency is the frequency at which the forward and backward wave modes intersect and where the tube tends to oscillate. The π-mode frequency must be above the highest operating band of the tube. The impedance and the resulting microwave properties of the circuit shown in Figure 1 are tabulated in Table 1. Shown is the frequency, the γa of the circuit, the interaction impedance and the Pierce parameter C at frequencies of 17, 20, 30, 40 and 50 GHz. For the calculation, the assumption is made that the helix pitches change at each frequency to give the optimum value of velocity synchronism parameter, so Table 1 represents how the helix shown in Figure 2 would be used in a design of a tube centered around 20, 30, 40 and 50 GHz. To obtain broadband performance across the full frequency range, dispersion loading shells would have to be used. Then a constant phase velocity vs frequency could be obtained but the interaction impedance would be only about one-half the value shown. It should be remembered in examining the characteristics of the helix assembly, shown in Table 1, that the gain per wavelength and the interaction efficiency are not determined by interaction impedance alone but are determined by the Pierce parameter C which is equal to the one-third power of the interaction impedance divided by the beam impedance and so depends on the perveance and operating voltage.

One value of microperveance chosen for the comparison chart of Table 1 is 0.04. A tube operating with this perveance at 8 kV would provide approximately 10 W of CW power. This design has been used in several TWT's currently under development in the microwave industry. The beam is relatively easy to focus but the Pierce gain parameter C is low and so the

gain per wavelength and the interaction efficiency is low. As discussed in a subsequent paragraph the loss parameter with this low perveance design is also high and this degrades tube performance. A better choice of microperveance which can be focused with PPM focusing with a beam filling factor of 0.5 with the circuit shown in Figure 1 would be a microperveance of 0.2. With this beam perveance operating at 8 kV the tube could provide approximately 50 W of CW power, and the Pierce gain parameter for this value of microperveance is shown in the last line of the table.

Table 1

Microwave Characteristics of Helix Assembly

Frequency (GHz)	17	20	30	40	50
Ya	0.762	0.897	1.346	1.794	2.242
v/c	0.169	0.169	0.169	0.169	0.169
K (0)	96.2	79.4	37.1	15.2	5.8
C (AT u P = 0.04, 8 kV)	0.045	0.043	0.034	0.026	0.020
C (AT uP = 0.2, 8 kV)	0.077	0.073	0.058	0.044	0.033

An extremely critical parameter for a 20 GHz helix is microwave loss. Microwave loss cannot be scaled from low frequency measurements and cannot be accurately calculated. Until the work done by Varian on these NASA programs was accomplished, no experimental measurements of the loss millimeter wave helix circuits had been published. One reason was that techniques first had to be developed to actually fabricate the helices and then suitable measurement techniques had to be developed. The exact fabrication techniques used had a major effect on the actual loss that was measured. During these programs, microwave loss was actually measured on the three types of circuits described above and the technique for making these loss measurements and the measured values themselves are reported in subsequent paragraphs.

The effect of helix circuit loss on interaction efficiency is shown in Figures 16 and 17; these figures show the significance of circuit loss and define the values of circuit loss that are required for a satisfactory helix tube. Figure 16 is taken from large signal calculations and shows the interaction efficiency as a function of Pierce loss parameter. Two curves are shown. The lower curve indicates that the velocity synchronism parameter has been adjusted for a maximum small-signal gain. The upper curve indicates that the velocity synchronism parameter has been adjusted for maximum interaction efficiency. The calculations are made with the helix circuit parameters shown in Table 1 at a frequency of 20 GHz. If the tube had no loss and the synchronism condition was adjusted for maximum interaction efficiency, the interaction efficiency would be 19%. Note, however, that as the loss increases the interaction efficiency drops drastically; and if the loss parameter were 0.5, the interaction efficiency would drop to under 7%. The same situation is true when the velocity synchronism parameter is adjusted for maximum small-signal gain. Because of the severe efficiency reduction effect of loss, most traveling wave tubes below the millimeter band are designed to operate with a loss parameter of less than 0.05. It must also be realized that the efficiency reduction due to circuit loss cannot be reclaimed by the use of a depressed collector. Figure 17 shows how the loss parameter depends on the helix circuit loss. The helix circuit loss is shown in dB/inch for a design using the helix dimensions of Figure 1 and calculated at a frequency of 20 GHz. The measured results obtained on the NASA programs are all given with loss in dB/inch so a direct comparison can be made with the measured results and the effect on TWT performance. The loss parameter d which controls the gain/inch and, most importantly, the interaction efficiency depends not only on the helix circuit loss but also on the gain parameter. Actually, the loss parameter d is approximately equal to the loss per wavelength divided by the gain per wavelength. (This would be strictly true if the growing wave parameter x_1 were equal to (1+Cb)). Therefore, if the loss parameter is 0.5 then the gain per wavelength is equal to twice the loss per wavelength and so forth. Consequently, the value of loss parameter depends on the actual helix loss and the gain parameter of the tube which, for a given circuit, depends on the microperveance. Two of the curves in Figure 17 show the value of d for any helix loss for two different values of beam

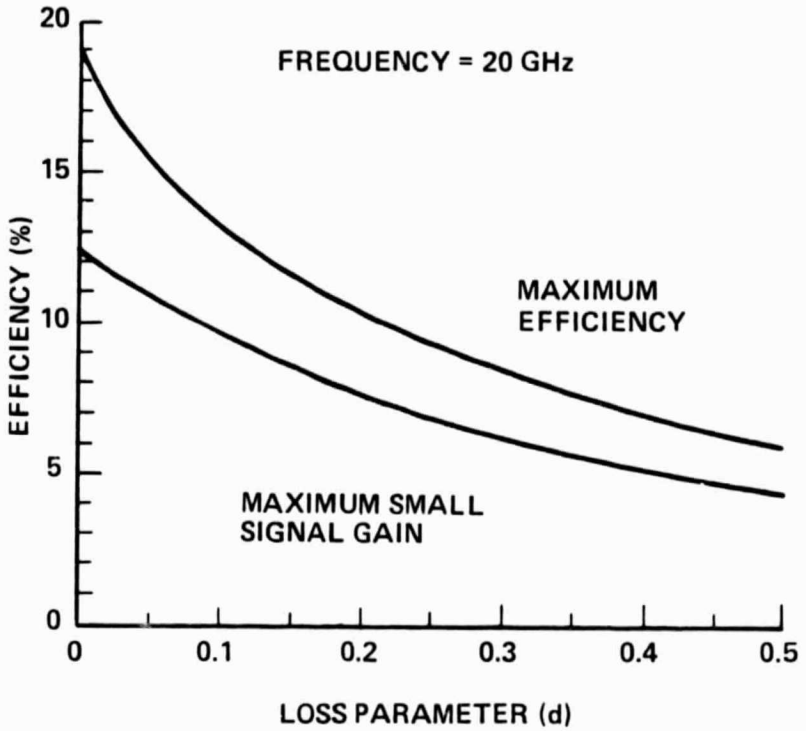

Figure 16. Interaction Efficiency as a Function of Loss Parameter

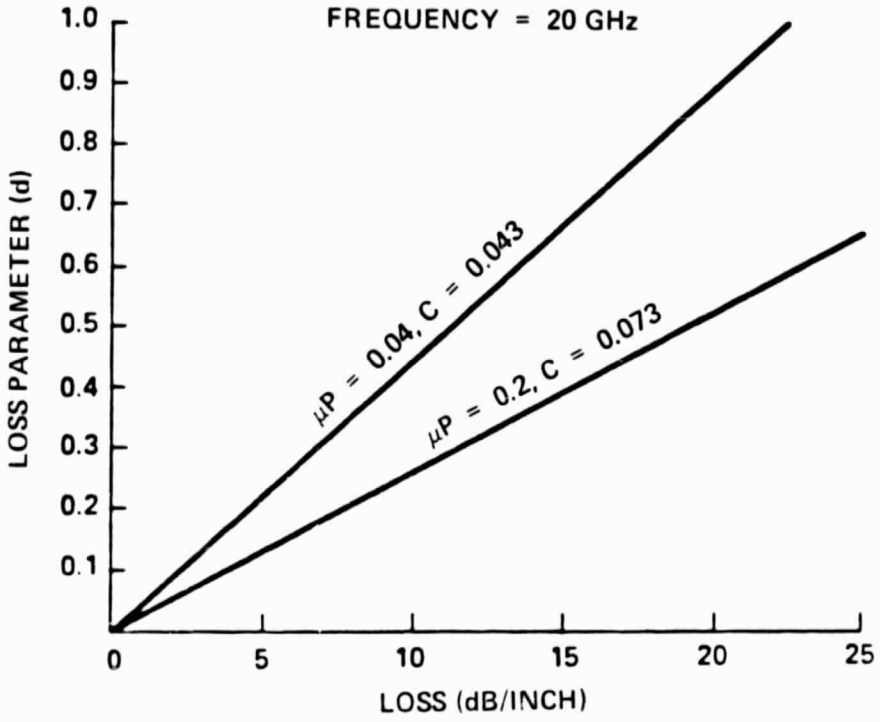

Figure 17. Loss Parameter as a Function of Helix Loss

micropervenace 0.2 and 0.04; and, of course, the higher the microperveance, the lower the value of loss parameter for a given helix loss. In order to achieve a loss parameter of 0.05, the helix loss should be less than 2 dB/inch.

2.2 LOSS MEASUREMENT TECHNIQUE

Nearly all of the loss measurements below 18 GHz are done using a coaxial coupled line to the helix structure. This is convenient as most tubes have been historically matched by a coaxial line through a ceramic window and the procedures to achieve this match are well known. This provides an excellent broadband vacuum window and allows the most flexibility for external packaging and interfacing with any rf connection, coaxial or waveguide. Circuit matching is performed by several methods, for example, by reducing the barrel diameter to reduce the helix impedance or by reducing the coaxial line diameter ratio to change its impedance. The matching transformer region is used by the designers as an area of individual tube design changes to compensate for impedance mismatches unknown to the tube designers and used by the technician to match the most difficult tube.

The initial loss measuring fixture was designed around a coaxial matching system. Considerable effort was expended on trying to match to a helix structure via a coaxial line to a coaxial ceramic window to a coaxial connector, either OSM or OSSM type, then transitioning to the waveguide measuring setup. The results of the matching experiments were poor. It became extremely difficult to use the same matching technique in a 0.070 BID compared to an I/J band body ID of 0.150. In addition to this difficulty the window and coaxial line tolerances became extremely critical as the size decreased in an attempt to maintain the fixture flexibility for matching. The variability of the coaxial connector to the window also became increasely important in reproductability of test results and all of the above adding to poor test results. The loss readings were higher than were thought to be reasonable and the variation of test data from a given

run, depending on the contact and position of coaxial components, made the data totally unrealistic. The best reasonable broadband match attained by this coaxial system was 2.5 to 3:1 which was also unacceptable.

As a result, the coaxial approach was dropped for a direct waveguide matching approach. This approach used a design procedure where the waveguide width and height dimension were modified to shape the waveguide impedance to the helix structure impedance. The matching results were acceptable over the waveguide bandwidth. To further improve the accuracy of the loss reading, E-H tuners were used on either side of the test fixture to assure a perfect match at each test frequency.

The unknown of the test was the losses in the transitions to the helix and in the matching elements of the transition. This covers the waveguide transition from full height waveguide to reduced height waveguide and the losses in the moveable waveguide short and the moveable antenna-body short.

The losses in the waveguide themselves have been fully understood and are well documented. The loses at millimeter frequencies have been higher than theoretical and an investigation of this has led to a knowledge of the effect of the surface roughness on the relative surface resistance. The effect of this finish is that a 8 micron finish would increase the relative surface resistance as much as 8% at 20 Ghz. Appendix C gives data on this effect.

As a result, the specified finish of all waveguide components was held to a 10 or better micron finish.

An estimate was not made during the study of the loss due to the back movable short or the antenna losses but it was apparent that the contact was extremely important.

2.2.1 Test Vehicle Design

As stated, the design of the loss vehicle test fixture started as a coaxial extension of lower frequency models. As the tests proceeded with unacceptable matches and unreproduciable data, the test vehicle was modified from the coaxial transformer to a direct waveguide transformer. Figure 18 shows the coaxial test fixture.

As design of the waveguide transformer proceeded, the addition of E-H tuners became necessary to reduce the transformer matches to an acceptable VSWR at each frequency. This eliminated the multiple reflection at each transformer which reduced the loss measurements to that only of the test waveguide transitions and the actual loss of the helix structure plus the unknown losses due to the waveguide back short and the antenna losses. Figure 18 shows the waveguide test fixture.

As can be seen in this figure the loss measurement is made by a transmission measurement. This requires a helix-waveguide transition at each end of the fixture with the match at each end contributing to the double-ended-match. A sample of one of the test matches is shown in Figure 19, and the long line effect of two mismatches is obvious. To assure that this double-ended-match does not contribute to the loss reading, E-H tuners were used at each end of the fixture. These were tuned at each frequency to maximize the transmitted power read on the output power bridge.

The theoretical losses of the waveguide are 13.3 to 9.5 dB/100 feet for WR 42 and therefore the transistions themselves contributed 0.08 dB which includes the increase in surface resistance due to the 10 micron finish.

2.2.2 Test Method

Several metnods are available for measuring rf loss. The method listed in the Statement of Work and used on these NASA contracts conducted by Varian used an attenuator substitution method. The helix assembly was matched on both ends to waveguide and the power passing through the

Figure 18. Waveguide and Coaxial Loss Test Circuit

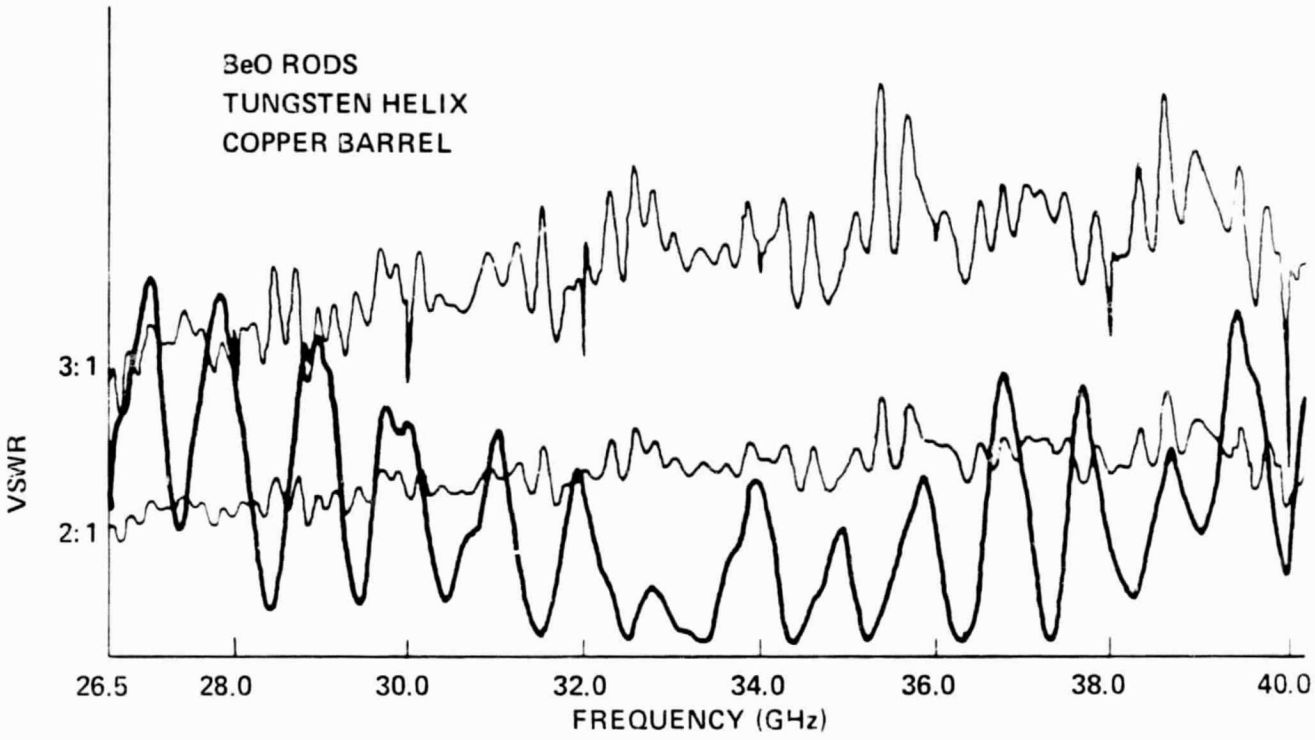

Figure 19. Double-ended Match of Helix Assembly

structure was measured, and the loss was then determined by substituting a precision attenuator for the test structure. The problem with the attenuation substitution method of measuring loss is that the loss in the couplers at either end of the helix is not known.

Another method of measuring rf loss which is described in Appendix D, and which is widely used at lower frequencies is to use a perturbing bead and measure the amount of reflected power with a network analyzer. The amount of power reflected from the bead of course depends on the amount of attenuation in the circuit. Appendix D shows a typical attenuation measurement. This method is much simpler, and eliminates the problem of coupler loss. It is much less expensive because only one helix needs to be made for each measurement. However, it is somewhat less accurate and can probably measure loss only to within $\pm$ 0.2 of a dB. As the results in (Figures 22,23 and 25) show, this may not be much worse than the error at a single frequency from the attenuator insertion loss measurements.

The microwave loss of the three different helix assemblies was measured with the setup shown in Figure 20. An attenuator substitution method was used in which the microwave power passing through the various helix assemblies mounted in the test fixture of Figure 18 was measured and then a precision rotary-vane attenuator was substituted for the test fixtures. The attenuator was adjusted until the same power reading was obtained and then the loss of the helix assembly was the same as the attenuator setting. The test fixture can be seen in the middle of the test setup of Figure 20 located in front of the microscope. E-H tuners are used on the input and output to obtain a perfect match at each measurement frequency. The helix circuit is in the center of the waveguide test fixture shown in Figure 18 and a match is made to both ends of the helix from the waveguide. The helix is matched with a tab which extends across narrow height waveguide and then the waveguide is tapered to the full waveguide height. A moveable backplate behind the match is adjusted to optimize the match and then at each frequency the remaining matching is done with the E-H tuners external to the test part. The fixture design shown in Figure 18 allows the helix assembly to be measured with different waveguide couplers. The setup shown in Figure 20 was designed with WR28 covering the 26-40 GHz

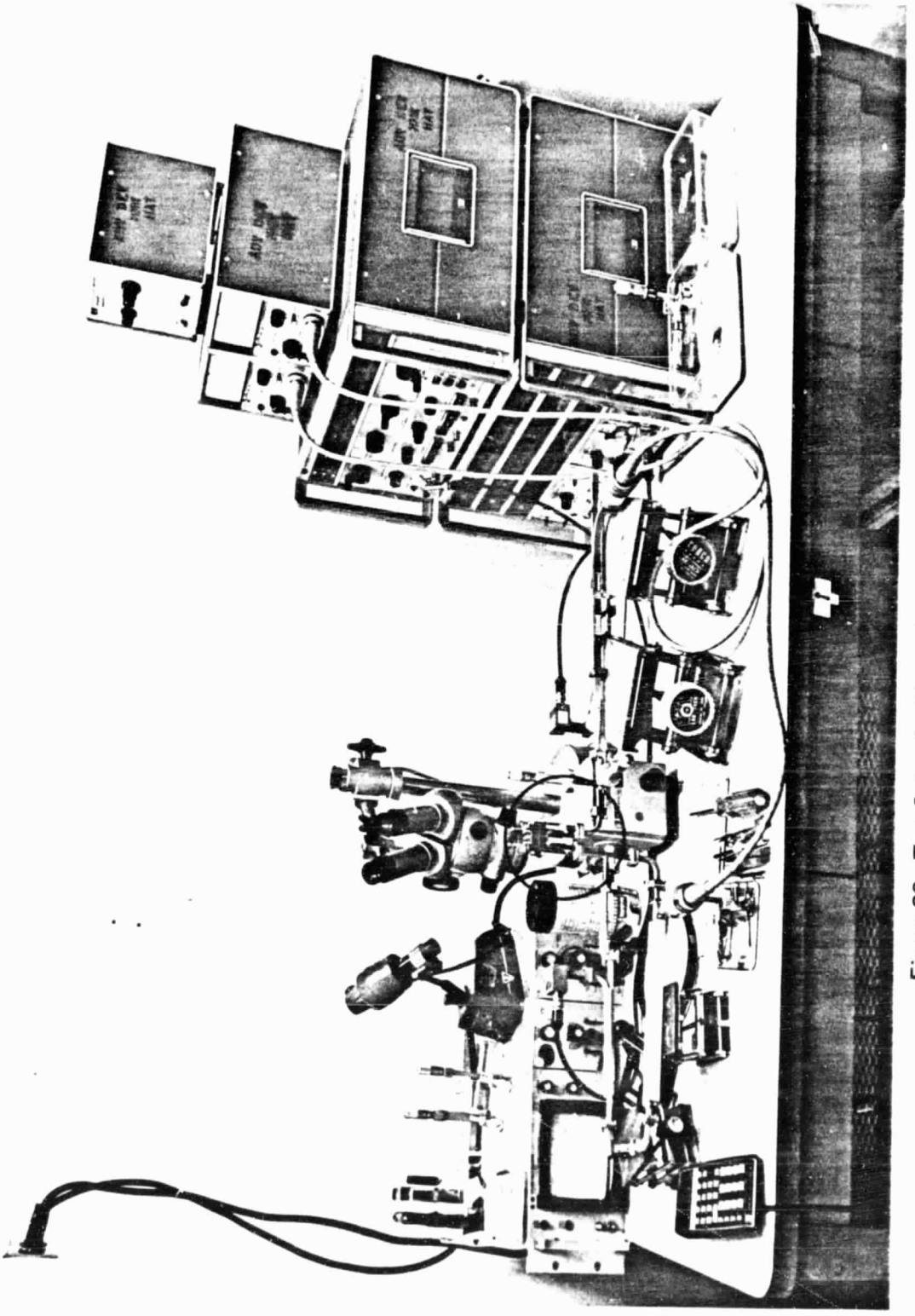

Figure 20. Test Setup for Measuring Helix Loss

band and most measurements were made in this band. Other couplers were designed and fabricated in WR42 to optimally cover measurements in the 18-26 GHz band.

2.3 LOSS MEASUREMENTS

This section will discuss the measurement of helix structure losses of the three structures actually studied. The fabrication of each of the circuits is discussed in detail in Sections 2.3.1 for APBN and for BeO interferenced fitted assemblies. The test results on these circuits are discussed in Section 2.3.2.

For the brazed circuits, the fabrication of the diamond brazed structure is discussed in Section 2.3.3, while the braze experiments required to finally achieve this brazed assembly are discussed in Section 2.3.4. Finally, the test results of the loss measurements on this brazed structure are discussed in Section 2.5.

The results of the programs assure the tube designer that at higher millimeter frequency the measured loss is not excessively higher than the extrapolated results of lower frequency measured data.

The results indicate the only added decrease in efficiency is due to the increase in the loss parameter because of the necessity of designing millimeter tubes with low Pierce gain parameter C for focusing considerations.

2.3.1 Interference Fitted Tungsten Helix with APBN Support Rods or BeO Rods

The interference fitted assembly using APBN support rods was assembled using the same techniques that are commonly used on lower frequency TWT's. The tungsten helix was wound on a molybdenum mandrel. After winding, the helix was brazed to the mandrel and was centerless ground. After grinding, the molybdenum mandrel is removed by selective etching and the helix is electropolished. The helix is then glued to a

stuffing mandrel using an acetone soluable glue. The APBN support rods are glued to the helix. The mandrel is then cold stuffed into the tube body. During the stuffing process the boron nitride contracts. A 0.2 mil interference fit can be obtained with this technique.

The interference fitted assembly using beryllia rods is assembled in a similar fashion to the assembly using the boron nitride rods. The tungsten helix is fabricated in exactly the same way. The beryllia rods however, are fabricated differently since it is difficult to make beryllia rods with a 0.010" x 0.010" cross section extending the full 1" length of the helix without breaking the rod. To solve this problem, sections of beryllia rods 0.010" x 0.010" in cross section and only 0.100" long are brazed to 0.006" x 0.015" Amzirc strips. These strips can be seen in cross section in the drawing of Figure 1. A picture of brazed BeO and diamond rods are shown in Figure 21. Amzirc is a dispersion strengthened copper containing 0.2% zirconium in pure copper. The zirconium addition not only strengthens the copper tape but also provides the active brazing alloy to bond the tape to the beryllia. Consequently, no metallizing processing is required. The zirconium in the tape itself forms the metallizing and strong reliable bonds are made when the Amzirc and Beryllia are heated to 850°C under pressure in an inert atmosphere such as helium.

The difference between this procedure and lower frequency tubes is the control of the body ID and the helix bundle OD. By use of special Deltronic gauges and special bushing gauges to measure the bundle OD, both of which were correlated to a specific air gauge, the helix bundle OD is controlled to within 2 microns, the same air gauge is used to measure the honed body ID which is controlled to 2 microns.

2.3.2 Assemblies Tested and Test Results

The two assemblies fabricated for the interference tests were measured by the substitution method. The tests were repeated several times. It was therefore assumed that all unknowns were accounted for and the measured losses were actual circuit losses.

Figure 21. Brazed BeO and Diamond Rods

ORIGINAL PAGE
BLACK AND WHITE PHOTOGRAPH

Figure 22 shows, on the same scale, measurements made on the tungsten helix mounted on APBN rods and interference fitted and the tungsten helix mounted on beryllia rods and interference fitted. The loss of the BeO supported assembly is slightly lower than the APBN supported assembly and so, extrapolated to 20 GHz, the loss of the APBN circuit is approximately 1.4 dB/inch and is 1.3 dB/inch for the tungsten helix mounted on beryllia rods. Note that these circuits used an unplated tungsten helix. The spread of experimental points gives an estimate of the accuracy of the measurements. The circuit with the beryllia rods has less loss; note that the beryllia rods are brazed on one surface to the rod supporting strip. In all cases, at 20 GHz, the loss is significantly less than 2 dB/inch, and even with the lowest perveance design discussed above, the loss parameter is less than 0.05. Figure 23 compares helix loss measurements made at Varian on a variety of helix assemblies across the frequency range from 4 - 40 GHz. All the circuits shown in Figure 23 are interference fitted and include the results shown previously in Figure 22. The helix support rods include APBN, IPBN, and beryllia. The helices are of tungsten or copper plated tungsten. The bodies are of cupronickel and of copper.

The difference between the measured losses of Figure 22 can be explained by the dielectric loading. The fact that the BeO structure loss was lower than the APBN, even though the dielectric constant of APBN is 5.12 while BeO is 6.0, was due to the effective dielectric loading. The APBN rods covered 31.3% of the area between the helix and the barrel compared to 14.8% for the BeO rods.

At first glance, all of the curves from Figures 22, 23 (and 25) suggest that the helix loss is increasing with frequency. That is because the attenuation is plotted in dB/inch. The TWT performance is all dependent on the loss per wavelength and for a helix at a given operating voltage, that is a given phase velocity, the wavelength is inversely proportional to frequency. Consequently, if the loss measurements all fall along a straight line as indicated, running diagonally across the curve of the graph of Figure 23, then the loss per wavelength of the circuits would be constant.

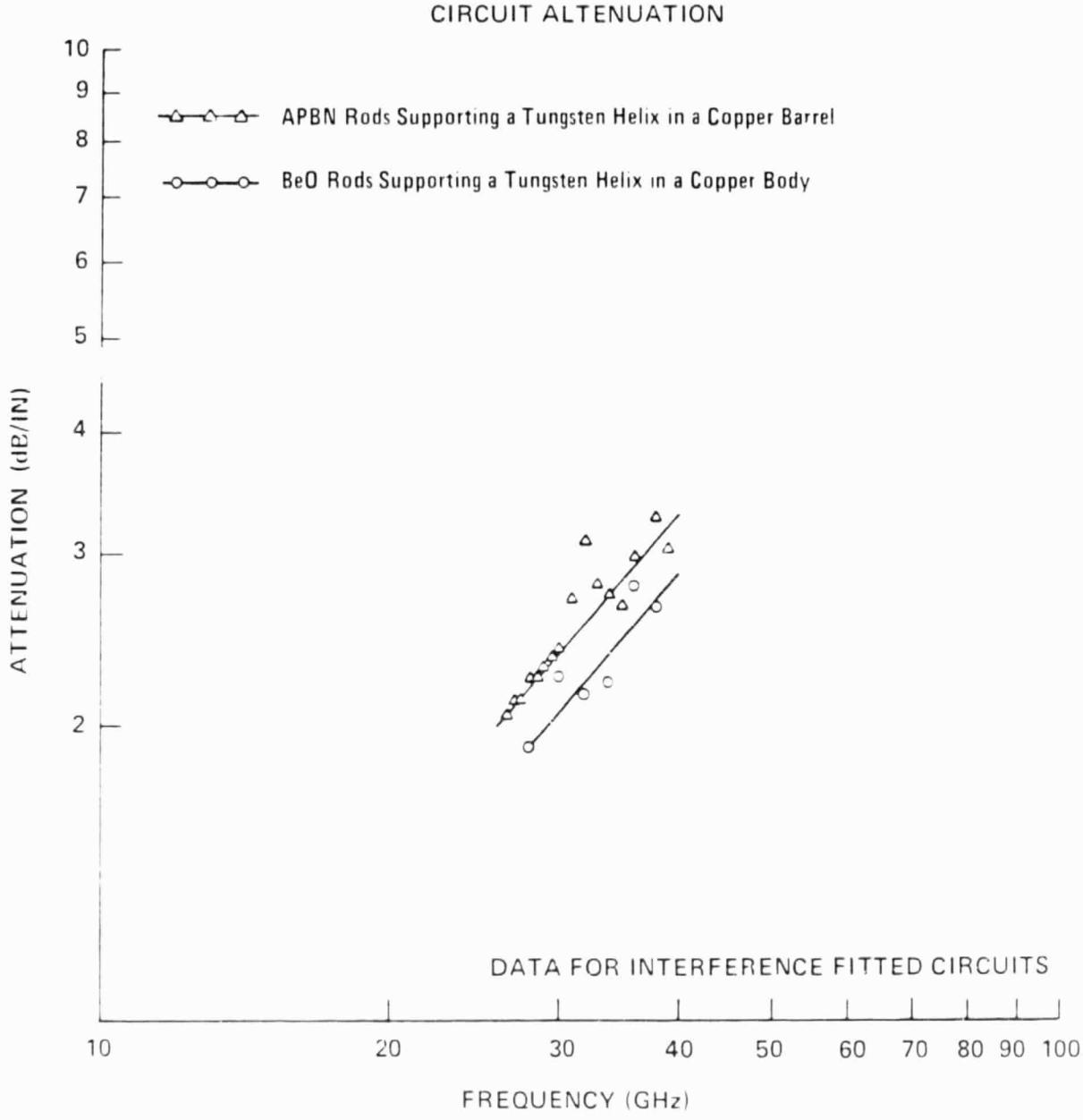

Figure 22. Attenuation of Interference Fitted Circuits

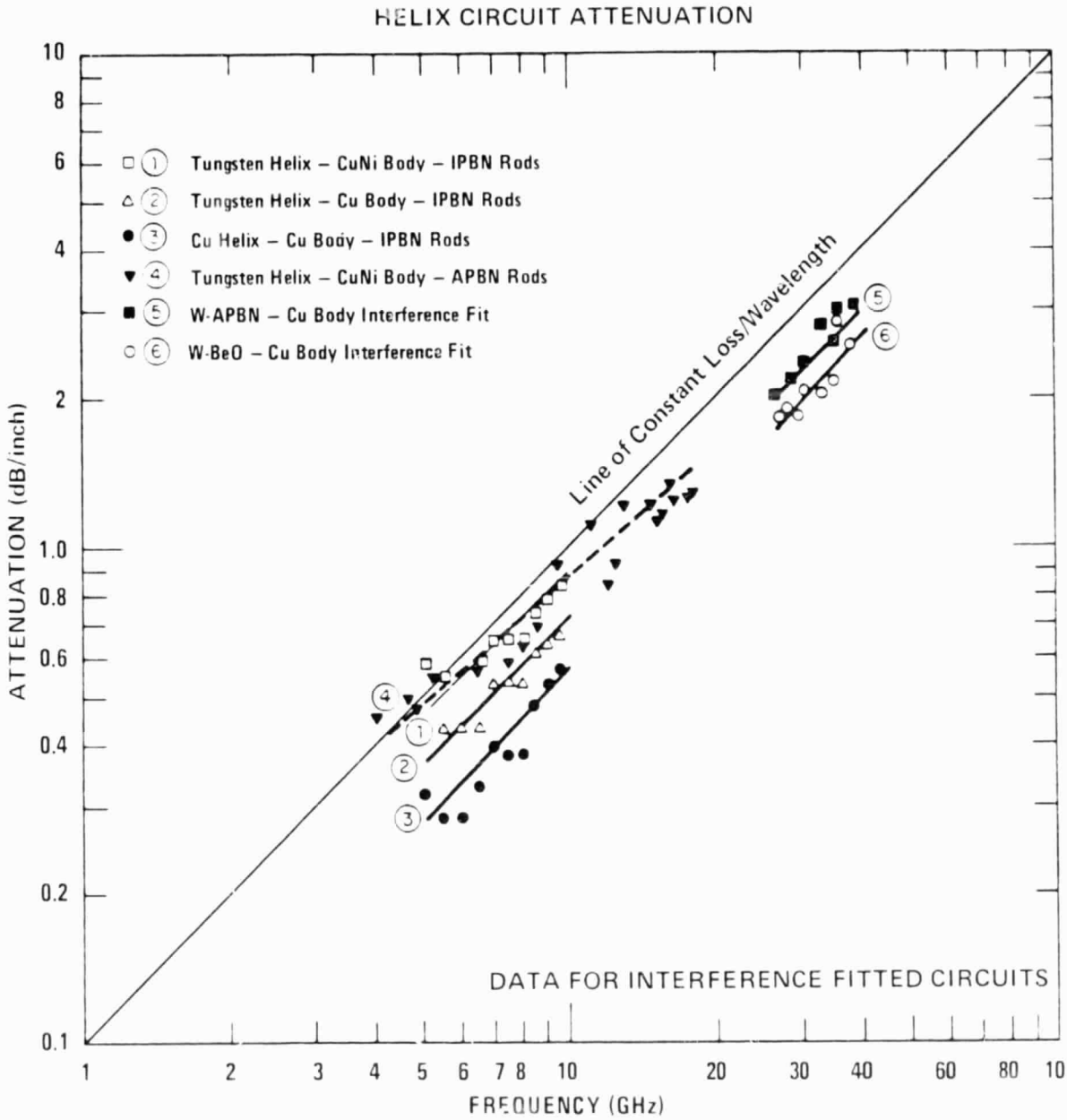

Figure 23. Attenuation of Interference Fitted Circuits as a Function of Frequency from 4-40 GHz

Note that the curves do fall approximately along a straight line, and so the loss per wavelength from 4 - 40 GHz is essentially constant.

2.3.3 Brazed Amzirc Helix with Diamond Support Rods

1. The brazed diamond assembly is made as follows. The rod assemblies are made in the same way as the beryllia rod assemblies described in the previous paragraph. Sections of diamond rod 0.010" x 0.010" in cross section and 0.100" long are brazed to the 0.006" x 0.015" Amzirc strips. The diamond rod assembly made in this way can be seen brazed to the helix in the photograph of Figure 2.

2. The next step is the helix fabrication which begins with the plating of a 0.0005" layer of chromium on a stainless steel helix mandrel. The chromium will ultimately be etched away after the helix is brazed to the support rods to allow the mandrel to be removed. Once the stainless steel mandrel with the chromium plating has been centerless ground, an Amzirc helix is wound onto the mandrel. Molybdenum spacing tape is used between the Amzirc helix turns to maintain the proper helix pitch tolerance during the following assembly operations. Ultimately, the spacer tape will be etched away after the helix has been brazed to the support rods.

3. The rods and helix made as described in Steps 1 and 2 are brazed together using the fixture shown in Figure 24. The helix and mandrel assembly are held in the center of the fixture. The diamond rods brazed to the Amzirc strip (which were fabricated as described in Step 1) are glued to the holding fixture, two of which can be seen at the bottom left of the photograph and the third of which can be seen held in the technician's hand. These holding strips are then inserted into the brazing jig. The parts of the brazing jig are made of stainless steel to provide a maximum expansion. The rings that surround the brazing jig are made of molybdenum, and when the brazing jig is then heated to the 800°C brazing temperature, the outer molybdenum rings provide the required pressure to push the diamond rods against the Amzirc helix assembly. The fixture has been carefully designed to provide sufficient pressure so that at the 850°C brazing temperature a

Figure 24. Helix Brazed Jig

strong mechanical and thermal bond is made between the support rods and the helix assembly. After this brazing operation, the helix and rod assembly is removed from the fixture and the molybdenum spacer tape and the chromium on the mandrel are selectively etched out of the assembly. The mandrel is easily removed, and the complete rod and helix assembly appears as shown in Figure 2.

4. The final step is to braze the helix and rod assembly into the tube body. The tube body contains a liner, the dimension of which is shown in Figure 1. The liner is initially brazed into the PPM body during the body fabrication procedure, the body inner diameter is plated with silver and a cusil braze is made between the Amzirc backing strips on the rod and the copper body when the complete assembly is fired at 800°C.

2.3.4 Braze Experiments

Considerable effort was spent in achieving a reliable braze to diamonds. Initial work done under an AFAL sponsored contract covered active braze experiments. These were done in a vacuum using Ti-Au-Moly or Zr-Au Moly sputtered on OFHC tape or copper coated tungsten tape. The test results were inconsistant and a reliable braze to diamond was not obtained. These were fired at 1000°C in the vacuum with pressure between the diamonds and the sputtered tapes.

Under an RADC sponsored contract, the work continued. The active braze gave way to a diffusion bond braze between the diamonds and Amzirc tape. These were still done in a vacuum at 1000°C and gave a more consistant braze. The resistance across the diamond rods varied from 200K to 100 G ohms after the brazes. It was under this contract that the first brazes were made in an inert atmosphere at 1000°C, the resulting brazes were extremely strong and reproducible. The resistances were still variable.

The work done under the NASA contracts improved the fixtures and lowered the temperature to improve the bond and decrease the variation of the resistance across a brazed rod. The temperature now used is 800°C and the cleaning process is a simple mechanical (way clean) cleaning of the

Amzirc tape prior to braze. The atmosphere is still helium and the brazed helix assembly which was tested was made by this process.

2.3.5 Brazed Assembly Tested and Test Results

The measured loss results are summarized in Figure 25 which shows the loss of the brazed circuit using the actual circuit with dimensions shown in Figure 1. This circuit used an Amzirc helix with diamond rods brazed to the helix and brazed to the copper barrel of the tube. The curve shows attenuation in dB/inch as a function of frequency across the 26 - 40 GHz band and can readily be extrapolated to 20 GHz where the loss is approximately 1.6 dB/inch.

2.4 THERMAL STUDY

The thermal characteristics of the different helix circuits were not measured on the NASA program because so much effort had to be expended in developing the fabrication techniques for the helices. However, the thermal characteristics were calculated and the results are shown in Table 2.

The calculations were made as follows. Each turn of the helix, with the dimensions shown in Figure 1, was assumed to dissipate 1 W of power. The dissipated power comes both from beam interception and from the rf power absorbed by the helix. The power is assumed to be uniformly distributed along the tape. With this power input, the temperature rise around the helix from the midpoint to the support rods was calculated. This is $\Delta T1$ in Table 2. Making this calculation requires a knowledge of the thermal conductivity of the helix material, and this data was obtained from Figure 26. The next temperature rise is between the helix and the support rod. There was assumed to be no temperature rise if the interface was brazed. If a pressure fit was used, the thermal resistance values of Figure 27 were used. The third temperature rise, $\Delta T3$, is through the support rod itself, and to make this calculation the thermal conductivity shown in Figure 26 was used at the appropriate temperature. The last temperature rise was the temperature rise between the support rod and the body itself. If this interface was brazed no temperature rise was assumed. If it was an

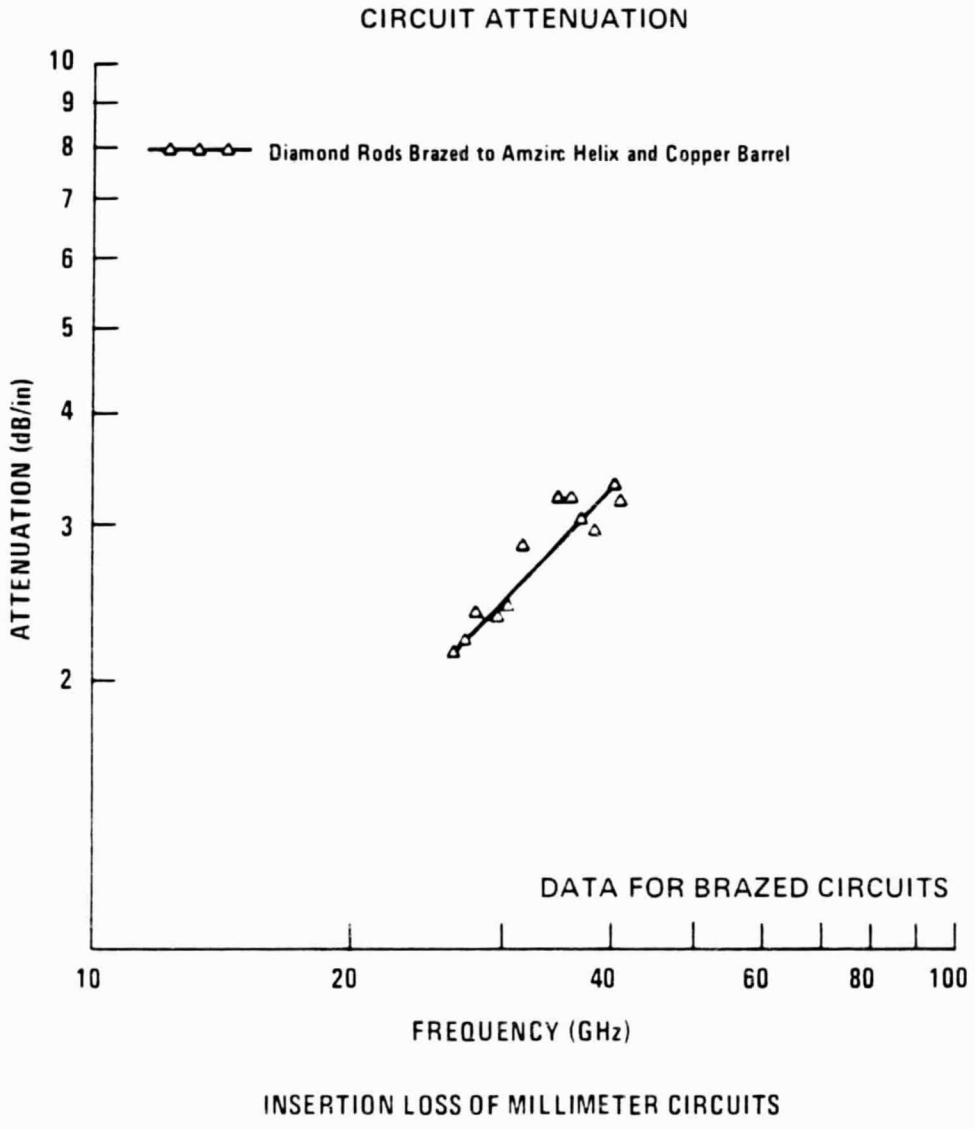

Figure 25. Attenuation of Brazed Circuit

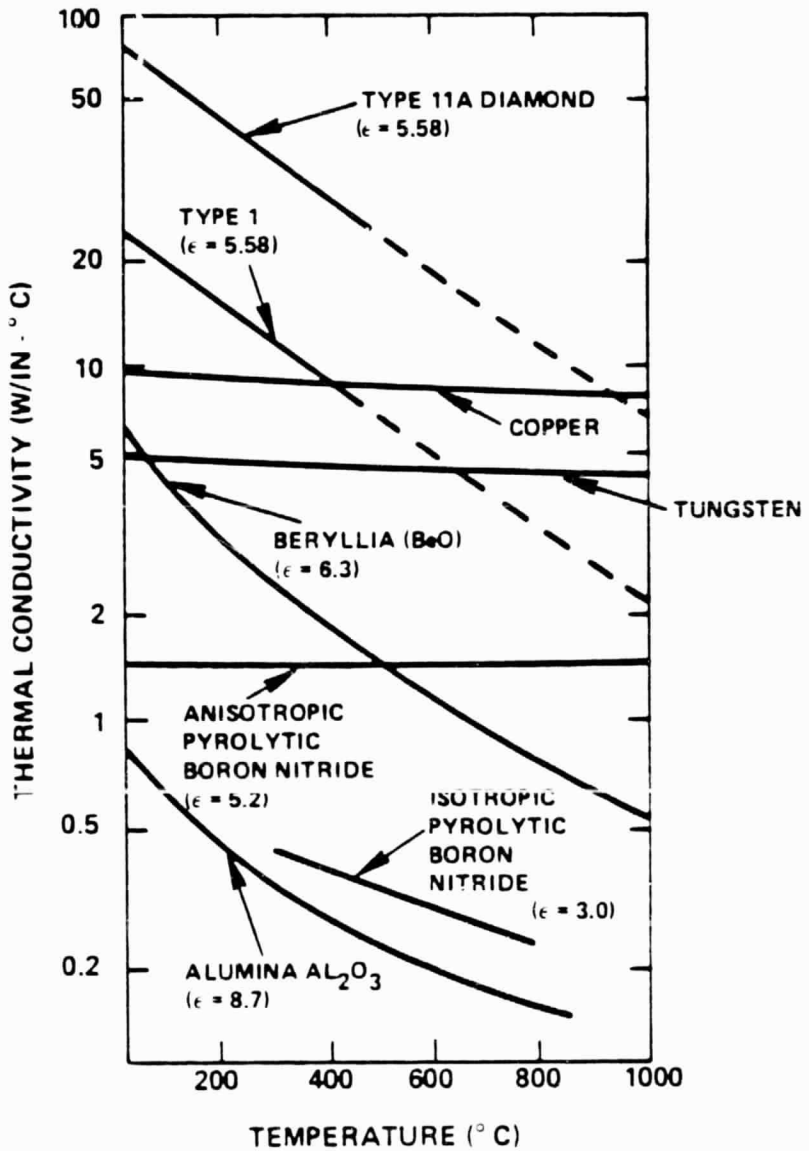

Figure 26. Thermal Conductivities of Helix and Support Materials as a Function of Temperature

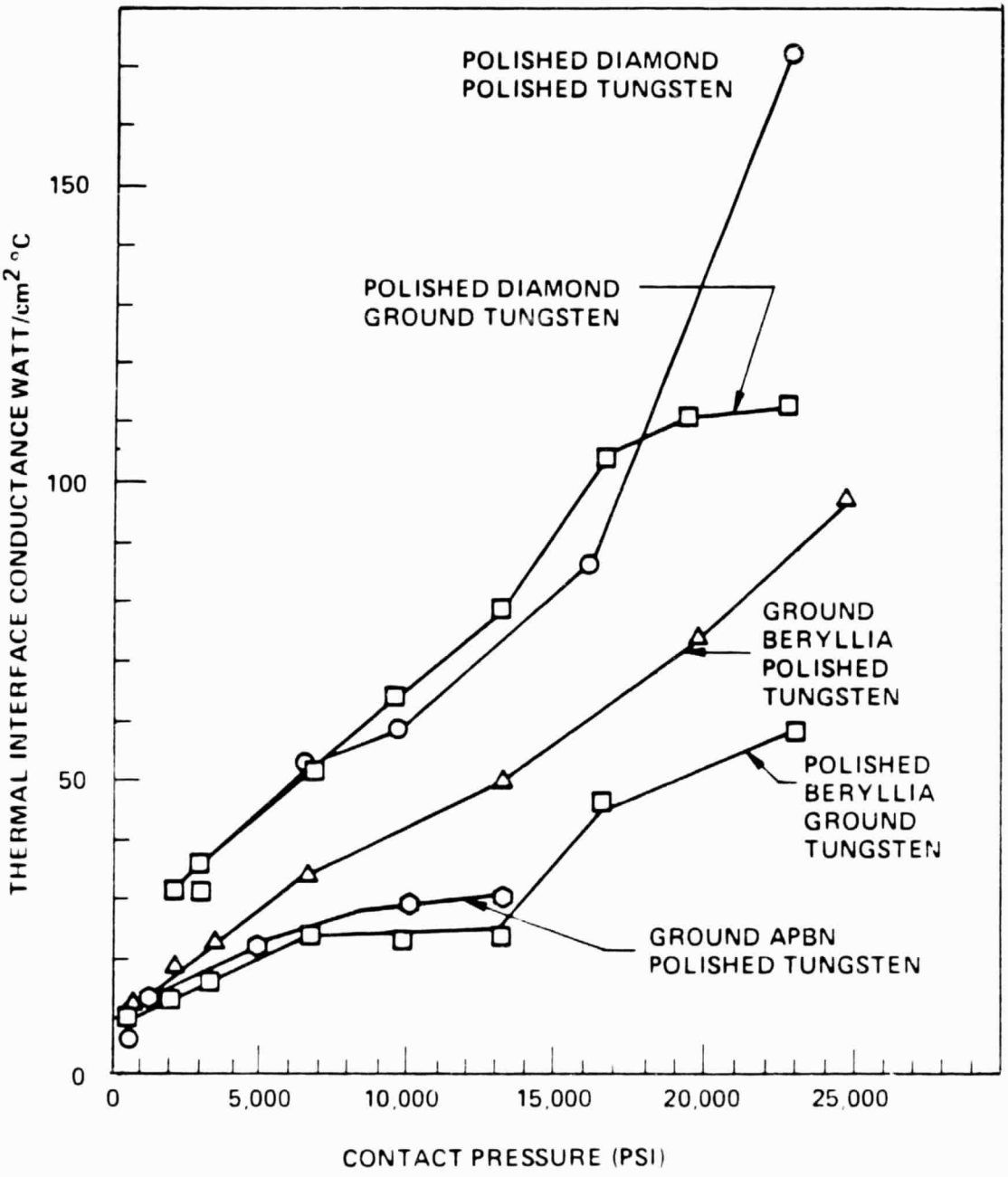

Figure 27. Thermal Interface Conductance as a Function of Contact Pressure

interference fit the thermal resistance measurements of Figure 27 were used. The sum of the four temperature rises give the total temperature rise from the hottest point on the helix to the tube body. With the tungsten helix interference fitted on three APBN rods, the temperature rise is 55.6°C/W of dissipated power. By using a copper helix or an Amzirc helix with three diamond rods brazed, the temperature rise is reduced by a factor of 10.

Table 2 gives an insight into the differences in thermal dissipation capability between the various circuit designs. The assumption is that the heat is transferred through the width of the rod. This assumes 100% helix contact to the rod thickness. If the helix-rod contact is less than 100%, then the temperature drop becomes a function of contact area and rod material. For example, APBN rods are anisotropic and the heat conductivity is very poor in the c direction and therefore if contact is made at a point the effective area is greatly reduced. On the other hand, if the rod material is BeO and the contact is a point then it is not as severe as the material is isotropic and although there is a "necking down effect" the heat transfer area to the body is still the total width of the rods.

Another property that affects the results is the change in thermal conductivity with the average rod temperature. For APBN, this thermal conductivity is fairly stable while BeO's thermal conductivity is highly temperature sensitive between 20 and 400°C.

To show these two effects, three calculations have been made showing

a. APBN vs area contact
b. BeO at 20°C
c. BeO at 400°C

Figure 28 indicates these curves and the importance of proper use of the support material for maximum thermal performance.

TABLE 2

THERMAL DISSIPATION CAPABILITY
(WHEN EACH HELIX TURN DISSIPATES 1 WATT)

	ΔT1 Around Helix (°C)	ΔT2 Helix Support Interface (°C)	ΔT3 Through Support (°C)	ΔT4 Support-Body Interface (°C)	ΔTotal Helix to Body (°C)	Clamping Pressure (psi)
1. Tungsten Helix 3 APBN Rods Interference fitted	8.7	20.7	15.9	10.3	55.6	10,000
2. Copper Helix 3 BeO Rods Brazed	4.4	0	7.9	0	12.3	---
3. Copper Helix 6 BeO Rods Brazed	1.1	0	4.0	0	5.1	---
4. Copper-Plated Tungsten Helix 3 Diamond Rods Interference fitted	8.7	6.5	0.8	3.8	19.8	20,000
5. Copper Helix 3 Diamond Rods Brazed	4.4	0	0.8	0	5.2	---
6. Copper Helix 4 Diamond Rods Brazed	2.5	0	0.6	0	3.1	---

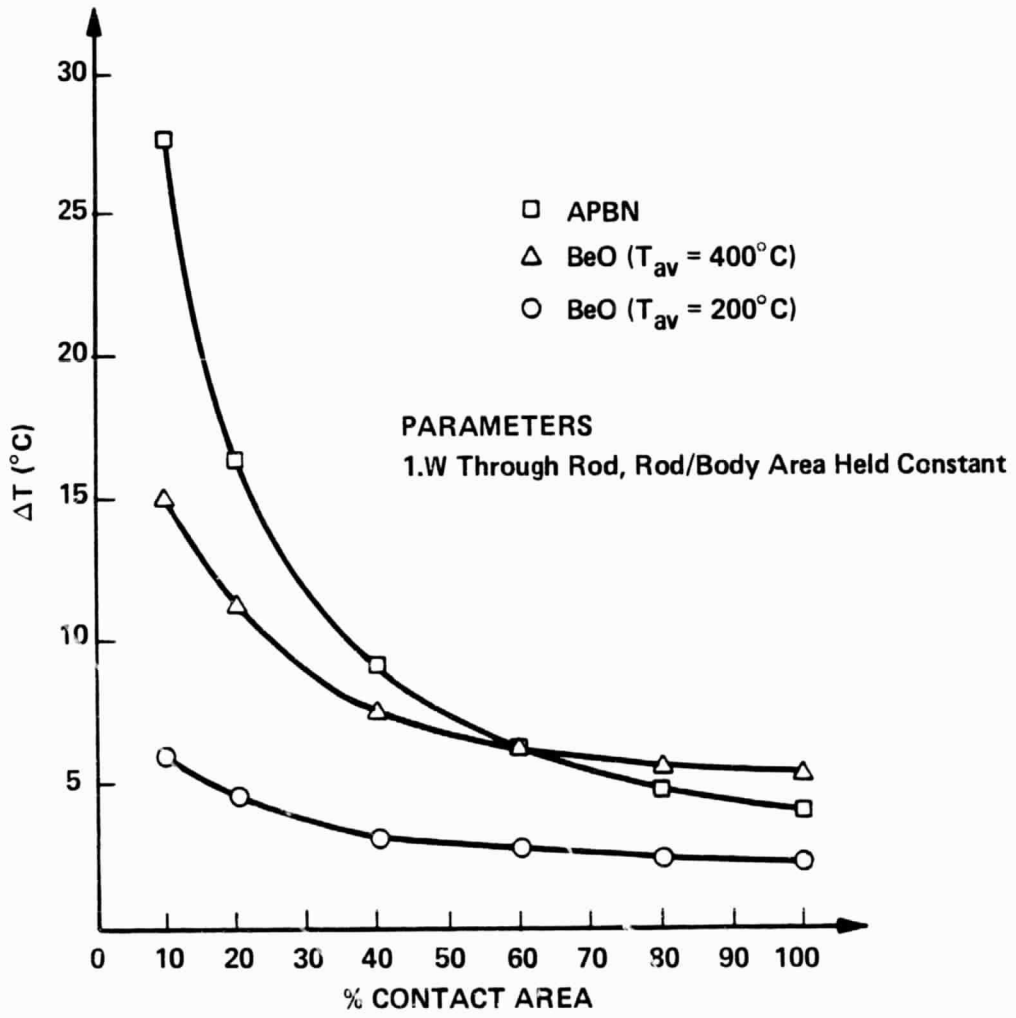

Figure 28. Temperature Drop Through Support Rod as a Function of Contact Area

3. CONCLUSIONS AND RECOMMENDATIONS

The study programs have produced considerable new data and results on circuit loss of interference and brazed circuits above 18 GHz and up to 40 GHz. It also has revealed the circuit and rod properties needing further control. This includes the processes used on the tape material and rod dielectric material during manufacturing as well as the in-process procedures and processing of these materials to make helices and final helix rods.

Essentially, the studies have measured the loss of circuits made by conventional interference fitted methods and by brazed methods. These losses are not any higher than expected from low frequency data. That is, the losses are acceptable and the circuits made by these methods will make a good millimeter tube in which the gain per inch will not be low due to excess circuit loss and the conversion efficiency will be acceptable due to the resulting loss parameter being around 0.05.

The studies indicate areas that need further detailed research and areas that have not been studied under the present programs. These areas are mainly in the material manufacturing and in-process processing and rods and helices manufacturing.

Details of these recommendations are as follows.

Helix Material and Manufacturing

Study and determine material acceptance specification and processing specifications.

Study methods of making helices and helix tapes.

Study process in fabricating wound helix and in-processes to produce the lowest loss surface.

Study helix materials to make brazed helix with lowest rf loss.

In addition to the above specific recommendations, the study should include the loss measurements of circuits made from these materials and processes, and a thermal study of those circuits to assess their thermal capability.

Dielectric Rod Material and Manufacturing

Study and determine material acceptance specification and processing specifications for optimizing low loss properties.

Study method of machining or making rods and in-process processing to reduce loss.

Study circuit rod support design to optimize thermal capability beyond those studied to data.

Study rod material and braze procedures and processes to make the lowest loss brazed assembly.

Again the recommendations include a loss and thermal study to evaluate circuits using material and rods from these materials.

APPENDIX A

THEORETICAL AND EXPERIMENTAL TWT HELIX LOSS DETERMINATION

A.S. Gilmour, Jr.
M.R. Gillette
J.T. Chen

Department of Electrical Engineering
State University of New York at Buffalo

ABSTRACT

As efficiency and power requirements for broad band traveling wave tubes increase, the necessity to reduce losses becomes more and more important. It is particularly important to reduce circuit losses because, when efficient multistage depressed collectors are used, each two percent increase in circuit efficiency yields a one percent increase in overall efficiency! Attempts to predict losses in helix structures have produced answers that were a factor of at least three below the measured loss. Historically, loss measurements have been very difficult to make, primarily, because of the small values of the quantities being measured. This paper presents an accurate theoretical analysis of the loss of a helix structure. The effect on loss of the dielectric support rods for the helix is taken into account. In addition, helix losses are separated from barrel losses. Functional variation are given of loss with frequency, helix pitch, helix radius, barrel to helix diameter ratio, helix and barrel resistivity and the effective relative dielectric constant of the helix support rods. Measurements of loss, made with a Hewlett Packard automatic network analyzer and a new automated measurement procedure, are presented. It is shown that excellent agreement between the predicted loss and the measured loss is obtained when helix surface roughness effects on resistivity are taken into account. Also, a correction is made for the increase in measured loss resulting from impedance mismatches between the helix and the measurement circuit and from loss in the sliding short.

I. INTRODUCTION

As power and efficiency requirements on broad band microwave amplifiers become more severe, attention is focused on the traveling wave tube and, more specifically, on the TWT slow-wave structure. For broad band (over an octave) TWTs the slow-wave structure universally used is the helix.

The effect of the intrinsic loss of the helix structure on the overall efficiency (η_{ov}) may be shown by considering the expression for η_{ov}. Following the work of Kosmahl, et al[1], η_{ov} may be written as

$$\eta_{ov} = \frac{\eta_e \eta_{ct}}{1 - \eta_c + \eta_c \eta_e + \eta_c \dfrac{P_{int} + P_{sig}}{P_o}}$$

where

η_e = electronic efficiency
η_{ct} = circuit efficiency
η_c = collector efficiency
P_{int} = beam power intercepted by helix
P_{sig} = harmonic and unuseable signal loss
P_o = beam power leaving gun.

Heater losses are assumed to be negligible.

In Figure 1 the overall efficiency is plotted as a function of the circuit efficiency for various values of collector efficiency.

Figure 1 illustrates the importance of maximizing circuit efficiency. For example, by increasing the value of circuit efficiency from 70 percent (a value not uncommon for a lossy helix material, such as rough tungsten, to 90 percent (for a properly finished copper plated helix) the increase in overall efficiency is nearly 10 percent when the collector efficiency is 95 percent!

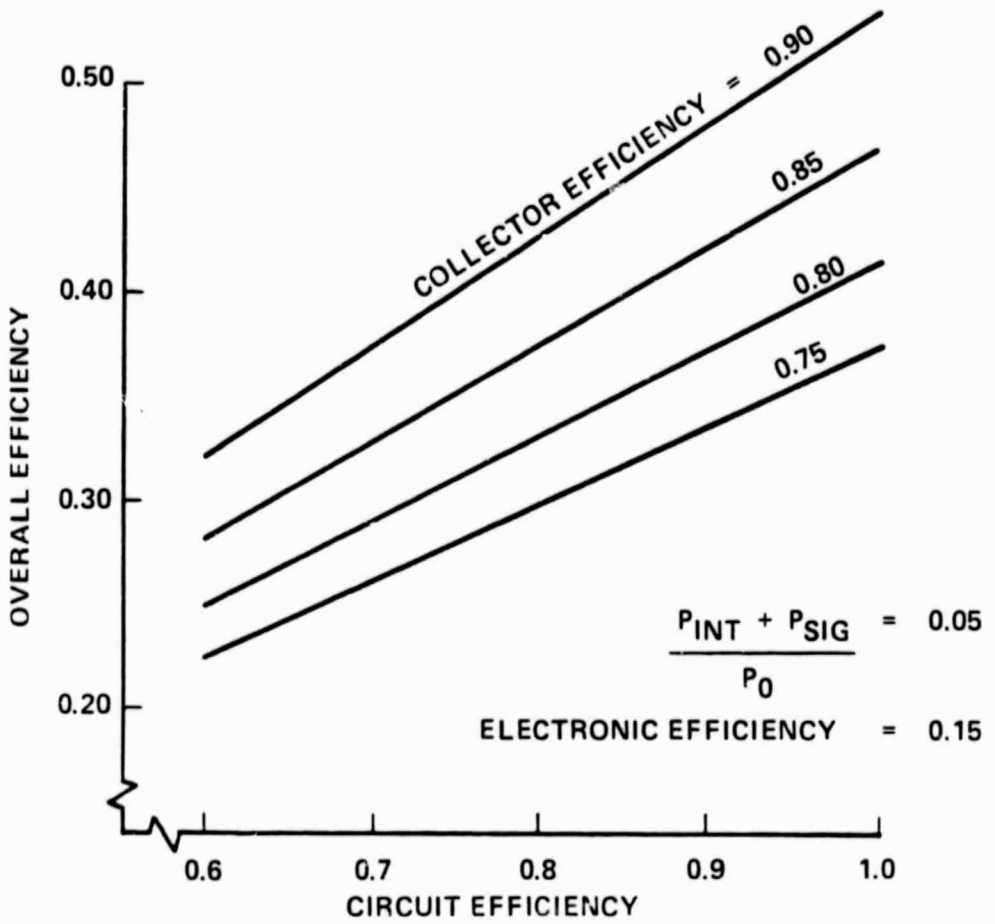

Figure 1. Overall Tube Efficiency as a Function of Circuit Efficiency for Various Values of Collector Efficiency

An additional benefit to increasing circuit efficiency, not evident from Figure 1, is that in some cases the upper limit for the power level of a helix-type tube is established by the circuit losses. By reducing circuit losses, the maximum power level can be increased. In fact, if circuit losses are the only limiting factor, as they sometimes are, and if all other factors remain equal, then a reduction in circuit losses by a factor of two would increase the maximum operating power level by a factor of two.

The foregoing analysis illustrates the importance of maximizing circuit efficiency. In spite of the fact that three decades have passed since the invention of the traveling wave tube and that several tens of thousands of helix-type TWT's have been fabricated, the functional variations of helix and support structure loss with frequency, geometry and material are not well understood. This is partly because analyses that have been performed have been inadequate and partly because accurate helix loss measurements are very difficult to make. The end result is that the circuit efficiency of the typical high-power helix-type TWT is much lower than it could be.

This paper presents a detailed theoretical analysis of the loss of a helix structure. Measurements of loss, made using a Hewlett Packard network analyzer and a new automated measurement procedure, especially suited for the meaurement of small loss values, are presented. Next, the effect of helix surface roughness effects in resistivity are accounted for. Finally, the increase in measured loss, resulting from impedance mismatches between the helix and the measurement circuit and from loss in the sliding short, is calculated. Excellent agreement between the predicted loss and the measured loss is obtained.

II. ANALYSIS OF LOSS OF HELIX AND SUPPORTING STRUCTURE

The following analysis is an expansion of earlier work by Bryant and White[2] and provides for the effects of dielectric helix support rods and for differences in resistivity between the helix and the surrounding barrel of the TWT. The intrinsic loss of the helix is separated from the loss of the barrel. Dielectric losses are not included in this analysis.

In this investigation, the usual Pierce helical sheath model[3,4] with an outer cylindrical shield is generalized so that dielectric loading is taken into account. Also, the resistivity of the barrel is permitted to differ from the resistivity of the helix. In this model, shown in Figure 2, current flows along the infinitely thin sheath surface in the pitch direction making an angle Ψ with the circumference.

In region A, which is the space inside the helix, the dielectric constant, ε_1, and the permeability, μ_1, are those of free-space. Corresponding to dielectric supporting rods, a material of effective dielectric constant, ε_2, and effective permeability, μ_2, is assumed to homogeneously fill region B. The resistivity of the sheath is ρ_1 and of the outer cylindrical conductor is ρ_2.

A. FIELD SOLUTION

Because the pitch angle is relatively small and because of the long helix length, perfect circular symmetry is assumed.

For plane waves propagating in the z-direction, it is assumed that fields vary as

$$\begin{bmatrix} \vec{E} \\ \vec{H} \end{bmatrix} = \begin{bmatrix} \vec{E}(r) \\ \vec{H}(r) \end{bmatrix} e^{j(\omega t - \beta_n z)}$$

The Floquet theorem may be applied to obtain the axial phase constant

$$\beta_n = \beta + 2\pi n/p,$$

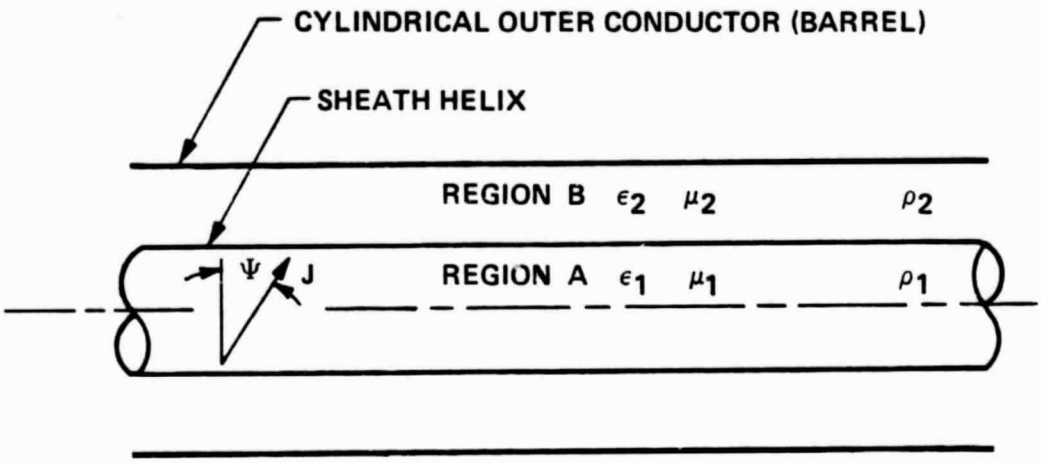

Figure 2. Model of Helix Structure Used in Analysis

where p is the period of the structure and n is the order of the mode. For the lowest order mode of transmission, n = 0. The following analysis is carried out for this lowest order mode.

In the analysis that follows, axial phase constants are separated while the radial propagation constants are assumed to be the same in both regions. Later in the numerical calculations, it will be seen that this separation produces no considerable difference.

For convenience, the following functions[5] in terms of combinations of modified Bessel functions are used.

$$G_{00} = G_{00}(\gamma a,\gamma b) = I_0(\gamma a)K_0(\gamma b) - K_0(\gamma a)I_0(\gamma b)$$

$$G_{11} = G_{11}(\gamma a,\gamma b) = I_1(\gamma a)K_1(\gamma b) - K_1(\gamma a)I_1(\gamma b)$$

$$G_{01} = G_{01}(\gamma a,\gamma b) = I_0(\gamma a)K_1(\gamma b) + K_0(\gamma a)I_1(\gamma b)$$

$$G_{10} = G_{10}(\gamma a,\gamma b) = I_1(\gamma a)K_0(\gamma b) + K_1(\gamma a)I_0(\gamma b)$$

and it is recognized that

$$\gamma b G_{10}(\gamma b,\gamma b) = \gamma b G_{01}(\gamma b,\gamma b) = 1.$$

Defining

$$\gamma^2 = \beta_i^2 - \omega^2\mu_i\varepsilon_i = \beta_i^2 - k_i^2$$

where i = 1 or 2 and assuming that the γ's are the same in both regions, then Maxwell's equations may be solved and the field components are as given in reference 4.

The characteristic equation obtained for the radial propagation constant is[6]:

$$\frac{k_1^2 \cot_\Psi^2}{\gamma^2} = \frac{I_0^2(\gamma a) - \frac{u_1}{u_2} I_0(\gamma a) I_1(\gamma a) \frac{G_{01}}{G_{11}}}{I_1^2(\gamma a) - \frac{\varepsilon_2}{\varepsilon_1} I_0(\gamma a) \frac{G_{10}}{G_{00}}}$$

B. ATTENUATION CONSTANT OF A DIELECTRICALLY LOADED HELICAL LINE WITH AN OUTER SHIELD

The Poynting vectors in regions A and B are determined separately. In region A, the Poynting vector is

$$S_1 = E_{r1} H_{\phi 1}^* - E_{\phi 1} H_{r1}^*$$

$$= \frac{k_1 \beta_1 A^2}{(u_1/\varepsilon_1)^{1/2} \gamma^2} \quad I_1^2(\gamma r) \left[1 + \left(\frac{\gamma}{k_1 \cot \Psi} \frac{I_o(\gamma a)}{I_1(\gamma a)} \right)^2 \right]$$

where E_{r1}, $H_{\phi 1}$, $E_{\phi 1}$, and H_{r1} are radial and azimuthal field components and A is a constant.

In region B, the Poynting vector is:

$$S_2 = E_{r2} H_{\phi 2}^* - E_{\phi 2} H_{r2}^*$$

$$= \frac{k_2 \beta_2 A^2}{(u_2/\varepsilon_2)^{1/2} \gamma^2} \quad I_0^2(\gamma a) \left[\left(\frac{I_1(\gamma r) K_o(\gamma b) + K_1(\gamma r) I_0(\gamma b)}{G_{00}} \right)^2 \right.$$

$$\left. + \left(\frac{\gamma}{k_2 \cot \Psi} \right)^2 \left(\frac{I_1(\gamma r) K_1(\gamma b) - K_1(\gamma r) I_1(\gamma b)}{G_{11}} \right)^2 \right]$$

The total power flow, Π_T, is obtained from the power flow in region A, Π_1, and in region B, Π_2, as follows:

$$\Pi_T = \Pi_1 + \Pi_2$$

$$= 1/2 \text{ Real} \int S_1 \cdot dA + 1/2 \text{ Real} \int S_2 \cdot dA$$

$$= 1/2 \text{ Real} \int S_1 \cdot 2\pi r dr + 1/2 \text{ Real} \int S_2 \cdot 2\pi r dr$$

$$= \pi \int_0^a S_1 r dr + \pi \int_a^b S_2 r dr$$

When the integrations are carried out, the following is obtained:

$$\Pi_T = \frac{\pi k_1 \beta_1 a^2 A^2}{2(\mu_1/\varepsilon_1)^{1/2} \gamma^2} L_T$$

where

$$L_T = M(\gamma a) \left[1 + \left(\frac{\gamma}{k_1 \cot \Psi} \right)^2 \frac{I_0^2(\gamma a)}{I_1^2(\gamma a)} \right]$$

$$+ \frac{\beta_2}{\beta_1} \frac{\varepsilon_2}{\varepsilon_1} I_0^2(\gamma a) \left\{ \left(\frac{b^2}{a^2} M(\gamma b) - M(\gamma a) \right) \left[\frac{K_0^2(\gamma b)}{G_{00}^2} + \left(\frac{\gamma}{k_2 \cot \Psi} \right)^2 \frac{K_1^2(\gamma b)}{G_{11}^2} \right] \right.$$

$$+ \left(\frac{b^2}{a^2} N(\gamma b) - N(\gamma a) \right) \left[\frac{I_0^2(\gamma b)}{G_{00}^2} + \left(\frac{\gamma}{k_2 \cot \Psi} \right)^2 \frac{I_1^2(\gamma b)}{G_{11}^2} \right]$$

$$\left. + 2 \left(\frac{b^2}{a^2} P(\gamma b) - P(\gamma a) \right) \left[\frac{K_0(\gamma b) I_0(\gamma b)}{G_{00}^2} \left(\frac{\gamma}{k_2 \cot \Psi} \right)^2 \frac{K_1(\gamma b) I_1(\gamma b)}{G_{11}^2} \right] \right\}$$

and where the following functions are defined.

$$M(x) = I_1^2(x) - I_0(x)I_2(x)$$

$$N(x) = K_1^2(x) - K_0(x)K_2(x)$$

$$P(x) = I_1(x)K_1(x) + I_0(x)K_2(x)$$

The insertion loss, α, of the helix structure may be determined as follows:

Since

$$\Pi_T = \Pi_0 \exp(-2\alpha z)$$

then

$$\alpha = -\frac{1}{2\Pi_T}\frac{d}{dz}\Pi_T,$$

where

$$\frac{d}{dz}\Pi_T = \frac{d}{dz}\Pi_1 + \frac{d}{dz}\Pi_2.$$

but

$$\frac{d}{dz}\Pi_1 = 2\pi a P_{L1}$$

$$= \frac{\pi R_1 \varepsilon_1 a k_1^2 A^2}{u_1 \gamma^2} \; I_0^2(\gamma a) \left[\left(\frac{I_1(\gamma a)}{I_0(\gamma a)} \right)^2 \right.$$

$$\left. + \left(\frac{\gamma^2}{k_1^2 \cot \Psi} \right)^2 \left(\frac{I_0(\gamma a)}{I_1(\gamma a)} \right)^2 + \left(\frac{\varepsilon_2 G_{10}}{\varepsilon_1 G_{00}} \right)^2 \right.$$

$$+ \left(\frac{\gamma^2}{k_2^2 \cot\Psi}\right)^2 \left(\frac{\varepsilon_2 G_{01}}{\varepsilon_1 G_{11}}\right)^2 \Bigg]$$

and

$$\frac{d}{dz}\Pi_2 = 2\pi b P_{L_2}$$

$$= \frac{\pi R_2 \varepsilon_2 b k_2^2 A^2}{\mu_2 \gamma^2} I_0^2(\gamma a) \left(\frac{1}{\gamma b}\right)^2 \left[\frac{1}{G_{00}^2}\right.$$

$$\left. + \left(\frac{\gamma^2}{k_2^2 \cot\Psi}\right)^2 \frac{1}{G_{11}^2}\right]$$

where P_{L1} and P_{L2} are the power losses per unit area in the helix and barrel respectively. They are determined from the Poynting vectors S_1 and S_2.

By combining the appropriate preceding equations, α is found to be

$$\alpha = \frac{2k_2 R_1}{\beta_1 a (\mu_2/\varepsilon_2)^{1/2} L_T} \left(\frac{\varepsilon_2}{\varepsilon_1}\right) I_0(\gamma a) \left\{\frac{bR_2}{aR_1}\left[\left(\frac{1}{\gamma b G_{00}^2}\right)^2 + \left(\frac{\gamma}{k_2 \cot\Psi}\right)^2 \frac{1}{K_2 b G_{11}^2}\right]\right.$$

$$+ \left(\frac{G_{10}}{G_{00}}\right)^2 + \left(\frac{\varepsilon_1}{\varepsilon_2} \frac{I_1(\gamma a)}{I_0(\gamma a)}\right)^2 + \left(\frac{\gamma 2}{k_1^2 \cot\Psi}\right)^2 \left(\frac{\varepsilon_1}{\varepsilon_2} \frac{I_0(\gamma a)}{I_1(\gamma a)}\right)^2$$

$$\left. + \left(\frac{\gamma^2}{k_2^2 \cot\Psi}\right)^2 \left(\frac{G_{01}}{G_{11}}\right)^2\right\}$$

This is the equation of the intrinsic insertion loss of a helix surrounded by dielectric materials and an outer cylindrical conductor.

If $\varepsilon_1 = \varepsilon_2 = \varepsilon$, $\mu_1 = \mu_2 = \mu$, and $k^2 = \omega^2\mu\varepsilon$, the equation for α reduces to

$$\alpha = \frac{F^3(\gamma a)^4 R_1}{2\pi a(120)^2(\beta a)(ka)} I_0^2(\gamma a)\left\{\frac{k^2}{\gamma^2}\left(\frac{I_1^2(\gamma a)}{I_0^2(\gamma a)} + \frac{G_{10}^2}{G_{00}^2}\right)\right.$$

$$+ \left(\frac{\gamma}{k\cot\Psi}\right)^2 \left(\frac{I_0^2(\gamma a)}{I_1^2(\gamma a)} + \frac{G_{01}^2}{G_{11}^2}\right)$$

$$\left. + \frac{b}{a}\frac{R_2}{R_1}\frac{k^2}{\gamma^2}\left[\frac{1}{\gamma^2 b^2 G_{00}^2} + \left(\frac{\gamma}{k\cot\Psi}\right)^2 \frac{1}{k^2 b^2 G_{01}^2}\right]\right\}$$

which is the main result of the paper by Bryant and White[2].

The skin effect resistance is obtained by using the relation

$$R_i = \sqrt{\pi\mu_o F\rho_i}$$

where i = 1 or 2.

Figures 3 through 9 contain plots of loss as a function of frequency. The frequency range chosen corresponds to that over which measurements of loss have been made on helix structures supplied to SUNYAB by industry. The normal values of various parameters used for Figures 3 through 9 are as follows.

Helix pitch	= 0.141 cm (18 TPI)
Helix radius	= 0.12 cm (0.047")
Barrel to helix diameter ratio	= 2.0
Helix resistivity	= 2.5×10^{-6} Ω - cm
Barrel resistivity	= 2.5×10^{-6} Ω - cm
Effective relative dielectric constant of support rods (ε_2)	= 1.5

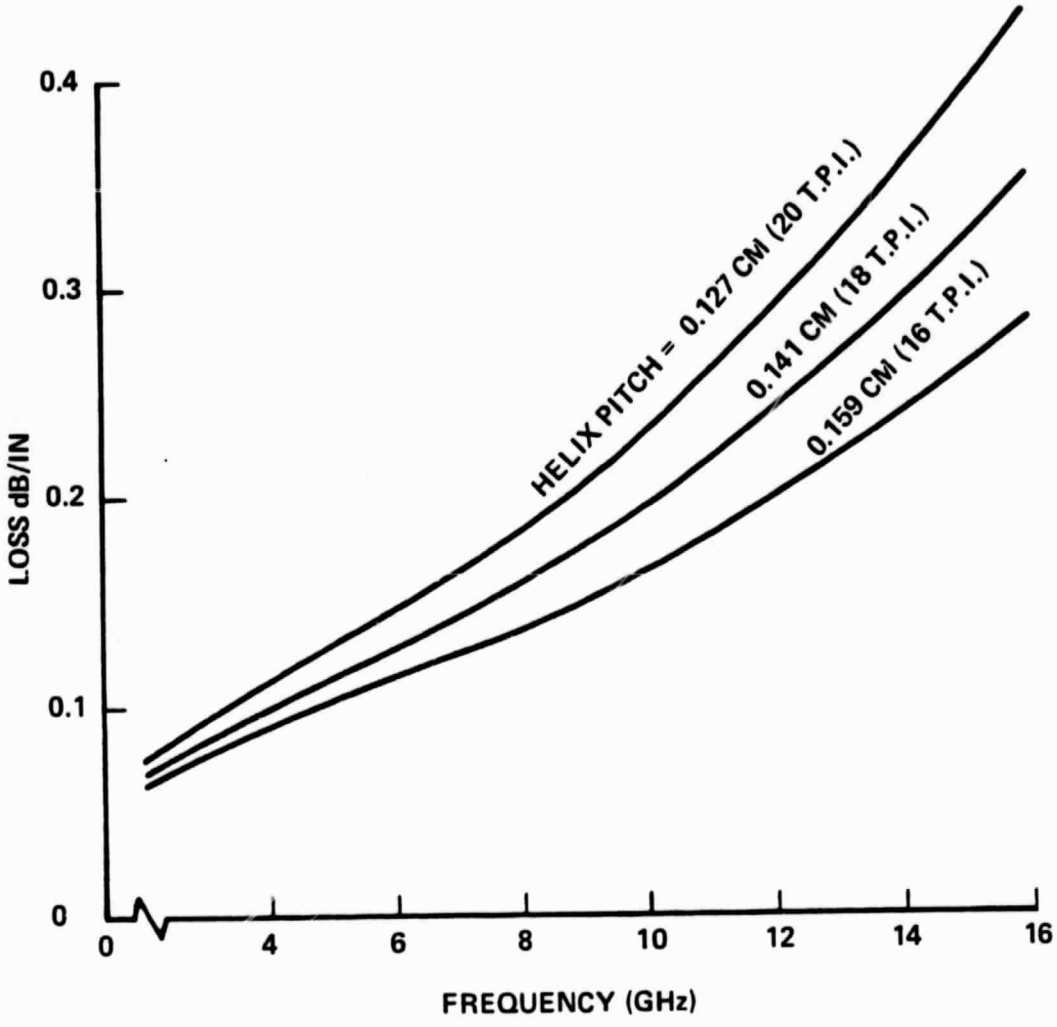

Figure 3. Loss as Functions of Frequency and Helix Pitch

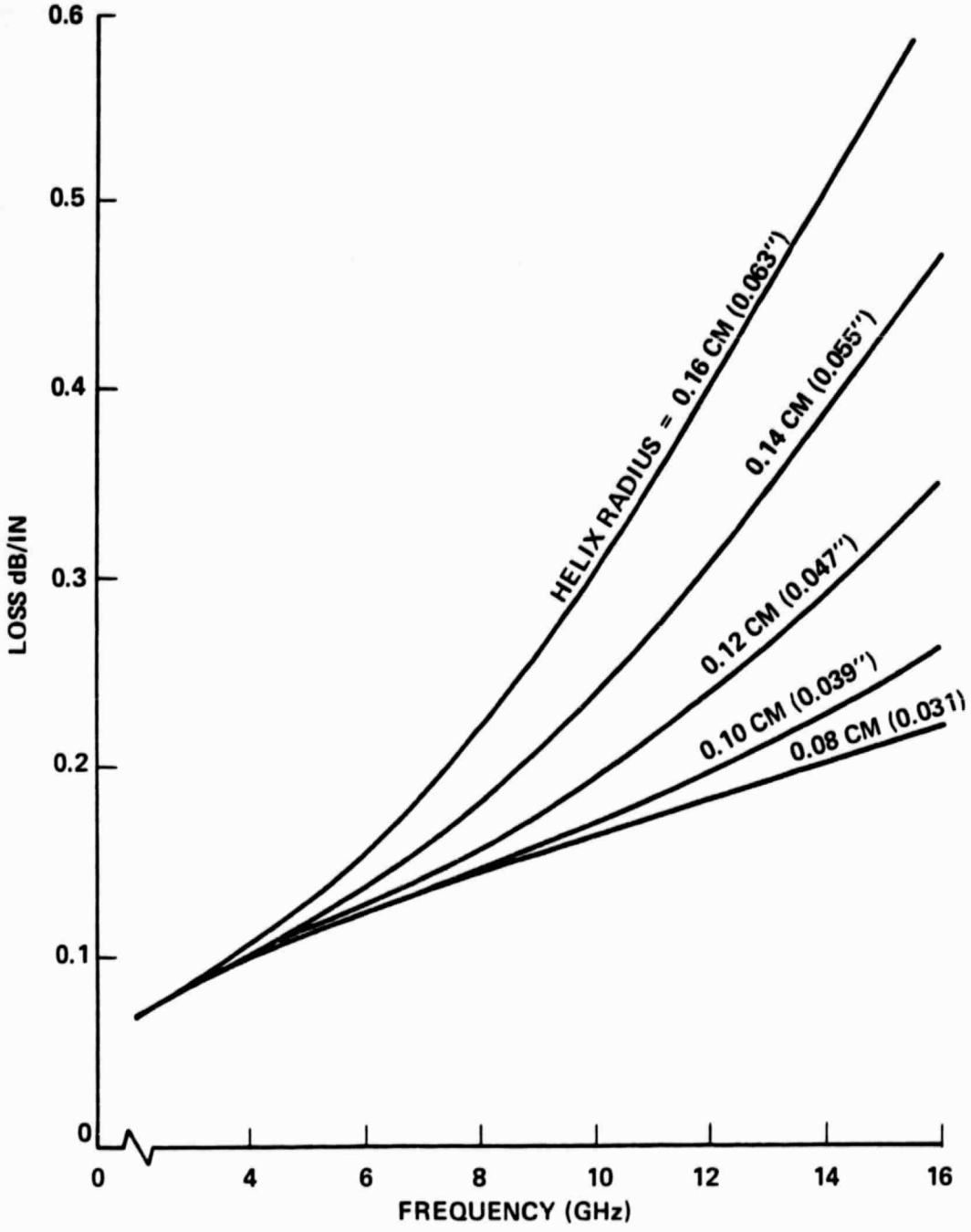

Figure 4. Loss as Functions of Frequency and Helix Radius

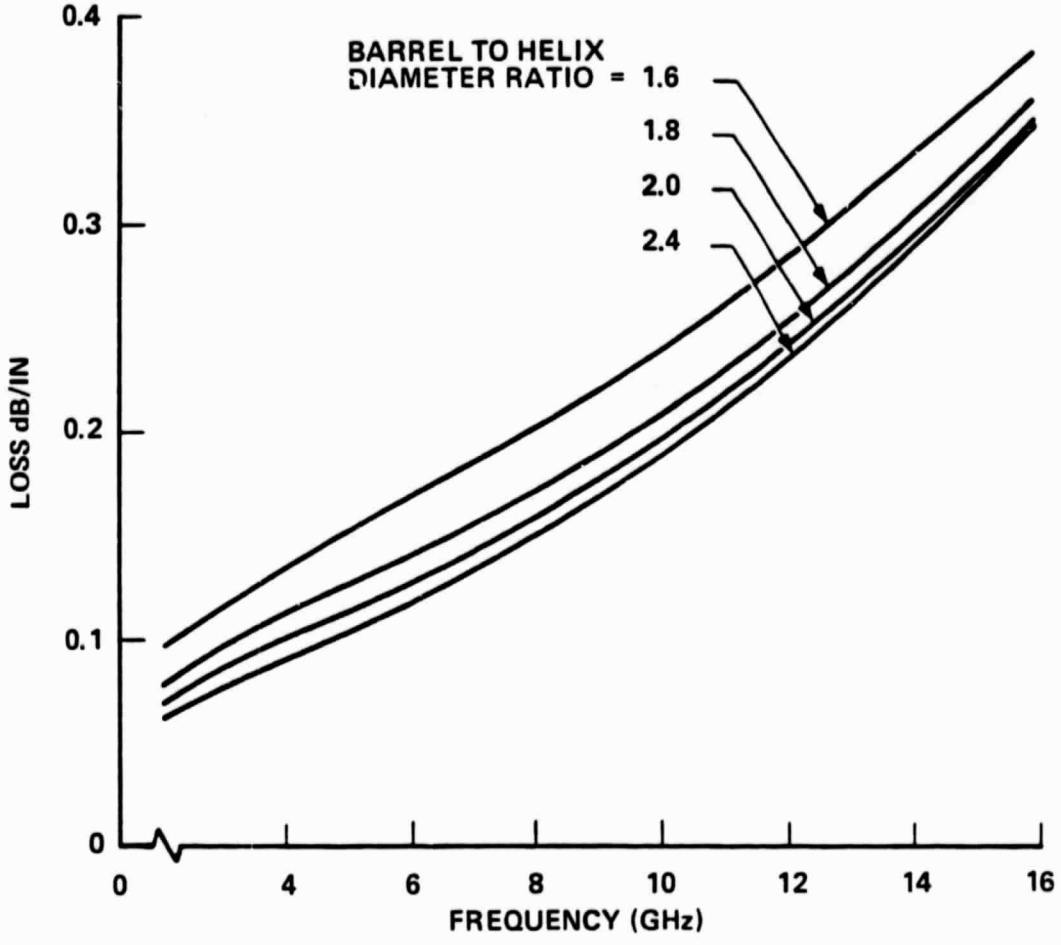

Figure 5. Loss as Functions of Frequency and Barrel to Helix Diameter Ratio

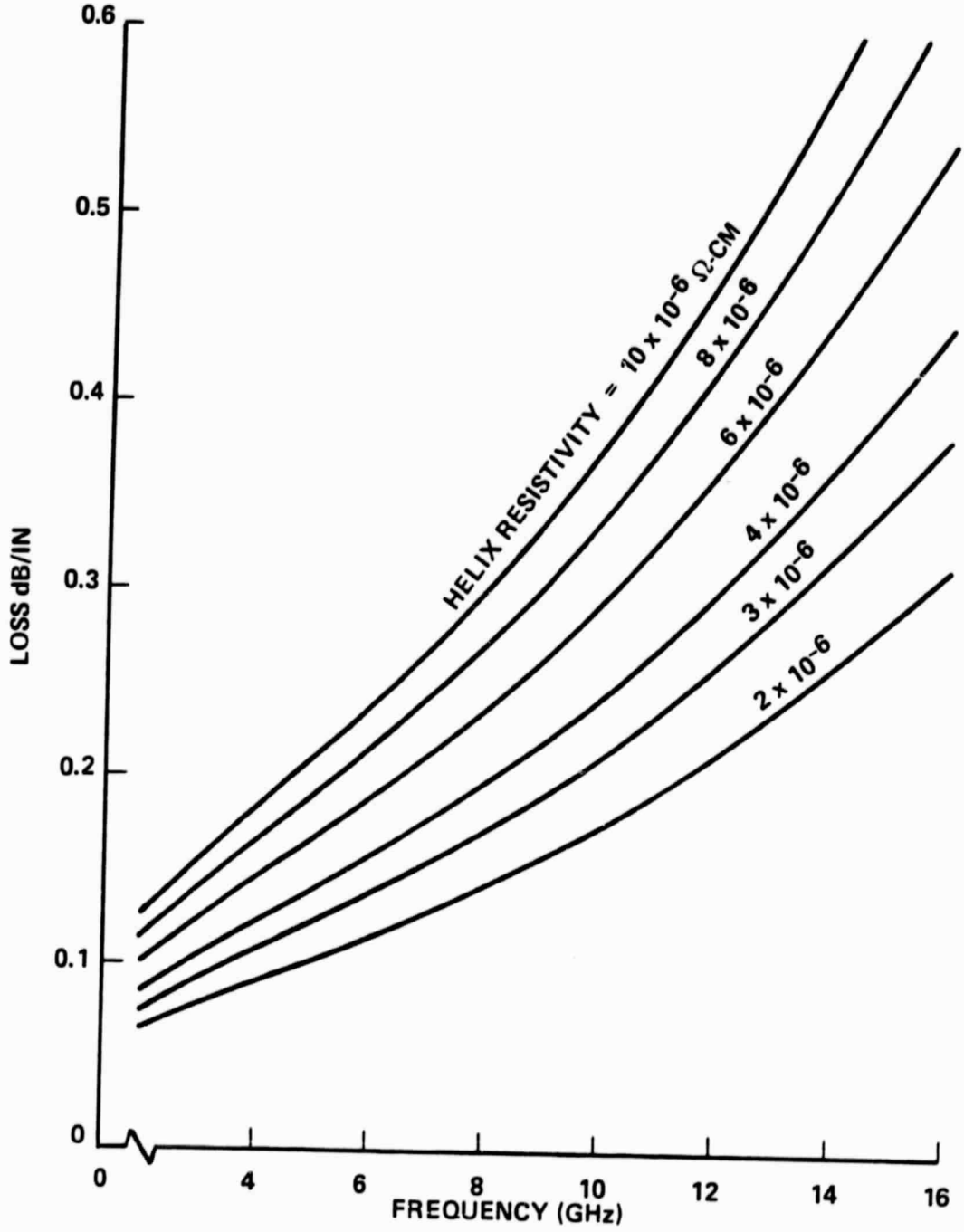

Figure 6. Loss as Functions of Frequency and Helix Resistivity

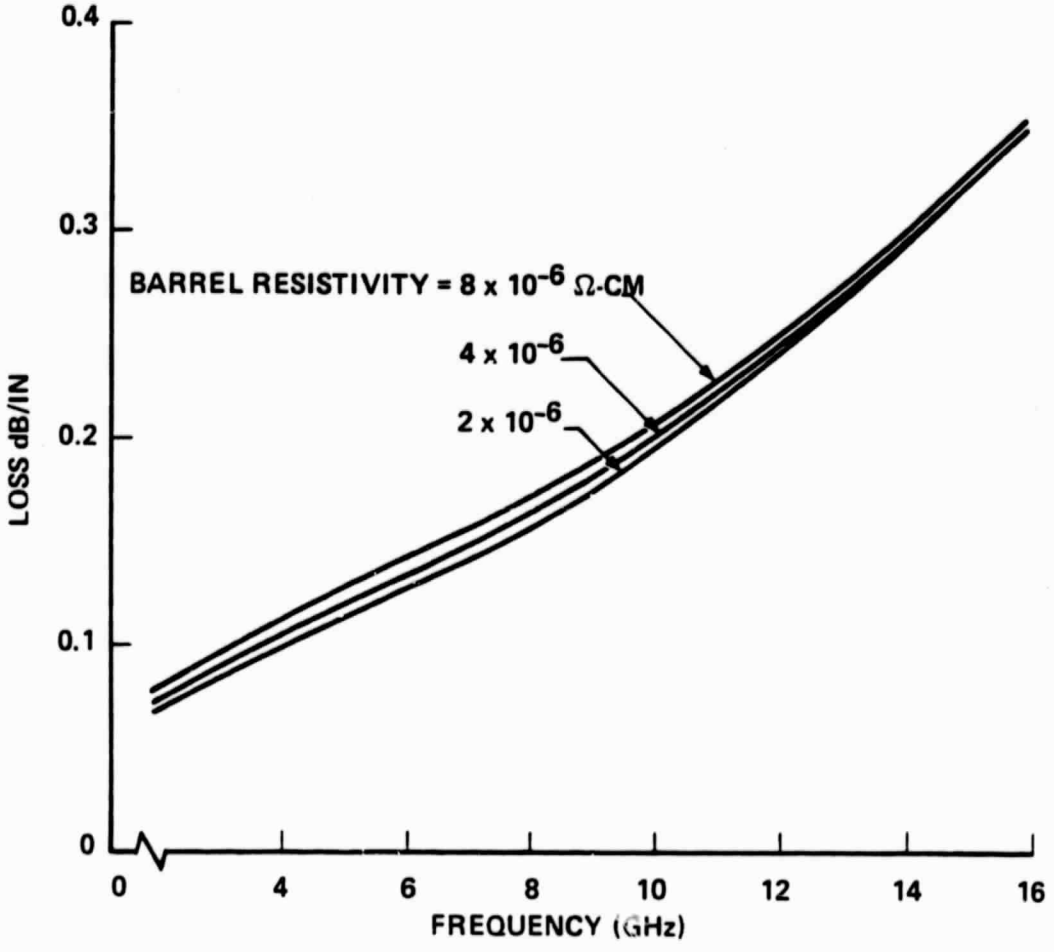

Figure 7. Loss as Functions of Frequency and Barrel Resistivity

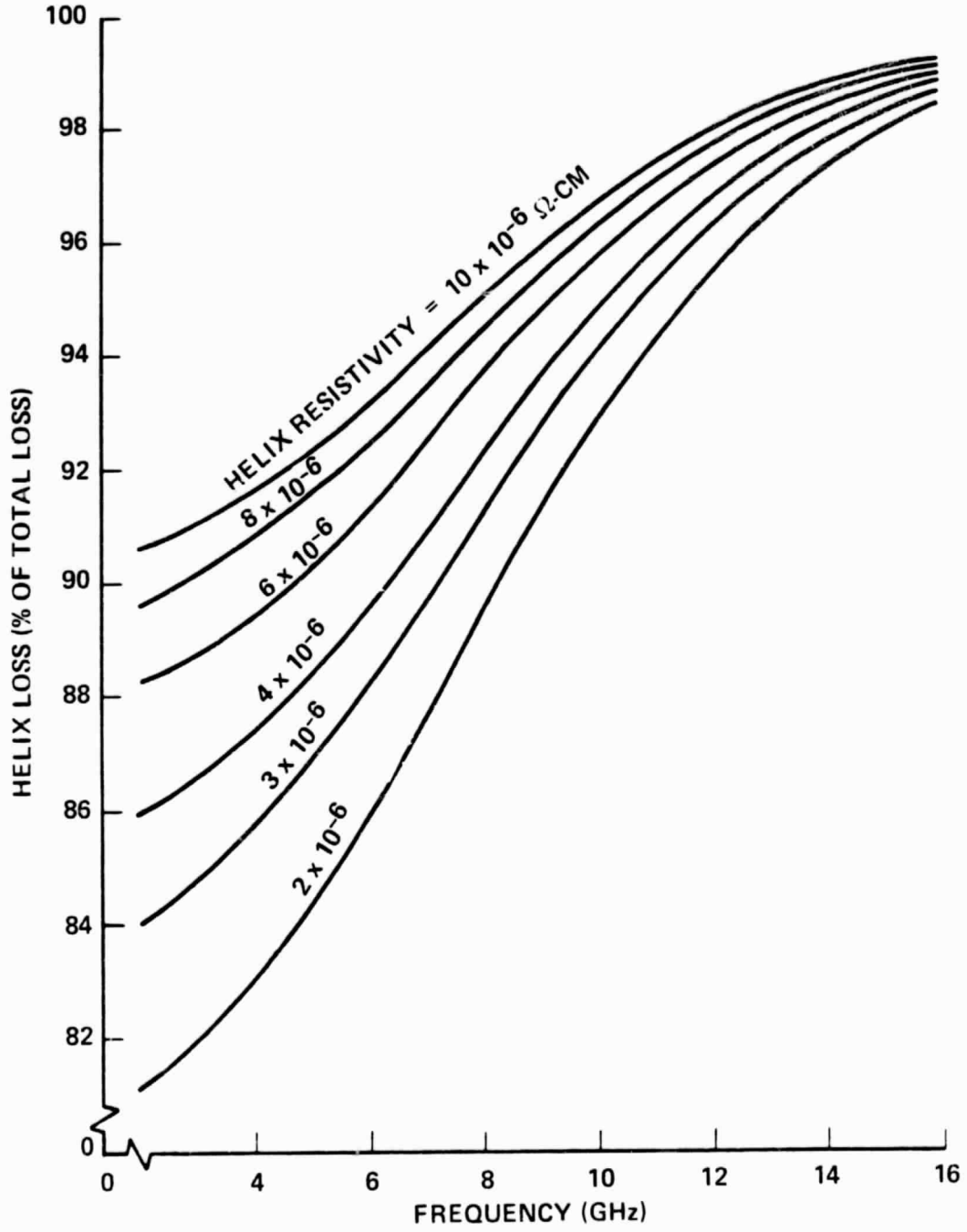

Figure 8. Helix Loss as Functions of Frequency and Helix Resistivity

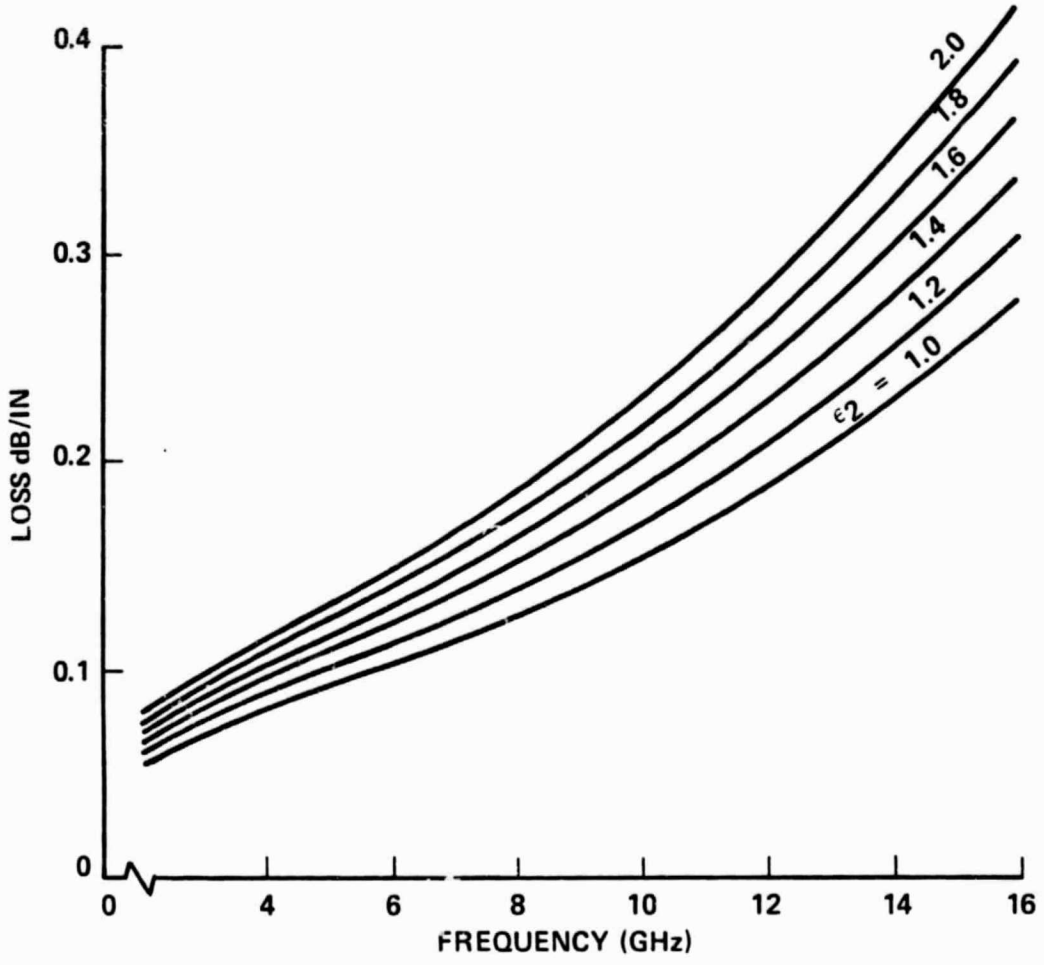

Figure 9. Loss as Functions of Frequency and Effective Relative Dielectric Constant of Support Rods (ϵ_2)

In each of the Figures 3 through 9, one of these parameters is varied while the others are held constant.

The effective relative dielectric constant, ε_2, is calculated as follows:

$$\varepsilon_2 = \varepsilon\ \alpha + (1-\alpha)$$

where ε is the relative dielectric constant of the support rods and α is the fraction of the cross-sectional area of the region between the helix and the barrel that is filled with dielectric material. In calculating ε_2 it is assumed that no azimuthal electric fields exist.

In Figures 3 and 4, it is shown that loss increases with decreasing helix pitch and with increasing helix radius. Certainly, an increase in loss would be expected because of the increase in conductor length per unit helix length accompanying a decrease in pitch or an increase in radius. However, the amount of loss increase is not proportional to the increase in conductor length.

As may be noted in Figure 6, the loss of the helix structure varies approximately as the square root of the helix resistivity. Figure 7 shows that the resistivity of the barrel has little effect on loss. As a result, as is shown in Figure 8, the helix loss represents a large percentage of the total loss of the entire structure.

Figure 9 shows the effect of the effective relative dielectric constant of the support rods on loss. Note that, to minimize loss, the dielectric constant and cross-sectional area of the support rods must be minimized. (Of course, these are the same requirements as those for maximizing interaction efficiency.)

In summary, to minimize loss, it is necessary to:

1. Maximize helix pitch
2. Minimize helix radius
3. Maximize barrel to helix diameter ratio
4. Minimize helix resistivity
5. Minimize support rod cross-sectional area and dielectric constant.

III. MEASUREMENT OF LOSS OF HELIX AND SUPPORTING STRUCTURE

The accurate measurement of the loss of a TWT helix structure is very difficult for two primary reasons. In the first place, the loss is normally relatively low (~ 0.5 to 1 dB). As a result, it is necessary to take precautions to eliminate and/or compensate for even relatively small losses in the transmission lines, connectors, etc. used in the measurement apparatus. In the second place, the impedance of the helix structure is a function of frequency. This is shown in Figure 10 for the helix structure for which loss measurements are reported later in this paper. The value of ε_2 for this structure was 1.9. The only frequency at which the impedance of the helix structure was matched to the 50 ohm measurement apparatus was approximately 8 GHz. Above and below this frequency, the impedance mismatches at the connections to the helix caused multiple reflections of signals in the helix structure and in some of the components in the measurement apparatus. The resulting multiple passes of the signal cause the measured loss of the helix structure to be higher than the actual loss.

The above two problems and their solutions are discussed in the following sections.

A. LOSS MEASUREMENTS ON LOW LOSS STRUCTURE

The manual measurement of the loss of a helix structure is an enormously time consuming task. As a result, manual measurements were made only occasionally to check results obtained by other techniques.

Most of the helix loss measurements were made with a Hewlett Packard Model 8542 B automatic network analyzer (ANA). The technique for using the ANA to make loss measurements on low loss structures has recently been described by one of the authors.[7] A BASIC language program using Deschamp's method[8] for the measurement of and data reduction for dissipative loss was written for the ANA. The use of this program with the ANA made it possible to readily compare results with the manual measurements and eliminated the flexible cables and internal switching of the ANA which

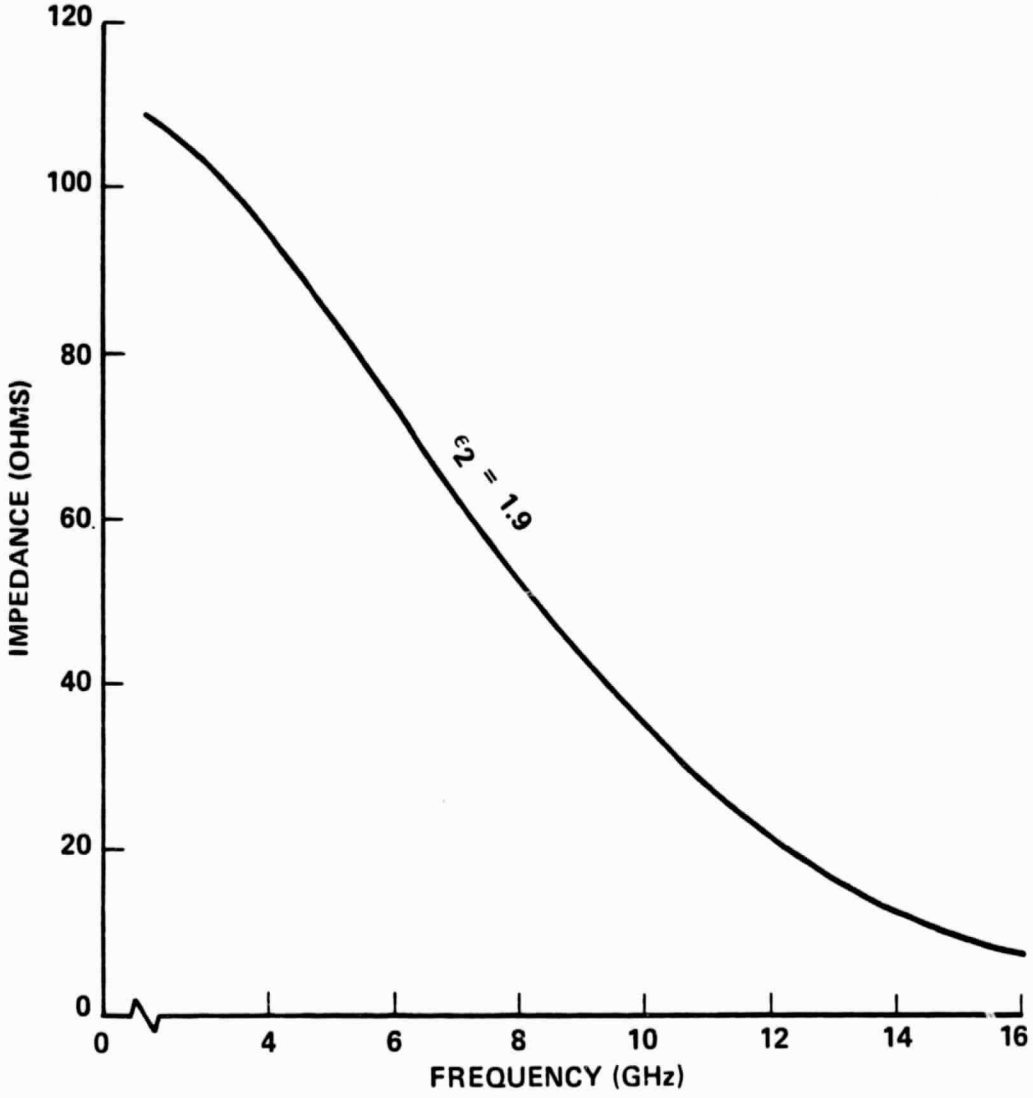

Figure 10. Impedance as a Function of Frequency

are requirements of the standard software packages (GPM-1 and GPM-2) available for the ANA.

It was necessary to eliminate the flexible cables because of the changes in impedance and loss characteristics of these cables and resulting measurement errors when the cables are flexed. It was necessary to eliminate internal switching in the ANA to prevent changes in calibration and the accompanying errors that resulted from switching during measurements.

The circled data points in Figure 11 resulted from loss measurements on a helix structure having the following characteristics.

Helix pitch	= 0.141 cm (18 TPS)
Helix radius	= 0.111 cm (0.0437")
Barrel to helix diameter ratio	= 2.02
Effective relative dielectric constant of support rods (ε_2)	= 1.9

The barrel and the helix were copper plated.

The lower curve in Figure 11 is the intrinsic loss of the helix structure calculated using the normally accepted resistivity value for copper (1.724×10^{-6} Ω - cm) 2.5×10^{-6} MPM manual.

In obtaining agreement (solid curve in Figure 11) between the calculated results and the measured results it was necessary first to consider the effect of the surface finish of the copper plated helix on the value of resistivity. It has previously been pointed out[9] that the surface irregularities on helix samples have dimensions of the same order of magnitude as the skin depth, calculated on a single-conductor, free-space basis. As a result a substantial increase in the resistivity of the helix would be expected.

Shown in Figure 12 are photomicrographs of the surface of a sample similar to that used for the measured results given in Figure 11. Notice

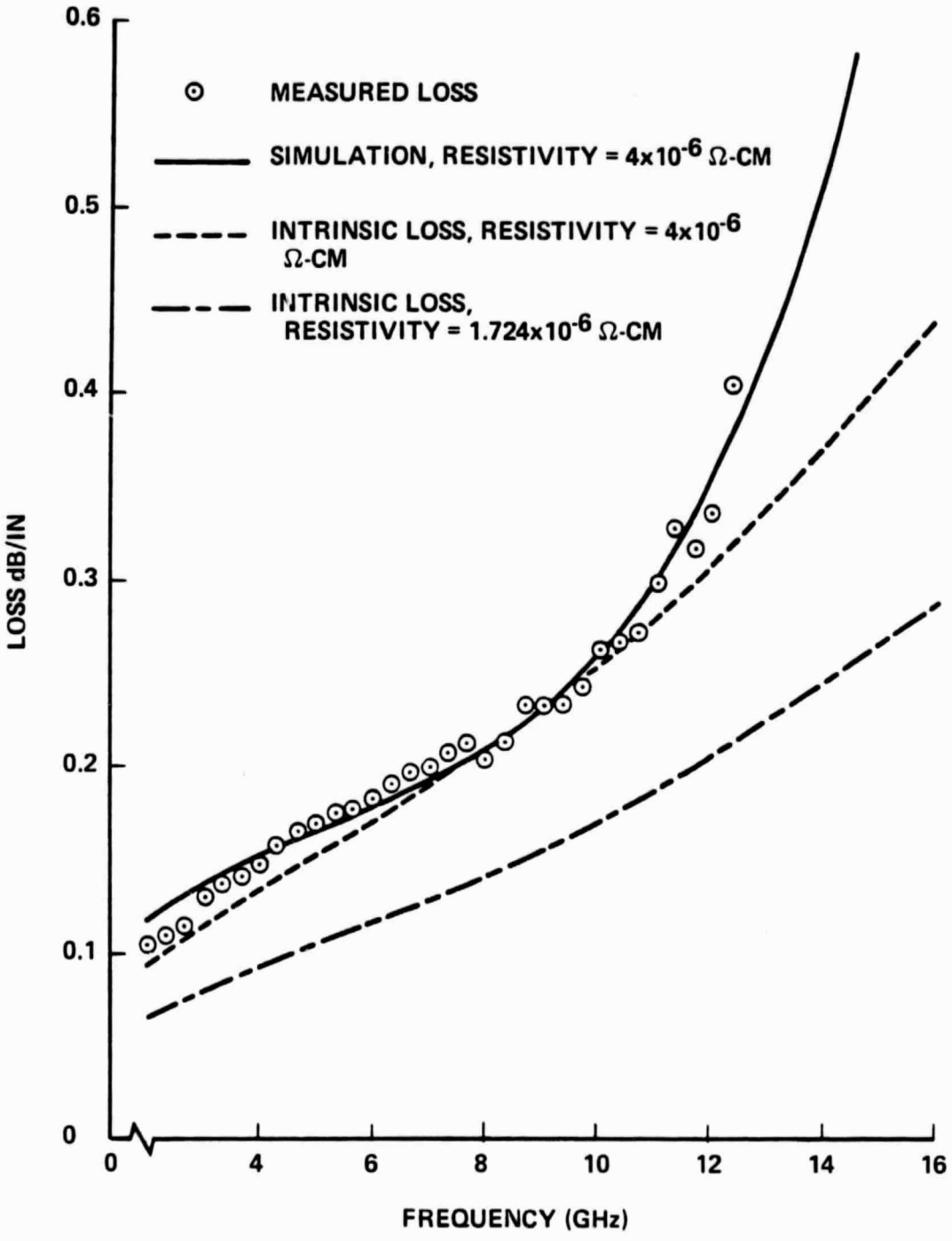

Figure 11. Measured and Theoretical Loss as a Function of Frequency

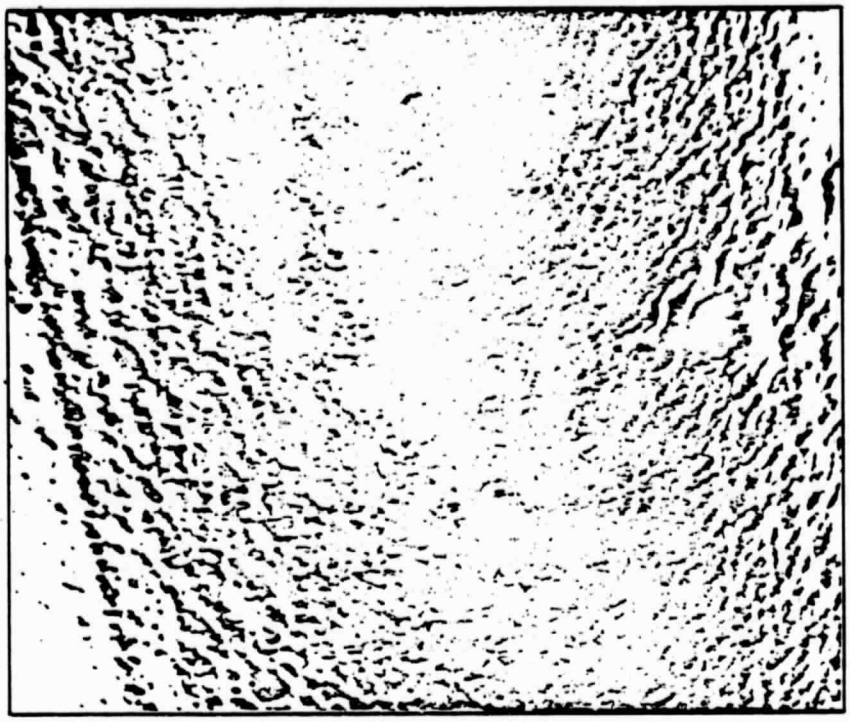

A Photomicrographic of the Surface of a Copper Plated Helix

MAGNIFICATION - 550X

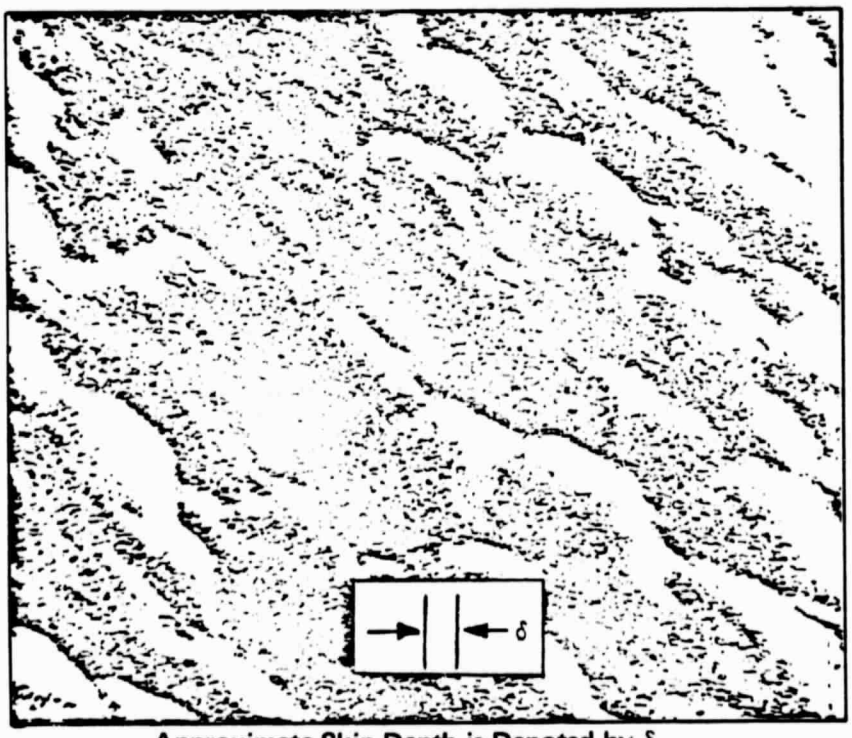

Approximate Skin Depth is Denoted by δ

MAGNIFICATION - 6000X

Figure 12.

that the surface is very rough and that the single-conductor, free-space skin depth at 10 GHz is smaller than the dimensions of the irregularities! As a result, it would be expected that the resistivity of the copper plated helix would be substantially higher than the value of 1.724×10^{-6} Ω - cm used for the calculation of the lower dashed curve in Figure 11. If it is assumed that the resistivity is 4×10^{-6} Ω - cm, then the upper dashed curve in Figure 11 is calculated for the intrinsic loss of the helix structure. It is suggested that a future research effort should be devoted to the problem of relating the roughness of a surface to resistance.

The second step taken to obtain agreement between the calculated and measured results was to account for the ohmic loss increase that occurred because of impedance mismatches and the multiple passes of the signal through the helix and the sliding short. This ohmic loss increase is discussed in the following section.

B. LOSS INCREASE RESULTING FROM IMPEDANCE MISMATCHES

The theory for Deschamp's method[8,10,11,12] considers an idealized case where the sliding short used does not have loss. For this case, the intrinsic insertion loss of a device can be measured directly without error for both mismatched and matched devices. However, the presence of loss in the sliding short requires additional information to determine an accurate value of device intrinsic insertion loss. The determination of the intrinsic loss of a well matched device requires the separate measurement of the loss of the sliding short and this can be substracted out. A lattice diagram in Figure 13 illustrates the signal flow for the well matched case. In this figure, the signal from the signal source is denoted by E^+. The signal enters the helix structure without reflection at plane 0 and then leaves the helix structure without reflection at plane L_2. The signal is then totally reflected from the sliding short and propagates back through the helix structure without reflection. Attenuation occurs in the helix structure and in the sliding short. The problem of mismatch in the device and loss in the sliding short is a situation where a knowledge of the sliding short loss and a correction for the increase in ohmic loss[13] must be used to determine an accurate value of test device intrinsic insertion

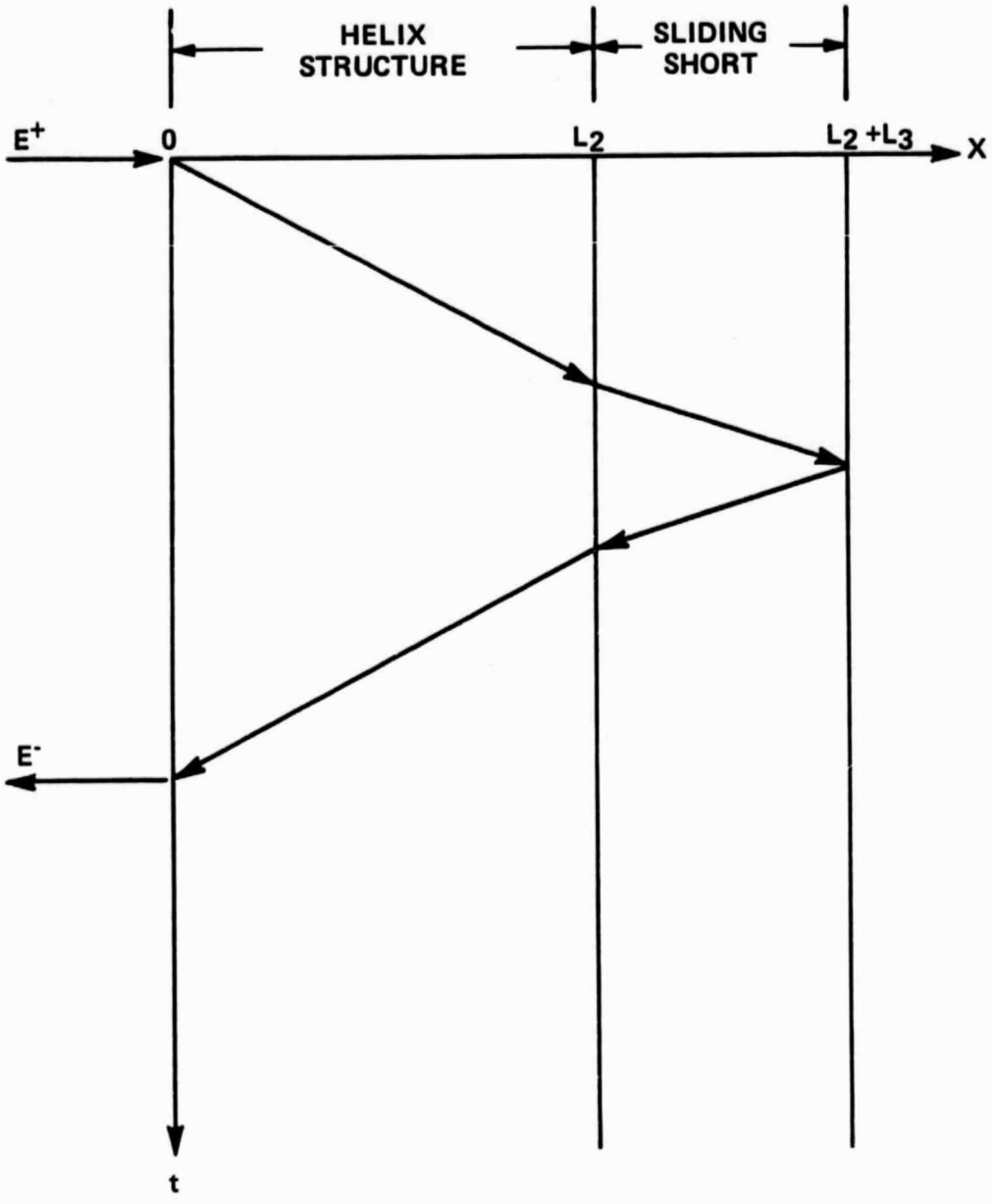

Figure 13. Lattice Diagram Illustration Signal Flow for the Well Matched Case

loss. The ohmic loss increase in the test device and in the sliding short is due to reflections and are rereflections caused by the mismatch. The lattice diagram in Figure 14 illustrates this situation. In this figure, the signal from the source, E^+, is partially reflected as it enters the helix structure. The portion of the signal transmitted through the helix structure is partially reflected at plane L_2 and this reflected portion is then partially reflected at plane 0, etc. Attenuation occurs on each pass of any portion of the wave through the helix.

Those portions of the wave that pass plane L_2 traveling toward the short at plane $L_2 + L_3$ are totally reflected by the short back toward L_2. When they are incident on L_2, they are partially transmitted to the helix and partially reflected toward the short, etc. Attenuation occurs on each pass of any portion of the wave in the region between L_2 and $L_2 + L_3$.

The above situation is carried to completion when all portions of all waves have been either completely attenuated or have been reflected to the generator which was assumed to be perfectly matched to Z_o.

A computer simulation of the experimental situation was used to determine the difference between the measured loss and the device intrinsic loss. Shown in Figure 15 is the circuit model of the experimental situation which was used for the computer simulation. The value of Z_{01} and of Z_{03} is 50 ohms, and the value of Z_{02} (the helix impedance) is a function of frequency as was shown in Figure 10. The solid curve in Figure 11 is the result of this simulation for the helix structure considered in Figure 11. Notice that there is excellent agreement between the simulated and measured results.

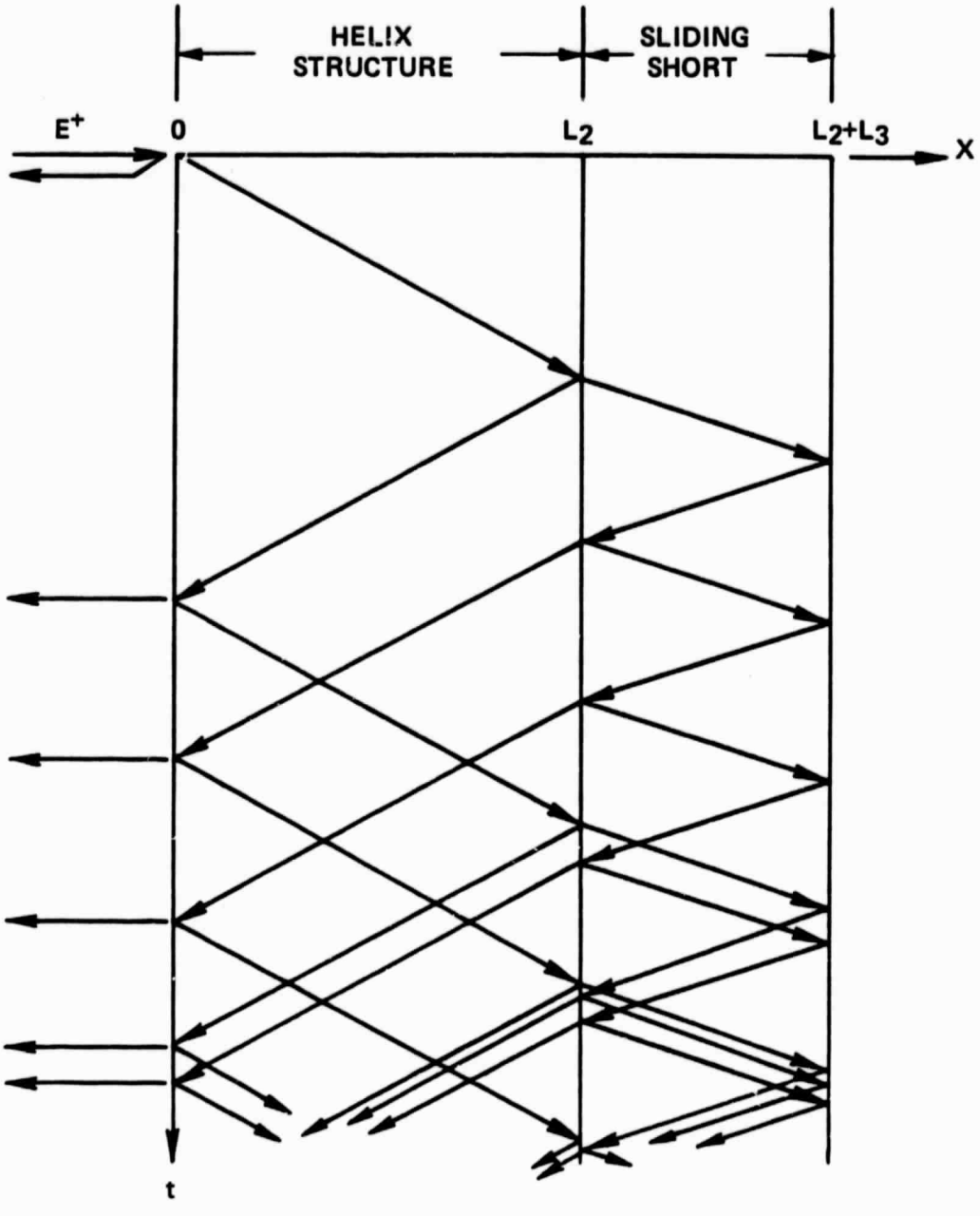

Figure 14. Signal Flow in Presents of Mismatch

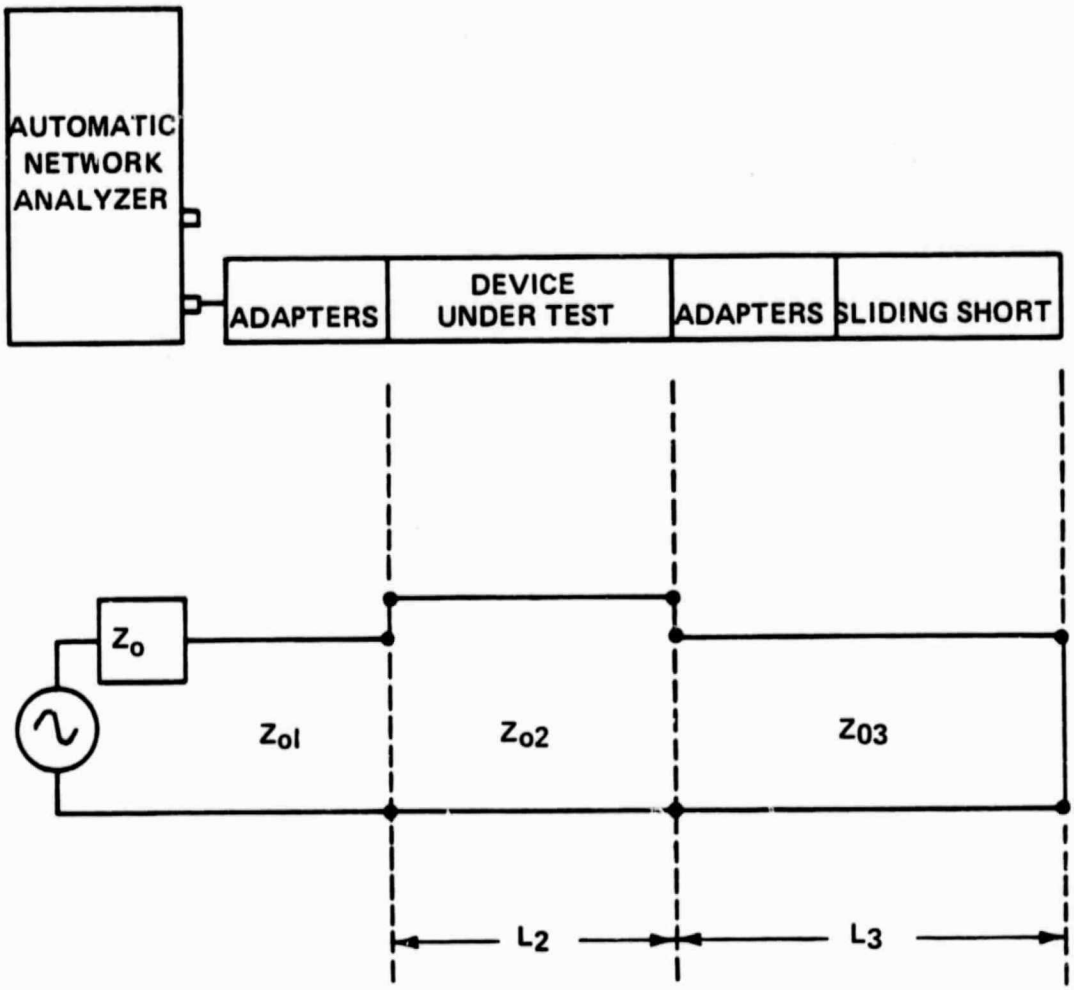

Figure 15. Circuit Model of Experimental Situation Which was Used for the Computer Simulation

IV. SUMMARY AND CONCLUSIONS

In summary, a program has been carried out to calculate and to measure the loss of traveling wave tube helix structures. Excellent agreement between the calculated and measured losses is obtained when it is assumed that the effects of helix surface roughness cause the resistivity to increase by a factor of approximately 2. Also, the increase in measured loss, resulting from impedance mismatches between the helix structure and the measurement circuitry and from losses in the sliding short, is accounted for.

It is shown that a very large fraction of the total loss of a helix structure (helix and supporting components) results from losses in the helix. Barrel losses are small and variations in total loss resulting from different values of barrel resistivity are negligible. Helix loss is shown to be minimized when helix pitch is maximized, when helix radius is minimized, when barrel to helix diameter ratio is maximized, when helix resistivity is minimized and when the effective dielectric constant of the support rods is minimized.

The implementation of the results contained in this paper should help increase the overall efficiency and power capabilities of helix-type traveling wave tubes.

C - 2

ACKNOWLEDGEMENT

The authors would like to thank Mr. Robert F. Bennett and Mr. Peter J. Talarico for their assistance during the course of this program. The support of a portion of this work by the Rome Air Development Center, Air Force Systems Command and the use of the Hewlett Packard Model 8542 B automatic network analyzer located at RADC are gratefully acknowledged. Finally, this program would not have been possible without the assistance and cooperation of microwave tube engineers at the following organizations; Hughes Aircraft Company, Litton Industries, Teledyne MEC, Varian Associates, and Watkins Johnson Company.

REFERENCES

1. H. G. Kosmahl and P. Ramins, "Small-size 81 - 83.5 Percent Efficient 2 - and 4 - Stage Depressed Collectors for Octave-bandwidth HIGH-Performance TWT's," IEEE Trans. Electron Devices, vol. ED-24, No. 1, pp. 36-44, Jan. 1977.

2. J. H. Bryant and E. J. White, "Attenuation and Power-handling Capability of Helical Radio-frequency Lines," Electrical Communication, pp. 278-282, Dec. 1954.

3. J. R. Pierce, "Traveling-Wave Tubes," D. Van Nostrand Co., New York, New York, 1950.

4. J. H. Bryant, "Some Wave Properties of Helical Conductors" Electrical Communiccation, pp. 50-56, March 1954.

5. G. W. C. Mathers and G. S. Kino, "Some Properties of a Sheath Helix with a Center Conductor or External Shield," Technical Report No. 65, June 17, 1953, Electronics Research Laboratory, Stanford University.

6. B. J. McMurtry, "Fundamental Interaction Impedance of a Helix Surrounded by a Dielectric and a Metal Shield," IRE Trans. Electron Devices, pp. 210-216, March 1962.

7. M. R. Gillette, "A Computer Aided Measurement Program for Dissipative Insertion Loss of Bilateral Microwave Devices," to be published, IEEE Trans. Microwave Theory and Techniques, special issue on 1979 MTT-S International Microwave Symposium, Dec., 1979.

8. G. A. Deschamp's, "Determination of Reflection Coefficients and Insertion Loss of a Waveguide Junction," J. App. Phys., vol. 24, No. 8, pp. 1046-1050, August 1953.

9. A. S. Gilmour, Jr. "SEM Analysis of TWT Helix Material Samples," IEEE Trans. Electron devices, vol. ED-24, No. 6, June 1977.

10. R. W. Beatty, "Determination of Attenuation from Impedance Measurements," Proc. IRE, vol. 28, No. 8, pp. 895-897, August 1950.

11. K. Tomiyasu, "Intrinsic Insertion Loss of a Mismatched Network, IRE Trans. Microwave Theory and Techniques, vol, MTT-3, No. 1, pp. 40-44, January 1955.

12. E. L. Ginzton, Microwave Measurements, McGraw Hill, 1957, Chapters 6 and 11.

13. G. L. Ragan, Microwave Transmission Circuits, Dover, 1965, pp. 29-36.

APPENDIX B

Measurement of the Dielectric Susceptibility with Resonator Having a Known Field Configuration

APPENDIX B

Measurement of the Dielectric Susceptibility with Resonator Having a Known Field Configuration

The factor $(\varepsilon_1/\varepsilon_0)$, the dielectric constant at a dielectric rod. can be determined by perturbing a resonant cavity having a known field configuration. For a cylindrical resonator operating in the TE_{010} mode, it can be shown that (Note 1)

$$(\varepsilon_1/\varepsilon_0-1) = -\frac{1}{1.85} \frac{\Delta f}{f} \frac{Vo}{\Delta V}$$

where $\Delta f/f$ is the fractional shift of resonant frequency caused by the dielectric rod of volume ΔV along the axis of a TM_{010} cylindrical cavity of volume Vo.

Note 1. See p. 445 Ramo and Whinnerg, "Fields and Waves in Modern Radio," Second Edition.

APPENDIX C

PAMTD Technical Memorandum No. 90

Estimating Accentuated Copper Loss at MM Wavelengths

APPENDIX C

PAMTD TECHNICAL MEMORANDUM NO. 90

ESTIMATING ACCENTUATED COPPER LOSS AT MM WAVELENGTHS

Arthur Karp

"Anomalous Skin Effect": The attached Figure 1 comes from Y.C. Wang's[1] "Screening Potential Theory," as adjusted by Wang to agree with two reliable room-temperature experimental data points due to F.J. Tischer.[2,3,4]

Example: At 90 GHz, cavity Q for perfectly stress-free and polished copper at room temperature should be about 22% lower than predicted "classically".

Roughness: Figure 2 (attached) uses, for 35 GHz, highly reliable experimental data due to Tischer[3]. The roughness profiles for which these data apply are those produced by abrasive gains (rubbed perpendicularly to the rf current direction). Since "increased surface area" appears to be involved, roughness profiles produced differently -- by EDM, chemicals or cutting tools, for example -- might yield more or less surface area for a given "rms roughness" depth. Note that the surface-resistance increase levels off when the rms roughness depth reaches about three times the classically calculated skin depth. Note also that Tischer generally found[3,5] conventional "profilometer" roughness readings to be much smaller than actual roughness; for this he very carefully measured profiles by Scanning-Electron and other Microphotography (and later found consistent correlation with the spreading after reflection of an initially collimated light beam).

The 90 GHz data have been derived from the 35 GHz data by assuming that the principal determinant of the surface-resistance increase is the ratio of the "rms roughness" depth to the classically calculated skin depth.

Example: A pure, totally stress-free copper cavity without brazed joints has surfae abrasions running normal to any direction of rf wall-current flow, with an rms roughness measure of 16 micro-inches, determined optically. At 90 GHz, the Q would then be about 24% lower than if the

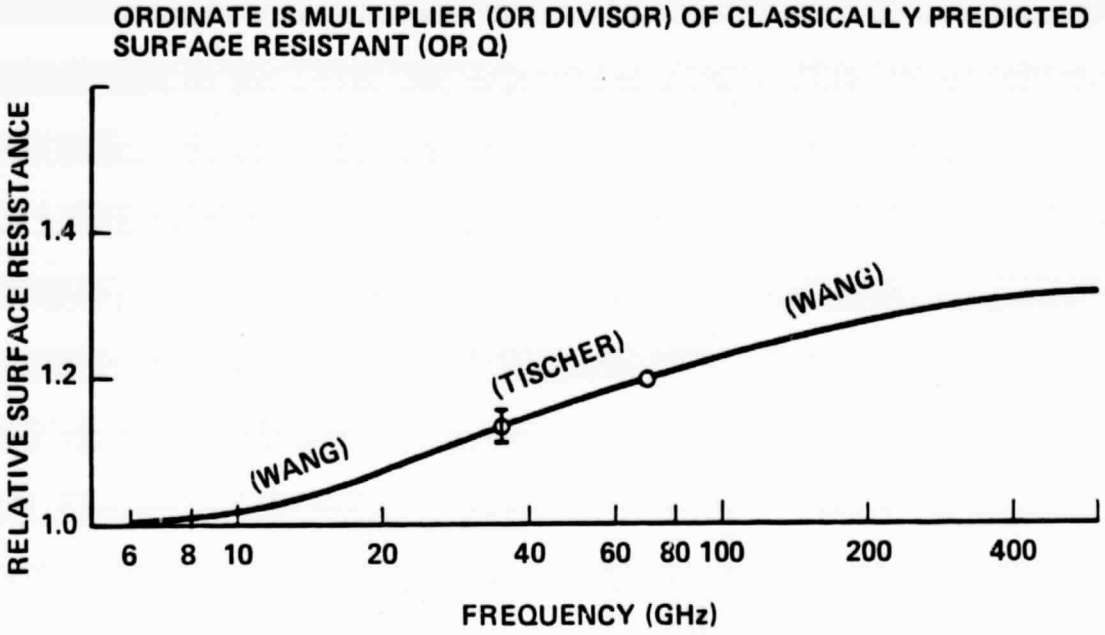

FIGURE 1. "ANOMALOUS SKIN EFFECT" AT ROOM TEMPERATURE

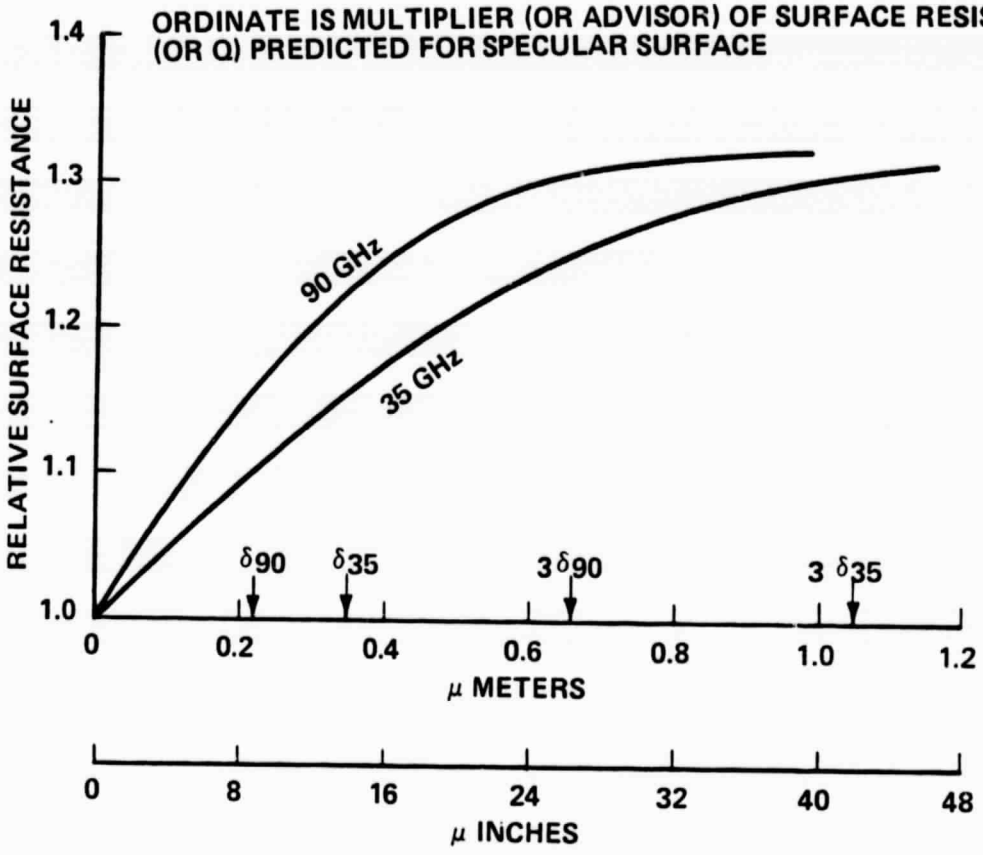

FIGURE 2. RELATIVE SURFACE RESISTANCE vs SURFACE ROUGHNESS

surfaces were specular. And so, at room temperature, the maximum Q attainable would then only be about 66% of that predicted in the absence of both roughness and "anomalous skin effect".

Further Notes

The copper is always assumed totally strain-relieved. (Even when not, a Q reduction of more than 2 -- at worst -- is not justified by the literature!) It is not clear whether conventional annealing will also relieve the "work-hardened" topmost micron (40 microinches) referred to in some references.[6,7] These stipulate that, in addition to general annealing, this thin layer of copper be removed, chemically or electro-chemically, or else "regenerated" by an oxidation/reduction process. Either procedure would significantly alter the roughness picture.

In cavities assembled with brazed joints, the extra resistance incurred by rf currents crossing a stripe of higher-resistance alloy might -- in especially small cavities -- come to dominate the Q picture, making the effects discussed above relatively less important. (Copper - only sintered or electroformed joints might be viewed as resistance-free - provided that appropriate inspection techniques confirmed complete unity of the metal across the join plane.) In periodic structures, random irregularities constitute an additional source of system loss having the potential to mask any of the sources already mentioned.

References Cited

1. Y.C. Wang, "The Screening Potential Theory of Excess Conduction Loss at Millimeter and Submillimeter Wavelengths," IEEE Trans. MTT, 26, pp. 858 - 861, Nov. 1978.

2. F. J. Tischer, "Measurement of the Surface Resistance of Single-Crystal Copper in the Millimeter-Wave Region at Room Temperature,' Appl. Phys. Lett., 5, pp. 285 - 286, 1974.

3. ---, 'Excess Conduction Losses at Millimeter Wavelengths," IEEE Trans. MTT, 24, pp. 853 - 858, Nov. 1976.

4. ---, "Experimental Attenuation of Rectangular Waveguides at Millimeter Wavelengths," IEEE Int. M-wave Symp. Digest (San Diego, CA), June 1977, pp. 492 - 494.

5. ---, "Excess Surface Resistance Due to Surface Roughness at 35 GHz," IEEE Trans. MTT, 22, pp. 566 - 569, May 1974.

6. J. S. Thorp, "RF Conductivity at 8 mm Wavelength," Proc. IEEE (British), 107, Part III, pp. 357 - 359, Nov. 1954.

7. R. L. Bell and M. Hillier, "An 8-mm Klystron Power Oscillator," Proc. I.R.E., 44, pp. 1155 - 1159, Sept 1956.

APPENDIX D

Measurement of Microwave Characteristics of Helix Traveling Wave Circuits

APPENDIX D

MEASUREMENT OF MICROWAVE CHARACTERISTICS OF HELIX TRAVELING WAVE CIRCUITS

James R. Legarra

Varian Associates, Inc.
611 Hansen Way
Palo Alto, CA 94303

ABSTRACT

A measurement technique has been developed for accurately and rapidly measuring phase velocity, loss profile, and Pierce impedance in helix traveling wave circuits. This technique employs an Automatic Network Analyzer to control a perturbation measurement sequence which generates amplitude and phase information on the microwave signals in the circuits. These data are statistically reduced in the computer and hard copy of the results is produced automatically in the form of graphs and tables. Phase velocity measurements are repeatable to within ± 0.05% and Pierce impedance to within ± 5%. Loss profiles are typically tracked down to the -20 dB level. Dispersion characteristics are measured over wide frequency ranges including the stopband regions of lossless circuits. Resonant loss profiles have been successfully measured. All these measurements can be made on production helix circuits which typically are one-port devices.

FUNDAMENTAL CONCEPTS

Non-Resonant Perturbation Theory

The theoretical basis for the method described in this paper for measuring the microwave properties of helix circuits is the non-resonant perturbation theory proposed ty C. W. Steele (1). This theory relates the change in the complex reflection coefficient, Γ, at the measurement port of a non-resonant microwave cavity to the complex electric and magnetic field components at a given position on the cavity due to the insertion of a perturbing object at that position.

$$\Delta\Gamma = (\Gamma-\Gamma o) = \frac{\omega}{2} \frac{\varepsilon \alpha_e E^2 - \mu \alpha_m H^2}{2Pin} \qquad (1)$$

α_e and α_m are the electric and magnetic polarizabilities of the perturber and Pin is the incident power at the measurement port. No attempt is made to separate electric and magnetic perturbations in helix circuits or to calibrate perturbers in terms of α_e and α_m. Instead, the assumption is made that E and H are so related in uniform sections of the helix that the right hand side of equation 1 is proportional to the square of a generalized field quantity, p, in which case (1) can be written as

$$|\Delta\Gamma| \, e^{j\phi} \propto |p|^2 e^{2(-j\beta z)} \qquad (2)$$

where $|p|^2$, and hence $|\Delta\Gamma|$, is proportional to the power flowing down the circuit and β is the propagation constant of the traveling wave. A measurement of $\Delta\Gamma$ as a perturber is pulled along the axis of the helix allows the calculation of loss profile from the $\Delta\Gamma$ versus z characteristic:

$$\text{Loss}\ (z) = 10 \times \log_{10} \left(|\Delta\Gamma|(z) / |\Delta\Gamma|_{max} \right) \qquad (3)$$

Furthermore β, and hence phase velocity, can be calculated from the slope of the phase vs z data:

$$\beta = -\frac{1}{2} \frac{d\phi}{dz} \qquad (4)$$

$$v_p = \frac{\omega}{\beta} \qquad (5)$$

It should be noted that if the helix circuit has a discontinuity in its structure which alters the relationship of the E and H fields, then $|\Delta\Gamma|$ may increase or decrease suddenly at that point due to the change in the circuit impedance. Thus, loss profiles can only be reliably interpreted within uniform sections of the helix.

Figure 1 illustrates the locus of Γ in the complex plane as a function of perturber position. Γ moves in a circle clockwise about Γo, the unperturbed reflection coefficient, as the perturber is moved away from the signal source. If there is loss in the circuit, Γ spirals in toward Γo and $\Delta\Gamma$ goes toward zero. Clearly, the dynamic range of

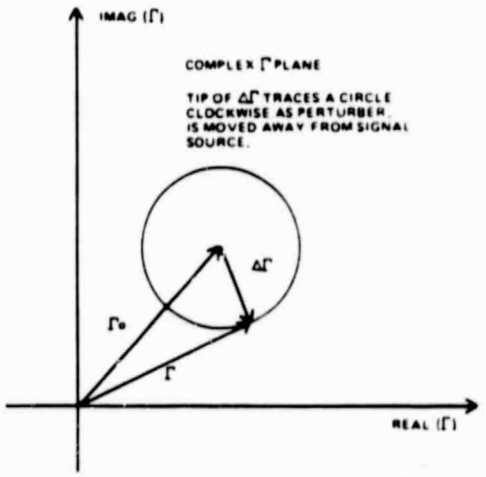

Figure 1. Locus of the complex reflection coefficient as the perturber is pulled through the helix.

Reprinted from INTERNATIONAL ELECTRON DEVICES MEETING, December 1979

the loss profile measurement depends upon the effectiveness of the perturber in producing a large and regular perturbation of the reflection coefficient. By "regular" it is meant that the locus of Γ be smooth and circular. Non-circular patterns result in ripple in both the Γ versus z and the ϕ vs z characteristics which limits the resolution in loss profile and phase velocity calculations.

Calculation of Pierce Impedance

R. P. Lagerstrom (2) showed that the Pierce impedance on the axis of a helix circuit is related to the change in propagation constant, β, due to the insertion of a dielectric rod on the axis:

$$K = \frac{E_z^2(o)}{2\beta^2 P} = \frac{1}{Pe} \frac{2(\beta' - \beta)}{\omega\beta(\varepsilon_r - 1)\varepsilon_o \pi b^2} \qquad (6)$$

β' is the dielectric loaded propagation constant, b is the radius of the rod, and ε_r is its relative dielectric constant. Pe is a correction factor which accounts for radial electric fields and radial field variation across the cross-section of the rod. Equation 6 assumes that TE fields are negligible in the region occupied by the rod. This assumption is best made for small diameter rods although, for good accuracy in the impedance calculation, it is desirable that the rod be large enough and have a nigh enough dielectric constant to produce at least a 2% change in β.

β' can be measured by putting a perturbing bead on the dielectric rod which is then pulled along the axis of the helix. If the rod is uniform the only perturbation is caused by the change in the bead position and β' can be calculated from the slope of the phase versus distance curve as previously described.

THE PERTURBATING OBJECTS

Finding perturbers which are effective over a wide frequency range and which produce a smooth and regular Γ locus in the complex plane has been a cut-and-try process. The best results have been obtained with a helical wire of about 3 turns wrapped around a dielectric core. The diameter of the perturber is approximately half the ID of the helix it will probe. This perturber is highly resonant in the sense that it produces an extremely large $\Delta\Gamma$ near its resonant frequency. It is desirable that the resonant frequency be approximately centered in the measurement band for best frequency coverage. A good rule-of-thumb seems to be that a 3 turn perturber will be effective over a broad frequency range which includes the operating band of the circuit.

For example, a 0.060" diameter helical perturber is used on circuits with helix ID's in the neighborhood of 0.120". The perturber is suspended on a thin nylon thread which has minimal dielectric loading effects. A sapphire rod (diameter = 0.040", ε_r = 11.34) is used for Pierce impedance measurements in the same circuits. The rod has a 3 turn helical wire wound around it and is otherwise uniform. In the class of circuits for which they were made, these perturbers resonate at about 6 GHz and are generally effective from 2 to 12 GHz.

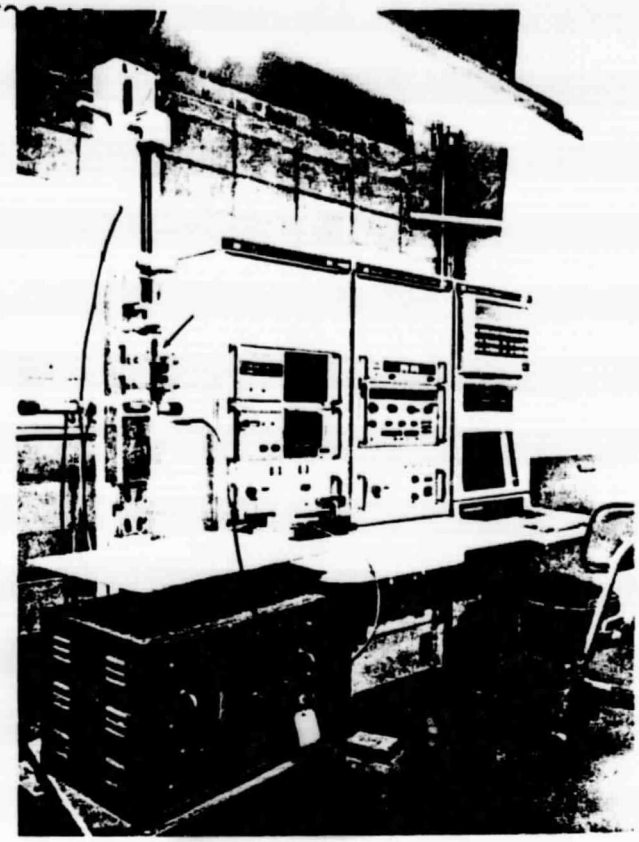

Figure 2. Automatic test system used in perturbation measurements on helix circuits consisting of an Automatic Network Analyzer and a mobile test apparatus which is used to position the perturbing probes. Arrow points to circuit under test.

THE MEASUREMENT EQUIPMENT

A Hewlett-Packard 8542B Automatic Network Analyzer is the centerpiece of an automatic test system for the perturbation measurements on helix circuits (see Figure 2). The positioning of the perturbers is accomplished accurately with a stepping motor driven linear slide which has been interfaced to the ANA computer. The motorized slide is part of a mobile test apparatus which holds the circuits under test and has adjustments for centering the perturbing probes. The ANA computer has been programmed to control a measurement sequence in which Γ is measured at each specified frequency for each position of the perturber which is stepped down the circuit in precise increments. There is also an initial measurement of Γ_o in which the perturber is pulled completely outside the fields in the helix. The sensitivity of the ANA in resolving small changes in Γ is a function of the absolute magnitude of Γ. The best resolution is obtained for good match conditions ($|\Gamma| < 0.2$) in which case $|\Delta\Gamma|$ down to 0.001 can be detected.

Data Reduction

$\Delta\Gamma$ is computed for each frequency at each perturber position. The loss profile is simply computed as a logarithmic plot of $|\Delta\Gamma|$ versus distance. Phase velocity is computed from the slope

of the ϕ versus z curve which is determined by means of a least-squares curve fit. Phase velocity can be computed in each section of a circuit with velocity steps (pitch changes) by limiting the data reduction for each velocity calculation to the appropriate range of axial distance.

If Pierce impedance is desired, the computer is progammed to perform another perturbation measurement on the helix with the dielectric rod probe which results in the calculation of the dielectric loaded β. Pierce impedance is then calculated according to equation 6, including the calculation of the Pe correction constant.

Finished hardcopy of all these helix characteristics is produced automatically in the form of plots and tables on an electrostatic printer-plotter following visual inspection and scaling on the console CRT.

TYPICAL RESULTS

The output section of a C-band production helix was measured from 4 to 12 GHz with the perturbers described earlier for use in 0.120" diameter circuits. The loss profile at 8 GHz (Figure 3) shows a lossless section near the output window followed by a section of low level distributed loss with lumped loss in the middle and finally terminated with heavy loss at the sever end of the circuit. There is a velocity step in this helix and the dispersion characteristics on each side of the step are superimposed in Figure 4. The Pierce impedance on the output side of the velocity step is shown in Figure 5.

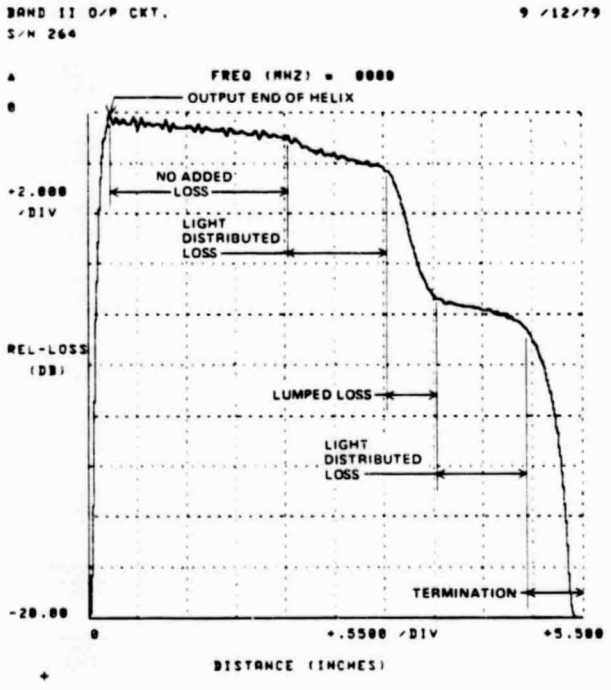

Figure 3. Loss profile for a C-band helix circuit with loss on the support rods. The test signal is injected through the output connector.

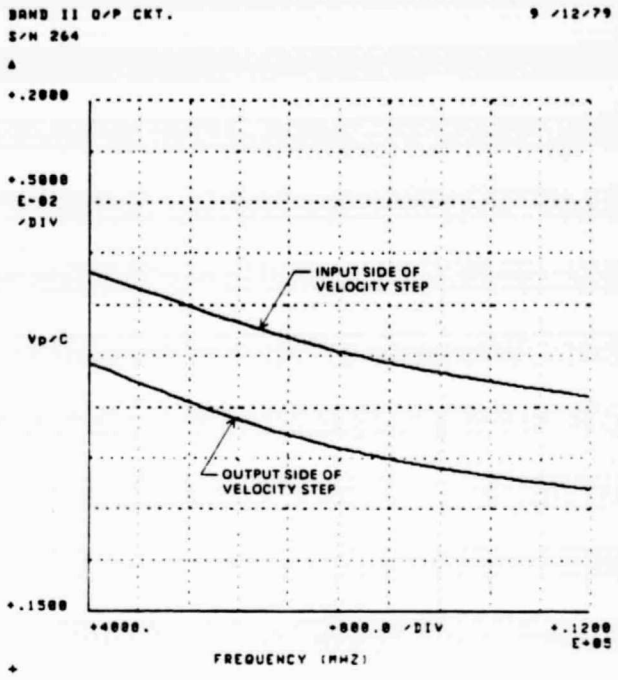

Figure 4. Measured dispersion characteristics for a C-band helix circuit with a velocity step.

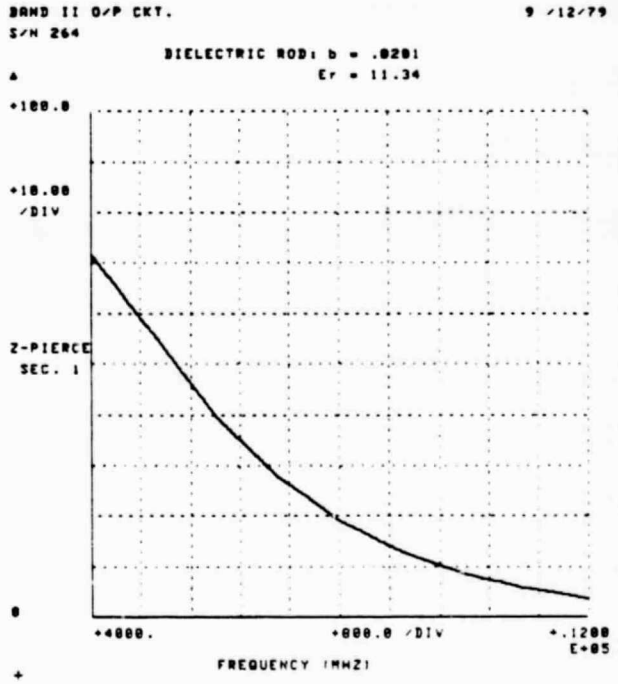

Figure 5. Measured Pierce impedance for C-band helix circuit on the output side of the velocity step.

Measurement Sensitivity and Repeatability

Loss profile can typically be tracked down to the -20 dB level if perturbers which are properly scaled to the helix are used. As much as 30 dB of dynamic range has been observed.

The measurement of phase velocity is repeatable to within ± 0.05% when there are sufficient wavelengths in the circuit section to insure a good data base for the least-squares curve fit algorithm. Typically, at least 5 wavelengths are desired.

The Pierce impedance measurement, if done carefully, is repeatable to within ±5%. To achieve this degree of repeatability the dielectric rod must produce a percentage change in β which is approximately 20 times the repeatability in the phase velocity calculation. Consequently, a change in β of about 2% is desired.

RANGE OF APPLICATIONS

This measurement technique has been used effectively in the following ways:

1. Cold testing production helix circuits for proper loss and velocity characteristics before final assembly.
2. Measuring experimental circuits designed to test dispersion control methods.
3. Providing loss, velocity, and impedance data for predicting the "hot" performance of new helix circuits.
4. Characterizing resonant loss in terms of a picture of the uniformity of the loss distribution as a function of distance.

REFERENCES

1. C. W. Steele, "A Nonresonant Perturbation Theory", IEEE Trans. MTT, Vol. MTT-14, No. 2, pp 70-74, February, 1966.

2. R. P. Lagerstron, "Interaction-Impedance Measurements by Perturbation of Traveling Waves," Technical Report No. 7, Stanford Electronics Laboratories, February 11, 1957.